Dear Editor, Dear Reviewers,

attached please find the revised version of the manuscript. For revision, we thoroughly followed the reviewer's comments as indicated in the attached point-by-point answers and as uploaded in the TCD discussion section.

As an overview, the main changes to the manuscript comprise:
- The manuscript has been slightly restructured to better focus on relevant aspects; three sections have been added to the appendix. They contain: A1) discussion of the fabric anisotropy, A2) Details of the weighted averages of the Maxwell-Garnett equations as suggested by Reviewer #1, A3) as in the original paper, A4: calibration of the snow scat instrument. (moved from the data section)
- The theory section has been split into two sections: Sec2: calculation of the permittivity, Sec3: Measuring the anisotropy via copolar phase differences.
- A section targeting the signal propagation and signal processing aspects to obtain the CPD from the copolar coherence has been added to clarify that the propagation paths can be calculated to a common point P (as questioned by reviewer #1).
- The SnowScat calibration has been moved from the measurement section to the appendix;
- The figures showing measurement data have been moved from the "Analysis" section to the "Measurement" section, including an interpretation of the measurements.
- a 4th computer tomography dataset has been added.
- a discussion with respect to the crystal fabric anisotropy has been added to the "Analysis"
- a section showing the author contributions has been added.

A latexdiff document indicating the changes made is attached to this letter for convenience.

Best regards,
Silvan Leinss

Anonymous Referee #1

General Changes:
Author: A forth validation data set from computer tomography has been added which shows similar results as the existing three datasets.
==========

General comments:

R1: Leinss et al. presented a method of microwave remote sensing to detect birefringence of electromagnetic waves that propagate through thicknesses of snow. First, dielectric mixture theory that relates between the geometrically anisotropic features of snow and the anisotropic dielectric permittivity is given. Then, microwave propagation model for the oblique incident angle and scattering at the bottom of the snow thickness was given. The authors performed radar measurement of snow at a test site in Finland. The authors demonstrated the copolar phase difference (CPD) had temporal variations in four winter seasons. With sets of data for snow thickness and snow density that was manually measured, the authors converted the CPD to the geometrical anisotropy of snow. The geometrical anisotropy of snow was verified by direct measurements of the snow microstructure using X-ray absorption micro-tomography. The authors demonstrated that settling of the snow particles that occur in several days after the deposition could be observed. The authors suggested that detection of the CPD variations are indicator of the fresh snow. In addition, the CPD observed from the satellite showed the same temporal variation that was observed at the test site.

R1: I evaluate that this is a nice paper that opens use of the birefringent features of snow for microwave remote sensing. Handling of the dielectric mixture theory seems sound and fair to me. Experimental settings, processing of the data and interpretation for the data were almost properly presented, with which I could agree. Overall, the readers of this paper can learn a lot about a remote sensing method that can provide progress in snow science related to metamorphism and remote sensing of snow metamorphic properties.

R1: I have relatively minor criticisms/concerns at points as listed below as the specific comments.

Comment: Frequent use of a term "recrystallization" does not seem proper to me to express metamorphism where vapor sublimation and condensation play major roles.

Answer: The term "recrystallization" has been removed from the paper and was replaced by the more appropriate term "metamorphism".

Comment: For explanation of the method in the abstract and conclusion, the authors tend to mention little about the principle of radio wave birefringence, whereas it is a key of the method. It should be explicitly mentioned.

Answer: The "principle of radio wave birefringence" is now mentioned in both, abstract and conclusion.

Comment: In the experimental method, to derive the snow anisotropy from the CPD, we need to know both thickness and density of snow independently. The authors tend to mention little on this point when the authors wrote summary of their experiment, for example, in the abstract and in the concluding remarks. Without providing such information, many readers may think that the snow anisotropy can be precisely determined by the CPD measurement alone, without any additional measurements. It seems more fair to me that prerequisite of the method is given.

Answer: The need for thickness and density/SWE has been added to the abstract, the conclusion and also the introduction of the method-section (sect. 2).

Comment: Besides, there are some misleading citations for the history of the measurement of the dielectric anisotropy of snow and firn, which should be fairly repaired.

Answer: We thank the reviewer for checking carefully the citations. We think, by answering your comments below, this point should be adressed adequately.

Comment: Though it is not mandatory, I recommend that author contributions are given at the end of this paper as a good habit of the collaborative paper.

Answer: This section has been added to the paper. A few people which also contributed to the paper were added to the acknowledgements.

Specific comments

Abstract in general
Comment: It seems to me that there is a big step of the context between lines 2-8 and lines 9-19. In the former, the authors' statement is that snow anisotropy can be remotely sensed. In the latter, the authors' statement is about observation. There is no mention for the basic principle in this abstract. A sentence should be given to fill the gap. My suggestion is something like "Snow is dielectrically anisotropic medium that has an axis of symmetry in the vertical due to anisotropic distribution of ice matrix and pore spaces. Such dielectric anisotropy can be detected by microwave remote sensing using a principle of radio wave birefringence and oblique wave propagation."
This kind of mention for the basic principle will better lead readers, I think.

Answer: Large parts of the abstract have been rewritten and your suggestions have been thankfully taken into account.

Abstract, L.2.
Comment: It seems to me that the term "recrystallize" is not proper. As many snow scientists have used, it seems better that the author choose a term "metamorphose". In crystal physics, "recrystallize" means more about migration of molecules within solid ice, from a domain of molecules (crystal lattice) to another. Such diffusion of molecules should exist in snow metamorphism. However, sublimation and condensation play major role in initial changes of the snow properties in particular 3D geometry. "recrystallize" is only one phase of various phenomena. Considering this, I suggest that a more general term "metamorphose" is a better choice.

Answer: Thanks for this nice explanation. We fully agree that the term "recrystallization" should be teplaced by "metamorphism". This was done where neccesary.

Abstract, L.3.
Comment: A term "oriented ice crystals" has vague meaning. Readers who know that ice crystal has c-axis and a-axis will wonder if this paper talks about either crystal axis orientation or macroscopic shape of ice matrix, or both. I understand, in this paper crystal axis orientation is not discussed. If it is so, some different expression seems better. It is mostly 3D geometry of ice and pore spaces that give such anisotropic effects (an anisotropy in mechanical, thermal, and dielectric properties). Not crystal-axis orientation.

Answer: The term "oriented" has been removed from the abstract and has been replaced by "spatially anisotropic distribution of the ice matrix".

Abstract, L.4-8.
Comment: I felt that the contrast or comparison was a bit strange here. Anisotropy of snow have been observed by many methods using snow samples. In this paper, the authors discuss microwave remote sensing method that can detect changes in average anisotropy over thick ice.
A problem in the expression is that the authors wrote a context as if microwave remote sensing were an alternative method to detect anisotropy in microscopic manner. It is a method to detect dielectric properties of the target (snow in this case) in macroscopic manner. I agree that such macroscopic properties in the media reflects microscopic properties in snow. However, the remote sensing method itself cannot clarify what is going on in microscopic scales. I suggest the authors to avoid to give an impression to readers that this paper gives an alternative method to detect microscopic features.

Answer: We replaced "alternative method (...) to determine the anisotropy" by "method to determine the depth-averaged anisotropy on macroscopic scales". This should clarify that microwaves cannot be used to determine the microstructure but that only the macroscopic effect due to the microstructure can be measured.

Main text:

L.23 in P.6062
Comment: I suggest that "metamorphism processes" is better than "recrystallization processes" with a reason same as abstract L.2.

Answer: agreed and changed.

L.24 in P.6062
Comment: The authors used a term "electromagnetic". I suggest that a term "dielectric" is better here. This word is more directly related to what the authors observed.

Answer: agreed and changed.

L.26 in P.6062 . L.2 in P.6063
Comment: The authors give introduction like this to show a contrast between sample measurement and the microwave remote sensing. However, microwave remote sensing is a method to detect macroscopic nature of the targets. It does not seem proper that the authors give an impression to readers that sample measurements have a problem of actions of sampling. Both are necessary scientific approaches.
Advantages of the microwave remote sensing include (i) repetitive measurements for inaccessible locations using satellites or airplanes, and (ii) the measurement can cover very wide area. Disadvantage is that it cannot be as detailed as the ground measurements. I suggest the authors to tell these aspects to readers. Destruction of samples by snow sampling does not seem to matter.

Answer: A short section about advantages and disadvantages of microscopic measurements vs. microwave remote sensing techniques have been added. The sentence about destructive sampling has been removed.

L.3 . 12 in P.6063
Comment: I felt a bid odd to find that an example of the polar snow first appeared in this paper. In the long history of seasonal snow studies, are there no studies that investigated anisotropy in the deposited snow?

Answer: This paragraph has been rewritten and early examples for anisotropy measurements of seasonal, deposited snow are cited.
eg. - Photographs by Kojima, Kenji (1960), in "Thin Section of Snow Cut by a Heated Wire.", Contributions from the Institute of Low Temperature Science, vol. 16.
- a review about dielectric measurements: Evan, S (1965) "Dielectric properties of ice and snow—A review", Journal of Glaciology vol 5.
- and the reference to the anisotropic thermal measurements of (Izumi, 1975). "Studies of metamorphism and thermal conductivity of snow, 1", Low Temperature Science Series A, vol. 33.
After that, the reference to (Alley, 1987) is given.

L.8 in P.6063
Comment: I suggest "metamorphism" rather than "recrystallization".

Answer: agreed and changed.

L.14 in P.6063
Comment: (Pfeffer and Mrugala, 2002) should be (e.g., Pfeffer and Mrugala, 2002) because there are earlier examples that these authors cited.
In addition "driven by a vertical water vapor flux under temperature gradients" seems better. I suggest to add "under temperature gradients".

Answer: agreed and corrected.

L.10 . 12 in P.6063
Comment: For the vertical anisotropy of geometry, the authors mentioned that it was driven by a vertical water vapor flux. The authors did not mentioned any cause of the horizontal anisotropy of geometry here. I think that a short mention will help readers' understanding.

Answer: This point is adressed later by the paper of Schleef (2013) and Löwe (2011).

L.13 . 16 in P.6063
Comment: The anisotropy of snow was determined from the computer tomography data by a paper Fujita et al. (2009) below as well. To be fair, I suggest this paper should be naturally added to citation with (Lowe et al., 2011, 2013).
Fujita, S., Okuyama, J., Hori, A., and Hondoh, T.: Metamorphism of stratified firn at Dome Fuji, Antarctica: a mechanism for local insolation modulation of gas transport conditions during bubble close off, J. Geophys. Res.-Earth, 114, 1.21, doi:10.1029/2008JF001143, 2009

Answer: The references to Lowe are given for the method of the statistical analysis. However, a reference to the paper of Fujita(2009) has been added later where anisotropies in polar firn are mentioned. This paper is indeed very interesting.

L.17 in P.6063
Comment: Vertical structures have been found in samples of polar firn (the same paper above and the paper below), too. To be fair, Fujita et al. (2009) and Fujita et al. (2014) should be naturally cited here.
Fujita, S., Hirabayashi, M., Goto-Azuma, K., Dallmayr, R., Satow, K., Zheng, J., and Dahl-Jensen, D.: Densification of layered firn of the ice sheet at NEEM, Greenland, J. Glaciol., 60, 905.921, doi:10.3189/2014JoG14J006, 2014

Answer: agreed and added.

L.2 . 3 in P.6064
Comment: The authors wrote "The origin of horizontally aligned structures has been discussed with respect to settling of fresh snow (Schleef and Lowe, 2013)".
However, I did not find such a context in the cited paper. Perhaps I did not read this paper deep enough to detect the cited context. However, the other readers may find the same problem. I suggest the authors to point out where readers should see in the citation.

Answer: We agree that here the wrong citation was given. The correct citation should be "Lowe (2011)" which is already given in the next sentence. We also added two references which indicate that snow crystals fall already with a preferentially horizontally aligned orientation.
- Garrett, T. J. and Fallgatter, C. and Shkurko, K. and Howlett, D. "Fall speed measurement and high-resolution multi-angle photography of hydrometeors in free fall", in Atmospheric Measurement Techniques (2012), vol 5 no 9.
- Matrosov, Sergey Y. and Reinking, Roger F. and Djalalova, Irina V. "Inferring Fall Attitudes of Pristine Dendritic Crystals from Polarimetric Radar Data", Journal of the Atmospheric Sciences (2005), vol 1 no 62.

L.2 . 6 in P.6064
Comment: The authors used several lines here to explain a relation between the isothermal metamorphism and the horizontally aligned structures. However, cited papers are all for artificial snow in the laboratory. Please mention how plausible such horizontally aligned structures of snow really appear in natural snow.

Answer: References have been added which show horizontal structures in natural snow (Mätzler, 87, Fig. 2.15) and Calonne (2012). Both papers are already referenced at other places in the paper.

L.7 in P.6064
Comment: I wonder why dielectric anisotropy was suddenly introduced here. Please provide an explanation. Why not mechanical properties, thermal properties or optical properties? It seems too sudden.

Answer: A paragraph has been added to the introduction to prepare the reader for different methods to determine the anisotropy of snow (microscopic, macroscopic in the field, and by remote sensing). I think this prepares the reader now that different scales are adressed. Additionally, we added "e.g." to the sentence to indicate that dielectric measurements are not the only method to determine the anisotropy.
The sentence was changed to "On macroscopic scales, the anisotropy of snow can be characterized by macroscopic properties of snow like e.g. the anisotropy of the dielectric permittivity".

L.9 . 11 in P.6064
Comment: The authors wrote, "the di-electric anisotropy can be measured with different polarizations of the electromagnetic field in microwave resonators filled with snow (Jones, 1976)."
Readers will surely read this sentence as if Jones (1976) had measured snow. It is not true. Note that "Jones (1976)" is a method paper and that only crystal quartz was measured. The authors sentence make readers misunderstand that Jones (1976) measured snow. Fujita et al. (2009) and Fujita et al. (2014) are real applications of the method to snow. Matsuoka et al. (1997) was the real application of the method to ice crystal. Please provide precise citations. Ignorance is insult to earlier studies.
Reference: Matsuoka, T., Fujita, S., Morishima, S., and Mae, S.: Precise measurement of dielectric anisotropy in ice Ih at 39 GHz., J. Appl. Phys., 81, 2344-2348, 1997.

Answer: I totally agree that this sentence is not clear and that this reference is misleading. See also comment/answer below.

L.13 . 15 in P.6064
Comment: Lytle and Jezek (1994) did not use open microwave resonator. They measured wave propagation speed. I find that the authors are sometimes misleading readers in terms of citations.
I suggest description something like below.
"Using open microwave resonators, different permittivities in the vertical and horizontal direction have been found in multi-year firn on the Greenland ice sheet (Fujita et al., 2014)

photographic (Lytle and Jezek, 1994) and computer tomographic analysis (Fujita et al.,2009).

Answer: Thanks for the suggestions. Your suggestion has been added in a slightly adapted form to mention the design of Jones (1979).
I'm not sure if the paper of Matsuoka et al. (1997) should be mentioned here as it focuses on the crystal anisotropy of ice and not the structural anisotropy of snow. However, I cited the paper Matsuoka et al. (1997) in the section about the definition of the "structural anisotropy". Here it is indeed relevant to consider the anisotropic properties of ice with respect to the crystal orientation/c-axis.

L.16 in P.6064
Comment: It seems to me that there are big steps in the context in this introduction here. It is the same problem that I pointed out for the abstract. The authors skipped introduction of the physical principle and earlier examples that used the principle.
First, if the media has dielectric anisotropy, in principle, electromagnetic waves propagating through the medium have polarization effects due to birefringent nature of the medium. Rather than suddenly introducing satellite-based observation, the authors should mention this basic physical principle to readers.
Second, it seems to me that the authors should tell to readers that there is no real measurement of dielectric anisotropy in seasonal snow.

"seasonal snow", "radar" and "satellites " are big steps in introduction, I felt.
I suggest that the authors should provide introduction something like below.

"Snow is dielectrically anisotropic medium that has an axis of symmetry in the vertical due to anisotropic distribution of ice matrix and pore spaces, as it has been observed. Such dielectric anisotropy can be detected by microwave remote sensing using a principle of radio wave birefringence of the electromagnetic wave propagation. The use of principle of the birefringence to remote sensing has been used to explore internal structure of the ice sheets and glaciers with radio wave (e.g., Hargreaves (1977, 1978), Fujita et al. (2006) and Matsuoka et al. (2009)). As for detection of birefringence of seasonal snow, Leinss et al. (2014) determined the anisotropy of seasonal snow with radar satellites; they analyzed propagation differences of differently polarized microwaves within snow."

References
Hargreaves, N. D.: The polarization of radio signals in the radio echo sounding of ice sheets, J. Phys. D. Appl. Phys., 10, 1285-1304, 1977.
Hargreaves, N. D.: The radio-frequency birefringence of polar ice, J.Glaciol., 21, 301-313, 1978.
Matsuoka, K., Wilen, L., Hurley, S. P., and Raymond, C. F.: Effects of birefringence within ice sheets on obliquely propagating radio waves, IEEE Trans. Geosci. Remote Sens., 47, 1429.1443, 10.1109/TGRS.2008.2005201, 2009.
Fujita, S., Maeno, H., and Matsuoka, K.: Radio-wave depolarization and scattering within ice sheets: A matrix-based model to link radar and ice-core measurements and its application, J. Glaciol., 52, 407-424, 2006.
The authors did not invent the use of principle of the birefringence to remote sensing. I suggest that earlier examples for snow and large ice masses should be naturally introduced to readers.

Answer: Thanks for this extended explanation for the history of remote sensing of anisotropic properties of ice sheets and also for the numerous references. I added your suggestion with very small modifications.
The following paragraph gives also historical reference for remote sensing of seasonal snow as Leinss (2014) was also not the first who observed birefringent effects in seasonal snow.

L.23 . 25 in P.6064
Comment: It seems to me that "a contactless, destruction-free" are not something to be emphasized. This aspect is clear if the authors tell it is radar remote sensing.
I suggest something like below.
"Polarimetric radar remote sensing methods can provide information of the dielectric anisotropy of snow from large distances. Areas of many thousands of km2 can be observed with air- and space-borne sensors repeatedly if it is observed from orbit of the satellite. They provide a complementary tool to detailed ground sampling/measurements such as computer tomography or dielectric anisotropy as large areas and volumes of natural snow can be observed as an averaged manner. h
I suggested here to mention the dielectric anisotropy. Indeed it is a measurable quantity and this is the very quantity that causes the birefringence. Between μCT measurement and the microwave remote sensing, a quantity dielectric anisotropy is necessary.

Answer: I agree and thankfully took your suggestion into account. I made also clear, that only "area-, depth- or volume-averaged properties are measured".

L.29 in P. 6064 . L. 3 in P.6065
Comment: The authors wrote "Currently, polarimetric radars are only used to characterize the anisotropy of falling snow or rain". To be precise, it is not true considering the radar remote sensing of the ice sheets and glaciers with radio wave (e.g., Hargreaves 1977, 1978, Fujita et al. 2006 and Matsuoka et al. 2009).

Answer: Considering your references concerning ice sheets which have been added, I changed this sentence to "Today, polarimetric upwards looking radars are used (...)"

L.3 . 5 in P.6065
Comment: This is repetitive statement about the dielectric anisotropy. The authors already gave statements snow is dielectrically anisotropic material. It is equivalent to the propagation speed difference.
I suggest that the statement here should be removed or rewritten.

Answer: as many examples are already given for the vertical dielectric anisotropy (eps_V > eps_H) this sentence has been removed.

L.5 and L.11
Comment: "opposite effect" meaning is unclear to me.

Answer: It has been clarified that for fresh snow a larger horizontal permittivity has been found (The "opposite effect" to firn, where eps_V > eps_H).

L.9
Comment: "both effects" meaning is unclear to me.

Answer: "both effects" means vertical and horizontal anisotropies. This has been clarified.

L.10
Comment: TerraSAR-X" appeared suddenly. The authors should give a short basic information for this instrument. Not all readers are familiar to this.

Answer: "sattelite time series of TerraSAR-X" has been replaced by "time series of polarimetric radar measurements using the satellite TerraSAR-X (Stangl et al., 2006; Werninghaus and Buckreuss, 2010)"
References:
M. Stangl and R. Werninghaus and B. Schweizer and C. Fischer and M. Brandfass and J. Mittermayer and H. Breit (2006) "TerraSAR-X technologies and first results", Radar, Sonar and Navigation, IEE Proceedings, vol 153, no 2.
Werninghaus, R. and Buckreuss, S. (2010) "The TerraSAR-X Mission and System Design", IEEE Transactions on Geoscience and Remote Sensing, vol 48 no 2.

L.13
Comment: "negative values" meaning is unclear to me.

Answer: (eps_x < eps_z) has been added.

L.14 . 16 in P.6065
Comment: Meaning is unclear to me. It seems that the statements are for detectable resolution. However, I did not understand. Why does this statement of the resolution in introduction? It does not seem important at all at this stage of this paper.

Answer: This paragraph has been clarified to point out that the CPD can be used to precisely measure the dielectric anisotropy of the snow pack. The dielectric anisotropy is now defined as $\Delta\epsilon =\eps_z - \eps_x$.
It has also been added (as suggested for the abstract) that snow depth and density are required to measure the dielectric contrast eps_x - eps_z.

L.17 in P.6065
Comment: What is dielectric anisotropy? Definition was not given so far anywhere.
Does it mean something measurable with a resolution of 0.0001? It seems unnecessary precision in practice. Can the authors provide?

Answer: See answer above.

L.27 in P.6065
Comment: "TanDEM-X" appeared suddenly. Please provide introductory information for this instrument.

Answer: "TanDEM-X" has been removed from the paper. This is not 100% correct, however it avoids a lot of confusion. TanDEM-X is often referred to a satellite formation consisting of two almost identical satellites, TerraSAR-X and TanDEM-X (TanDEM-X = TerraSAR-X-Add-on for Digital Elevation Measurements). The measurements of both satellites are (with respect to the application in the paper) identical. Therefore, I think it is justified to claim that a few datapoints which actually were measured by the "other" satellite TanDEM-X were measured by TerraSAR-X.

L.11 in P.6066
Comment: It was written as "different choices for the length scales". It is not clear that the authors have shown two or more different choices. Different from what? What does a choice of the exponential correlation length mean as compared to the other correlation? An explanation to readers seems to help. What "choice" do the authors suggest to use for studies of the snow?

Answer: A reference (Loewe 2011) was given which describes different correlation lengths. We use the exponential correlation length as it has been commonly used in microwave modeling. ("microwave modeling" has been added). It has further been added, that the exponential correlation length is conveniently fitted to the correlation functions, but that for scattering effects limitations occur. New reference to (Löwe, 2015) added.
Reference: L\"owe, H. and Picard, G., "Microwave scattering coefficient of snow in MEMLS and DMRT-ML revisited: the relevance of sticky hard spheres and tomography-based estimates of stickiness", The Cryosphere (2015), vol. 9, no 6.

L.14 . 16 in P.6066
Comment: It seems to me ax and az are dimensions in the horizontal axis and in the vertical axis, respectively. Then, the magnitude of A for grains with given ratio between longest and shortest length seems dependent on whether the longest length is vertically or horizontally oriented. Is there my misunderstanding by me somewhere?

Answer: "magnitude of A" means "|A|" (without sign). According to Eq. (1), when e.g. ax = 2 and az = 1, then A = 0.66. Swapping ax and az leads to A = -0.66. (Same magnitude, opposite sign.). This is not the case in the definition A' where for the same numbers (ax = {2, 1} and az = {1, 2}) A' = 2 and A' = 0.5 follows which has a difference of 1 and 0.5 to the isotropic case of A' = 1.
"the magnitude of A" has been changed to "the magnitude |A|". The given example has been added.

L.6 in P.6067
Comment: The authors wrote "In the following we define the coordinate axes such that z is parallel to the normal vector of the earth surface and the x and y plane is parallel to the flat earth surface."
It seems that this was already assumed in eq. 1. I am confused to see that this definition appeared only here.

Answer: I moved this definition before the definition of the anisotropy. Thereby, z is defined by gravity (analog to the definition of vertical) and x,y is defined as horizontal.

L.20 . 22 in P.6067
Comment: The authors wrote "However, the relative permittivity, eps_{eff, MG} calculated with the Maxwell-Garnett formula underestimates the measured permittivity."
Does this mean that the measured permittivity of the isotropic snow was higher that the model calculations or opposite? This point is unclear to me. Please clarify.

Answer: To me "underestimate" means that the MG result is lower than the measured values. I added: to "the measured permitticity (Mätzler 96)" "which is slightly higher" to clarify this.

L.26 in P.6067 . L.2 in P.6068 "We found...."
Comment: Meaning of this sentence is unclear to me and probably to the other readers.
Do the authors intend to claim that the weighted average of the Maxwell-Garnett formula and the "inverse" Maxwell-Garnett formula agree with the empirical data of the permittivity of snow measured with the resometer method (Matzler, 1996). Is it correct? Please clarify to readers.

In addition, the authors wrote that deviation was within 0.7 %. 0.7% of what?
I suggest authors to develop their analysis in the appendix of this paper or as supplementary information. Otherwise, I am afraid that this part of the analyses are left as a black box for readers, which readers cannot digest only by reading this paper.

Answer: This has detailed in Appendix A: Effective permittivity from weighted average of Maxwell-Garnett equations

Comment: As for the footnote #2 in P.6068, it is not understandable for me, too. What are ƒÃh or ƒÃs? What is 3.171/3?

Answer: This has also been clarified in Apprendix A.

Equation 3
Comment: Please provide physical meaning of this equation to readers if it is possible.

Answer: Eq. (3) considers that for a low ice volume f_vol eps_eff,MG should provide better results as here, a few ice particles are embedded in a matrix of air. For large snow densities, it is better to model the permitticity by air inclusions in ice. The equations provides therefore a smooth interpolation of both boundary cases. (This arguments have been added to the appendix).

L.4 in P.6068
Comment: Please provide unit of ƒÏ.

Answer: This is also mass per volume and can be g/cm^3 or kg/m^3.

L.7 . 9 in P.6068
Comment: Please indicate temperature range that this study is applied. It seems that temperature range for this study is above about -10 degrees C. Is it correct? How did the authors handle temperature dependence of the permittivity? Did the authors approximate values of the permittivity?

Answer: For the entire paper, a fixed permittivity for ice of 3.179 was used. This corresponds to -10 degree C. The temperature dependence of the permittivity is about 1% in the range of the experiment (-30 ... 0 degree C) and therefore smaller than the uncertainty in density of a few percent.

Comment: In addition, nothing is mentioned for the fact that ice crystal has dielectric anisotropy with a size more than 1 % of the ice permittivity (Fujita et al., 1993; Matsuoka et al., 1996). Did the authors think that effects from this is negligibly small? Please explain to readers.

Answer: This is an important point and has been added in a separate subsection (including the reference to (Fujita et al., 1993; Matsuoka et al., 1997). Currently, it is not clear how large the crystal anisotropy of natural snow is, but evidence exists that the crystal anisotropy could have a small effect on the dielectric anisotropy (Riche et al, 2013). However, the dielectric anisotropy due to crystal orientation would have the opposite sign than the dielectric anisotropy due to a structural anisotropy.
Reference: Riche, Fabienne and Montagnat, Maurine and Schneebeli, Martin "Evolution of crystal orientation in snow during temperature gradient metamorphism" (2013) in Journal of Glaciology vol. 59 no 513.

EQ.7 in P.6069
Comment: "s" is not defined or explained here. In addition, what is physical meaning of this assumption? Please provide explanation to readers if possible.

Answer: Here, I refer already to (Sihvola, 2000) which provides this equation. "s" is a integration variable which can be substituted by a dimensionless quantity u = s/a_x^2 as mentioned later.

L.24 in P.6070
Comment: Meaning of "spatially anisotropic microstructure" is unclear to me. Does it mean that anisotropic microstructure is variable from one location to another? If so, please write so.

Answer: "spatially" has been removed. We mean only "anisotropic microstructure".

L.24 . 26 in P.6070
Comment: The authors wrote "The effective permittivity can be measured when snow is observed with a polarimetric radar system by analyzing the Copolar Phase Difference, CPD." It does not seem true to me. How can we detect the permittivity by microwave remote sensing?

Answer: This sentence has been corrected to " The difference of the vertical to the horizontal permittivity of snow can be measured when snow is observed with a~polarimetric radar system by analyzing the Copolar Phase Difference, CPD, when snow depth and density are known."

L.1 . 2 in P.6071
Comment: To be precise. I suggest the authors to express "measuring the vertical anisotropy of snow". Nadir-looking radar systems can still measure the horizontal anisotropy of snow if there are such structures.

Answer: Thanks for the suggestions. "vertical" has been added.

L.3 in P.6071
Comment: The authors mentioned "a requirement ".
It seems to me that another requirement is that microwave signals that were scattered at the distinct boundary with snow, such as soil, should be detected. The authors need to analyze CPD form such distinct target. Propagation "through" snow is an important experimental setting. In case of very cold glaciers or ice sheets without such clear "bottom" of snow, it seems that a method described here cannot be used. Please clarify such points to readers.

Answer: Thanks for pointing this out. Indeed, this is an important requirement.

L.6 . 9 in P.6071
Comment: The authors wrote here as "several GHz". However, in this paper, the authors used 10 - 17 GHz. These numbers seem more than "several".
Please inform readers of what will happen if we use higher frequencies, for example, 17 - 30 GHz?

Answer: I think, this is covered in the section "Generalization for scattering multilayer systems".

L.10 in P.6071
Comment: The authors wrote "The dielectric anisotropy can precisely be measured with the CPD". It does not seem true to me. It is CPD that can be measured precisely in a condition that there is a clear scattering object behind the snow as propagation path. Average of the dielectric anisotropy over propagation paths can be calculated only if observers can determine lengths of the propagation paths and density of snow. Even if the radar system is capable of detecting precise CPD, it does not necessarily mean that precise dielectric anisotropy can be detected.

Answer: I think this point has been adressed above where I mention, that ground is required below the snow pack.

Comment: In addition to this aspect, I did not see in this paper any discussion about effects from footprint. It seems that footprint width can give some averaging effects for the wave propagation of the side-looking radar.

Answer: Generally, radar systems have a very good range resolution of a few meters therefore, within one pixel, there is almost no variation in incidence angle. In our paper, we indeed averaged the CPD over the footprint of the antenna which covered an incidence angle range of about 5 - 12 degree (depending on frequency).
It has been added to the paper, that 1) the incidence angle with in the area of interest should be considered, and 2) (in the data processing section) that the CPD within the antenna footprint has been averaged. However, the effect of averaging is small as the CPD depends sufficiently linear on the incidence angle within the range of incidence angles of 5 - 8 degree.

L.5 . 6 in P.6072
Comment: The authors wrote "Hence, the H-polarization is delayed by the ordinary refractive index n0"
Meaning of this sentence is unclear to me. What does this delay mean? Delay as compared to propagation in air or delay as compared to the extraordinary wave?

Answer: The sentence has been rephrased to "Hence, the propagation velocity of the H-polarization is determined by the ordinary refractive index n_0".

Figure 2
Comment: This figure seems to show slightly tricky geometry. It seems untrue that paths of the VV wave and HH wave meet at the same point of the target of the snow/soil boundary.

Answer: This seems indeed a bit arbitrarily chosen. However, it is a strict requirement otherwise the copolar-coherence is lost. Only common scatterers within one range resolution cell of the radar contribute to the CPD. When the delay between the HH and VV polarization is larger than the range-resolution of the radar, this condition is not anymore fulfilled and the coherence is lost. This has been discussed in detail in a new section "Copolar phase difference of polarimetric radar systems".

L.1 in P.6076
Comment: The authors are using approximation that ice has no dielectric anisotropy. Please clarify it to readers.

Answer: We added a sentence: "We note here, that $\Delta \zeta$ vanishes only for isotropic ice which is not generally the case for ice on glaciers and ice sheets where the crystal axis of ice (c-axis) has a preferential orientation (e.g. \citealp{matsuoka97, fujita14})".

L.12 in P.6076
Comment: "Delta epsilon" should be minus (-0.05) if we exactly follow the definition of "Delta epsilon" in this paper (eps_x - eps_z).
gas observed in Fujita et al. (2014) h at a site in Greenland ice sheet. I suggest to add this.

Answer: Thanks for finding this typo. From this value, a negative CPD of -70° per meter would be expected. This has been corrected and "at a site in Greenland ice sheet" has been added.

L.16 . 17 in P.6076
Comment: "Similar anisotropy values have been observed in Alley (1987); Schneebeli and Sokratov (2004)."
It was not clear to me similar to what. I read these two papers but I could not identify what was really cited here. In addition, the authors should mention what kind of snow they are talking about. The former is the Antarctic firn. The latter seems to be artificial snow under temperature gradient. In contrast the authors' major topic in this paper seems seasonal snow. It seems that all these types of snow and firn are treated equally.

Answer: It has been added, that Antarctic firn was used by (Alley 1987) and natural and sieved seasonal snow by (Schneebeli 2004). "similar" refers to the range of the determined structural anisotropy. This has been clarified by citing numbers for A' as given in the two papers.

L.23 in P.6077
Comment: What does "SDvar" stand for? Snow Depth variability or something like that? An explanation will help readers.

Answer: The abreviation "SDvar" for Snow Depth variability course is now given.

L.17 in P.6078
Comment: "sectors can be found in (Leinss et al., 2015)."
This way of citation occurred at many points in this paper. I think that "sectors can be found in Leinss et al. (2015)" is correct. If so, please repair many such points in this paper.

Answer: I think, both styles are correct. On http://www.the-cryosphere.net/for_authors/manuscript_preparation.html it is written: In general, in-text citations can be displayed as "[…] Smith (2009) […]", or "[…] (Smith, 2009) […]".
To me "can be found in Leinss" sounds a bit like it can be found inside the body of Leinss. Of course, correct would be "can be found in the publication of Leinss (2015)" but I see "can be found in (Leinss, 2015)" as a shorter version of "in the publication of ~". Please correct me if I'm wrong here.

Section 3.2
Comment: A lot of abbreviations started to appear, such as SSI, SDTA1, SMT etc. It is hard to remember everything for readers. I suggest that a list for abbreviations is provided.

Answer: A table listing the abbreviations is now provided.

Section 3.3 First line
Comment: The authors wrote "Snow density was manually measured in the snow pit once every week." Was it measured over the entire thickness? If so, please inform readers of it already here.
In addition, in this paper, it is important to inform readers that manual measurement of density and independent measurement of the snow thickness is necessary to derive snow anisotropy from the CPD.

Answer: Both, the depth-average and the vertically resolved density were measured. However, for this paper, no vertical density profiles are required, therefore we wrote "The depth-averaged snow density was measured manually..."
Your second point is already adressed in comments above.

L.3 in P.6079

Comment: Please let readers know what SWE means when it is used first in this paper.

Answer: "snow water equivalent" was added.

L.5 in P.6079
Comment: What is GWI? Please explain to readers briefly. Is there any good citation for this instrument? What is the measurement principle?

Answer: It has been added that SWE was determined "from measurements of gamma ray absorption within the snowpack using the Gamma Water Instrument".
The measurement principle is described in the given reference about SWE determination (Leinss, 2015). Unfortunately, there is no reference for the GWI.

L.9 in P.6079
Comment: "where" -> "were" ?

Answer: corrected.

L.10 . 12, in P.6083
Comment: The authors wrote "For three dates anisotropy measurements are compared with anisotropy data from computer tomography." It should be clarified for which three dates. It took time for me to understand. Perhaps it should be as follows.
For the three dates when the muCT measurements were done, anisotropy measurements are compared with anisotropy data from computer tomography.

Answer: This has been clarified by writing: "The anisotropy obtained from the computer tomography analysis of the four profiles CT-1 to CT-4 were compared with the anisotropy obtained from the CPD for the four corresponding dates when the samples were taken in the field". Note, that we added a forth anisotropy profile.

L.19 . 20, in P.6083
Comment: The authors wrote "The snow density was determined by dividing SWE, as determined in (Leinss et al., 2015), by the snow depth measured by the sensor SDAT1."
Readers will not understand this sentence unless they know physical meaning of SWE.

Answer: The definition of SWE = average snow density x Snow depth is given to provide the reader the physical meaning of SWE.

L.24, in P.6084
Comment: "Lemmetyinen et al. (2013, p. 399(49))" Is this paper publicly available and accessible? If it is not to access for readers, perhaps the authors provide the data in the appendix or as the supplementary information.

Answer: The NOSREX report (Lemmetyinen et al, 2013) is available on the ESA datahub for campaign data. The URL is provided now in the references.

L.29, in P.6084
Comment: The authors wrote "melt-refreeze events caused the formation of a crust at the bottom of the snow pack". It seems crust should appear at the surface of the snow pack. Like me, the other readers may not imagine a crust at the bottom of the snow pack.

Answer: Of course, the crust appeared first at the top of a very shallow early winter snow pack but was then covered by snow therefore, the crust is situated at the bottom of the snow pack. The sentence has been rephrased to: "Due to warm temperatures, depth hoar was largely absent and melt-refreeze events in early December caused the formation of a~crust in the shallow snow pack which was later covered by snow."

L.25, in P.6085
Comment: Again I suggest that "recrystallization" should be replaced by "metamorphism".

Answer: done.

L.12, in P.6086
Comment: Citation of Bormann et al. paper is a bit confusing. It is not very clear if the citation is for the density range or the density dependency of the CPD. Please clarify.

Answer: This paragraph has been rephrased:
"The average anisotropy of the snow pack can be estimated, because the CPD shows only a~weak density dependence for the density range of seasonal snow. For seasonal snow, densities of 0.15 and 0.4\,\unit{g\,\unit{cm^{-3}}} have been reported \citep{bormann13}. Within this range, the

L.14, in P.6086
Comment: There seems no "Figure 3a". It is Figure 3 (right).

Answer: yes. This has been corrected.

Section 4.2
Comment: So far when I read this paper, I had an impression that the dielectric anisotropy could be calculated purely by remote sensing (contactless, destruction free, according to the authors). However, I noticed that an important point of the method in that the data of the ice thickness and the snow density should be observed independently.

Answer: This has been clarified in several points; also here it has been added that the CPD "can be inverted with the additional information of snow depth and a good approximation of snow density to get a CPD based estimate for teh depth-average anisotropy."

Comment: Also, it seems unclear that observations using multiple angles of theta and multiple frequencies are necessary for data processing. I think that such information should be provided in the abstract and the conclusion. Otherwise, until readers reach this section 4.2, readers will think that the dielectric anisotropy of snow may be observed by a method of microwave remote sensing alone. In reality, ground observations for density and snow thickness are necessary. In addition, it seems that the readers should know what will happen if the remote sensing data with only single theta value and single frequency is available.

Answer: Only snow density and snow depth are reqired. Different frequencies provided redundant estimates for the ansisotropy. Different incidence angles could in principle be used to eliminate either snow depth or density due to the nonlinear dependence in incidence angle. However, I think the nonlinearity is too small to be used.
The anisotropy was determined independently for all different incidence angles and the results for different incidence angles were compared. This requires the assumption that the snow properties do not vary spatially for different antenna footprints. The careful preparation of the test site and the snow depth variability measurements support this statement.

Comment: The authors showed that the standard deviation of the anisotropy of snow is very small. But this small standard deviation can be attained based on multiple settings of \theta values and frequencies. Is it so?

Answer: I'm not sure, if I understand your comment correctly. The standard deviation is the standard deviation based on multiple settings of theta and frequencies. I rephrased the sentence to:
"The standard deviation for each time is given by the scatter of the individual estimates $A(\theta_0, f)$ for each θ_0, and f." I hope this clarifies / answers your question.

L.24 . 25, in P.6087
Comment: I did not understand meaning of an expression "wavelengths "fit" into the snow volume".

Answer: I hope, "wavelengths ``fit'' into the propagation path through the snow volume" is more clear.

L.16, in P.6089
Comment: Please specify +4% and -8% relative to what.

Answer: Relative to the anisotropy measured by computer tomography. This has been corrected.

L.1 . 2, in P.6090
Comment: "as it is expect for snow recrystallized by temperature gradient metamorphism"
I suggest as follows.
"as it is expected for snow geometry modified by temperature gradient metamorphism h
Here, I consider definition of recrystallization in metallurgy or ice crystal. If the authors feel that this term can be still used for sublimation and condensation, please explain basis for it.

Answer: As in other cases, also here the term "recrystallized" has been replaced by "metamorphic" and the sentence has been rephrased to: "as it is expected for the geometry of metamorphic snow which was exposed to temperature gradients"

L.12 . 14, in P.6090
Comment: "Further, the CPD decreases during periods of cold temperatures due to temperature gradient metamorphism." To clarify more, I suggest to modify "due to growth of the vertical

Answer: Thanks for the suggestion. It has been clarified as suggested.

Equation 26
Comment: Please provide readers what "SD" means. I think it is snow depth.

Answer: SD = snow depth has been added.

In the equation 26 and Figure 18
Based on my poor understanding, I did not understand what "tau" meant and how I should see Figure 18 right top and right bottom. Please better explain meaning of these to me and to readers.

Answer: The parameter "tau" is the temporal offset between the time series snow depth, SD(t), and the time series CPD(t). This is now explained more in detail.

L.11, in P.6091
Comment: fresh "snow"?

Answer: thanks, "snow" was missing here.

L.12 . 14, in P.6093
Comment: The authors wrote as "The propagation delay difference of orthogonally polarized microwaves was measured by the CPD which was then used to determine the structural anisotropy of snow."
I suggest to clarify that the method is for snow with known thickness to derive average anisotropy over the thickness. For example, geometry of the optics is clearer if it is written as follows.
"The propagation delay difference of orthogonally polarized microwaves through known thickness of snow was measured by the CPD which was then used to determine the structural anisotropy of snow averaged over the snow thickness."

Answer: This suggestion has thankfully been included together with the comment below: This sentence reads now: "The propagation delay difference of orthogonally polarized microwaves through known thickness of snow was measured by the CPD which was used to estimate the dielectric anisotropy of snow to determine then the structural anisotropy of snow averaged over the snow thickness."

L.16 . 19, in P.6093
Comment: I would suggest that the authors explicitly tells to readers that the CPD values were converted to the dielectric anisotropy of snow using the snow thickness that were determined independently. Otherwise, many readers may misunderstand that the CPD alone can determine the pricese snow anisotropy.

Answer: see answer above.

Comment:
The authors wrote that the standard deviation of 0.005 as small numbers. However, this evaluation is a result of measurements using multiple theta and multiple frequencies. In addition, snow thickness and the density should be known independently. These experimental settings should be mentioned.

Answer: I see your point. I added: "The standard deviation is based on measurements of different incidence angles and frequencies and confirms the provided theory though does not represent systematic errors due to uncertainties in snow depth and density."

L.19 . 20, in P.6093
Comment: The authors wrote, "Copolar phase differences ranging from -30 to +135°C were measured for 50-60 cm deep snow at a frequency of 13.5 GHz."
Readers may wonder why these numbers are specifically given here. Are these numbers symbolic for the present study? In addition, actual snow depth ranged up to ~100 cm. Readers will wonder why 50 - 60 cm deep snow was highlighted.

Answer: "The large variation of CPD values shows that the anisotropy of snow must be considered when the CPD is analyzed in polarimetric studies of snow covered regions." (this sentence has been added.)

L.22 . 24, in P.6093
Comment: The authors wrote, "Only small deviations of 5 - 10 degree"
Readers will not understand whether this angle is for incidence angle or the CPD. In case this is the CPD, readers feel hard to understand how deviations of 5 - 10 dgree mean as a size of uncertainty.

Answer: It has been clarified that here I mean the deviations of the CPD from the modeled data. Further, the 5-10 degree have been put into relation with the range between -30 and +135 degree in order to provide an idea about the relative accurary.

L.25, in P.6093
Comment: I hope to find one of keywords "dielectric anisotropy" somewhere in this line, to tell basic principle of the birefringence.

Answer: the keywords "dielectric anisotropy" have been added: "The linear frequency dependence verifies our assumption that the CPD is a~volumetric property of snow which is determined by the dielectric anisotropy and is which is related to the structural anisotropy of the ice matrix and pore spaces of snow." In the second sentence of the conclusion, the keyword "birefringence" has been added.

L.6 . 10, in P.6094
Comment: "A weak correlation was found and an optimal acquisition interval of 8.15 days was determined to detect the depth of fresh snow . It was observed that the evolution of the CPD shows a delay of about 2.3 days compared to the evolution of snow depth, which indicates an average settling time of a few days."
Due to my poor understanding, I did not understand the relation between tau and the optimal acquisition interval in this paper.

Answer: As answered on your comment further above, I hope that this has been clarified now. The parameter tau has been described more detailed there.

Around L.18 in P.6094
Comment: The authors wrote "The possibility to observe the anisotropy of the snow pack by remote sensing techniques". This technique require independent determination of the snow thickness and the snow density. Readers should know how this requirement can be satisfied in the practical remote sensing. A short paragraph to discuss this point will help. Otherwise, some readers may think there is no such requirement.

Answer: A short paragraph providing some information about independent determination of snow depth and snow density using remote sensing data has been added.

L.20 . 23, in P.6094
Comment: I did not understand at all what kind of principle was meant here.

Answer: The paragraph has been rephrased.

L.14, in P.6095
Comment: "Dielectric anisotropy" should be explicitly stated here, because it was exactly used in experimental principle used in this paper.

Answer: "especially the dielectric anisotropy" has been added.

Technical corrections
Comment: L.19 in P.6064
(Li et al., 2008) should be Li et al. (2008).
Answer: corrected.

Anonymous Referee #2

General comments: This paper describes the measurement of CPD and its relationship to snow's anisotropy and SWE/density. Multiple seasons of snow measurements were conducted and the measured data were compared to the model described in the paper. The measured anisotropy of snow showed a good agreement with the results obtained from the micro-CT scan of the snow pack.

General comments:

Comment: What is the transmit power used?

Answer: The transmit power is approximately 10 mW. However, the SnowScat Instrument is a "Stepped Frequency Contineous Wave" Radar, therefore a good SNR is achieved by an integration time of about 5 ms for each frequency. The transmit power is not relevant for the content of the paper. To give a reference for technical data, a reference where this specification (10 mW) can be found was added in section 3.1 (Micrwave measurements). (See p. 9 in "SnowScat, X- to Ku-Band Scatterometer Development: D13 SnowScat User Manual" ESTEC/AO1-5311/06/NL/EL) This paper is available on request via ESA or from Gamma Remote Sensing.

Comment: What is the effect of surface roughness and features on the measured CPD? How is the effect being isolated from the anisotropic of snow?

Answer: The effect of a rough snow surface and also of rough layer boundaries within the snow pack is now more clearly discussed in the section "Generalization for scattering multilayer systems". An additional section discusses the effect of a rough underlying ground surface in "Contribution of a rough ground surface".

In the present work, scattering contributions from the snow surface and layers within the snow pack are shown to be small, as the snow water equivalent could be precisely determined using differential interferometry as shown in the paper "Snow Water Equivalent of Dry Snow Measured by Differential Interferometry" by Leinss et al in IEEE Journal of Selected Topics in Applied Earth Observations and Remote Sensing (2015), vol. 8 no 8.
The reference and argumentation has been added to the section "Microwave Measurements".

The effect of the underlying ground has already been discussed in section 4.7 "Effect of Underlying Ground". The time series data (Fig. 7 - 10) show, that during dry snow conditions, the CPD is very close to zero.

Specific comments:

Comment: p. 6071; line 1-3: Nadir-looking radars can also measure 2D anisotropy if there is a difference in crystal orientation along the xy-plane.

Answer: Of course, this is correct. But we do not see any reason which could cause any anisotropy in the xy-plane in a snow pack situated in flat terrain. As mentioned in the last paragraph of the section "Definition of structural anisotropy" "We restrict
our model to flat terrain and do not consider shear stress or temperature gradients not parallel to gravity, which can both occur on steep terrain."

Comment: p. 6071; line 6: It appears the statement is a bit contradicting as the anisotropy is caused by the particle scattering

Answer: I disagree. In the present paper, snow is considered as an effective medium (see 1st paragraph of section "Relative permittivity as a function of anisotropic inclusions") which is transparent but which has a dielectric anisotropy. The dielectric anisotropy is caused by a different polarizability of the anisotropic ice grains and not by scattering effects.

Comment: p. 6080, line 10: Is it possible to show a raw radargram of the quad-pol data as well as the SLC radargram with reference to the geometry depicted in Figure 5? It is interesting to see the spatial variability of the raw radar signal.

Answer: Here I refere to Figure 3 in the paper "Snow Water Equivalent of Dry Snow Measured by Differential Interferometry" by Leinss et al in IEEE Journal of Selected Topics in Applied Earth Observations and Remote Sensing (2015), vol. 8 no 8. The figure shows a time-averaged "radargramm" with respect to the imaging geometry as shown in Fig. 5 our paper. Please note, that the SnowScat system is a side-looking radar therefore each range cell contains the integrated backscatter signal of the snow surface, snow volume and the underlying ground.
I like to refer also to the conference paper "Snow Structure Evolution Measured by Ground Based Polarimetric Phase Differences" by
S. Leinss; J. Lemmetyinen; A. Wiesmann; I. Hajnsek, (2014); in Proceedings of 10th European Conference on Synthetic Aperture Radar (EUSAR). In this proceeding paper, time-resolved radargrams are shown which indicate that the microwaves completely penetrate the snow volume as long as the snow is dry. In this paper, the delay difference between dry snow and wet snow at

Comment: p.6086, line 21: Can the authors show a comparison between CPD_meas and CPD_model before optimization and after optimization, and the corresponding number of iterations and change in fitting parameters? Is the data in Figure 14 before or after optimization?

Answer: Equation (19) contains only one free parameters, the Anisotropy A. As written in section 4.2 "Estimation of the average anisotropy of snow", all other parameters (wavelength or frequency, snow depth, incidence angle, density) are known. The minimization of Eq. (24) is done by simply testing about 2000 anisotropy values between -1 and 1. The anisotropy value which minimizes Eq. (24) is defined as A(theta, f) and depends on incidence angle and frequency. To avoid confusion with iterative optimization algorithms, the term "iterative" has been removed from the caption of Fig. 11 and replaced by "minimization with respect to A".
Figure 14 shows the standard deviation and mean difference between measured and modeled CPD values. The modeled CPD values are based on the average of the anisotropy values obtained by minimization. The standard deviation of the anisotropy A(\theta,f) is snown in Fig. 12.

Manuscript prepared for J. Name
with version 2015/04/24 7.83 Copernicus papers of the LaTeX class copernicus.cls.
Date: 9 May 2016

Anisotropy of seasonal snow measured by polarimetric phase differences in radar time series

S. Leinss[1], H. Löwe[2], M. Proksch[2], J. Lemmetyinen[3], A. Wiesmann[4], and I. Hajnsek[1,5]

[1]Institute of Environmental Engineering, Swiss Federal Institute of Technology (ETH), Zürich, Switzerland
[2]Institute for Snow and Avalanche Research SLF, Davos, Switzerland
[3]Finnish Meteorological Institute FMI, Arctic Research, Sodankylä, Finland
[4]GAMMA Remote Sensing AG, Gümlingen, Switzerland
[5]Microwaves and Radar Institute, German Aerospace Center (DLR), Wessling, Germany

Correspondence to: S. Leinss (leinss@ifu.baug.ethz.ch)

Abstract. ~~Snow settles under the force of gravity and recrystallizes by vertical temperature gradients . Both effects are assumed to form oriented ice crystals which induce an anisotropy in~~ The snow microstructure, i.e. the spatial distribution of ice and pores generally shows an anisotropy which is driven by gravity and temperature gradients and commonly determined from stereology or computer tomography. The structural anisotropy induces anisotropic mechanical, thermal, and dielectric properties~~of the snow pack. On microscopic scales, the anisotropy could be hitherto determined only from stereology or computer tomography of samples taken from snow pits. In this paper we present an alternative method and show how the anisotropy of a natural snow pack can be observed contact- and destruction-free with polarimetric radar measurements. The copolar phase differences~~ . We present a method based on radio wave birefringence to determine the depth-averaged, dielectric anisotropy of seasonal snow with radar instruments from space, air or ground. When snow depth and density are known, the birefringence allows determination of the dielectric anisotropy by measuring the copolar phase difference (CPD) ~~of polarized microwaves transmitted through dry snow were analyzed for four winter seasons (2009–2013) from the SnowScat Instrument, installed at a test site near the town of Sodankylä, Finnland. An electrodynamic model was established based on anisotropic optics and on~~ between linearly polarized microwaves propagating obliquely through the snow pack. The dielectric and structural anisotropy are linked by Maxwell–Garnett-type mixing formulas~~to provide a link between the structural anisotropy and the measured CPD. The anisotropy values derived from the CPD were compared with~~ . The anisotropy evolution of a natural snow pack in Finland was observed over four winters (2009–2013) using the ground-based radar instrument "SnowScat". The evolution indicates horizontal structures for fresh snow and vertical structures in old snow which is confirmed by computer tomographic in-situ ~~anisotropy measurements obtained by computer tomography. In addition, we show that the CPD measurements obtained from SnowScat show the same temporal evolution as~~ measurements. The ground based CPD measurements were compared with space-borne ~~CPD~~ measurements from the satellite TerraSAR-X ~~.~~ which showed the same temporal evolution. The presented dataset provides a valuable basis for the ~~future development of snow models capable of including the anisotropic structure of snow~~development of new snow models which include the anisotropy of the snow microstructure.

1 Introduction

~~Deposited snow is~~

After deposition on the ground, snow crystals form a porous~~and highly metamorphic material~~ , sintered material which continuously undergoes ~~recrystallization processes~~ metamorphism to adapt to the ~~external thermodynamic forcing determined~~ thermodynamic forcing imposed by the atmosphere and the ~~underlying~~ soil. The ~~microstructure of the sintered snow crystals constitutes~~ porous microstructure, defined by the 3D distribution of the ice matrix and the pores space, determines the thermal, mechanical and ~~electromagnetic properties of snow~~dielectric properties of the snow pack. Hence, ~~an anisotropic~~ a spatially anisotropic

distribution of the microstructure leads to a macroscopic anisotropy of snow properties.

Characterization of the microstructure is difficult and requires work intensive sampling~~which can disturb the natural snow structure irreversibly by snow pits, sieving, sample-taking or cutting of samples.~~ , sample preparation, and data processing but enables a unique insight into the structure at micrometer scales. Macroscopic (point) methods commonly applied in the field can be used to determine snow properties averaged over sample volumes of several centimeters. Methods based on remote sensing complement these point methods in providing large spatial coverage of repetitive measurements with a sampling resolution between meters and kilometers also for inaccessible locations. For snow, radar remote sensing methods measurement of snow properties averaged over the microwave penetration depth. This makes it possible to estimate the depth-averaged dielectric anisotropy of seasonal snow with radar instruments.

~~Before the introduction of micro computer-tomography (μCT) , microscopic data about the snow structure was rare. The only method providing microscopic information was stereology, which is based on cutting snow into thin sections. Nevertheless, vertical~~

1.1 Observations and cause of the structural anisotropy of the snow

Anisotropic structures have been identified in ~~thin sections of polar snow (Alley, 1987).Furthermore,~~ photographs of thin section cuts of seasonal snow with preferentially horizontal structures for fresh snow and vertical structures in old snow (Kojima, 1960; Davis and Dozier, 1989; Mätzler, 1987, Fig. 2.15[1]). Vertical structures have been reported also in thin sections cuts of polar firn (e.g. Alley, 1987). The formation of anisotropic, vertical snow structures has been observed by thin section photography, when snow ~~recrystallization~~ metamorphism was driven by a vertical water vapor flux ~~(Pfeffer and Mrugala, 2002).Vertical structures have also been found in conjunction with anisotropic thermal conductivities (Izumi and Huzioka, 1975). Also horizontal structures have been identified using stereology in fresh snow (Davis and Dozier, 1989), (Mätzler, 1987, Fig. 2.15, left[2]).~~under temperature gradients (e.g. Pfeffer and Mrugala, 2002).

The anisotropy of snow can ~~statistically be~~ be statistically determined from the ~~heterogeneous snow matrix~~ snow microstructure by spatial correlation functions (Vallese and Kong, 1981; Mätzler, 1997) ~~of~~ computed from stereological (Alley, 1987; Mätzler, 2002) or computer tomography data ~~(Löwe et al., 2011, 2013)~~(Löwe et al., 2011, 2013). Today, computer tomography is often considered as the "state of the art" for destruction-free ~~observation~~ observations of the snow microstructure within volumes of a ~~few~~ cm^3 and with a spatial resolution ~~of a few micrometers. Even a temporal resolution is possible for snow samples which are~~ on the micrometer-scale. The non-destructive CT measurements allow imaging of the same sample multiple times to observe the temporal evolution of the microstructure for samples kept under laboratory conditions (Schneebeli and Sokratov, 2004). ~~Laboratory experiments~~

Laboratory experiments using computer tomography revealed the characteristics of grain growth and sintering during isothermal metamorphism (Kaempfer and Schneebeli, 2007) ~~as well as during~~ or alternating temperature gradients ~~which occur on daily cycles (Pinzer and Schneebeli, 2009). Anisotropic structures have been identified and the recrystallization process was observed where initially horizontally oriented ice grains recrystallized to vertical structures during exposure to a vertical temperature gradient~~ (Pinzer and Schneebeli, 2009). The formation of vertical structures from initially horizontal structures has been observed in laboratory samples if vertical temperature gradients are applied (Schneebeli and Sokratov, 2004; Riche et al., 2013; Calonne et al., 2014). Vertical ~~structures have also~~ and horizontal structures have been found in artificial snow from the cold-laboratory but also in natural seasonal snow (Calonne et al., 2012). Vertical structures have also been found in samples of polar firn ~~(Hörhold et al., 2009; Lomonaco et al., 2011) and vertical and~~ (Hörhold et al., 2009; Fujita et al., 2009; Lomonaco et al., 2011; Fuj

In contrast to vertical structures which are known to be caused by vertical temperature gradients, horizontal structures have ~~been found in seasonal snow (Calonne et al., 2012). The originof horizontally aligned structures has been discussed with respect to settling of fresh snow (Schleef and Löwe, 2013). Settling is also assumed to be the reason for horizontal anisotropies which were found~~ a different origin. A predomininant horizontal orientation is initially created by the deposition of anisotropic, atmospheric growth forms (plates, needles, dendrites) which predominantly align horizontally in the gravity field Matrosov et al. (2005); Garrett et al. (2012). Snow settling can further contribute to horizontal anisotropies in the intermediate stage of isothermal metamorphism ~~, since for isothermal conditions~~ (Löwe et al., 2011), where only gravity breaks the symmetry between vertical and horizontal directions~~(Löwe et al., 2011)~~.

1.2 Field observations of the dielectric anisotropy

On macroscopic scales, the anisotropy of snow can be ~~determined~~ characterized by measuring the anisotropy of the thermal conductivity (e.g. Izumi and Huzioka, 1975) or of the dielectric permittivity. ~~Despite the fact that the dielectric anisotropy is much smaller than~~ Due to the contrast in thermal conductivity between ice and air, the anisotropy of the thermal conductivity is much

stronger compared to the anisotropy of the ~~thermal conductivity (Löwe et al., 2013)~~dielectric permittivity, which is determined by the contrast in permittivity between ice and air, $\varepsilon_{ice}/\varepsilon_{air} \approx 3$ (Löwe et al., 2013). Still, dielectric measurements have been discussed already in 1965 with respect to the shape and orientation of ice crystals (e.g. Evan, 1965).

The dielectric anisotropy of snow, $\Delta\varepsilon$, in the following defined as the difference between the horizontal and vertical permittivities, $\Delta\varepsilon = \varepsilon_x - \varepsilon_z$, ~~the dielectric anisotropy~~ can be measured ~~with~~ precisely using different polarizations of the electromagnetic field~~in microwave resonators filled with snow (Jones, 1976). Using~~. The dielectric anisotropy due to the c-axis orientation of the crystal fabric of ice (Matsuoka et al., 1996, 1997) has been measured with open microwave resonators ~~, different permittivities~~ of the design of e.g. Saito and Kurokawa (1956); Jones (1976). With the same method, the dielectric anisotropy due to a structural anisotropy has been measured and higher permittivities have been found in the vertical ~~and horizontal direction have been found~~ direction compared to the horizontal direction in multi-year firn on both, the Greenland ice sheet (Fujita et al., 2014) ~~. Anisotropy measurements with microwave resonators were also~~ and on the Antarctic ice sheet (Fujita et al., 2009). Using a method of microwave propagation, Lytle and Jezek (1994) also detected a larger vertical permittivity in multi-year firn on the Greenland ice sheet and Sugiyama et al. (2010) found similar results in Antarctica. Some of these anisotropy measurements were performed in conjunction with photographic (Lytle and Jezek, 1994) and computer tomographic analysis (Fujita et al., 2009) ~~. It is even possible to determine the anisotropy of seasonal snow with radar satellites, when~~ which both showed vertical structures in the snow microstructure.

1.3 Dielectric anisotropy observed by microwave remote sensing

The observation of structural anisotropy in seasonal snow together with the observations of a dielectric anisotropy in polar firn indicate that also seasonal snow is a dielectrically anisotropic medium that has an axis of symmetry in the vertical. Such dielectric anisotropy can be detected by microwave remote sensing methods using the principle of radio wave birefringence for the propagation of electromagnetic waves. The radio wave birefringence has been used to explore internal structures of ice sheets and glaciers with radio waves (e.g., Hargreaves, 1977, 1978; Fujita et al., 2006 and Matsuoka et al., 2009). The birefringence of seasonal snow was observed in radar satellite data by Leinss et al. (2014b); they determined the dielectric anisotropy by analyzing the propagation differences of differently polarized microwaves ~~are analyzed (?).~~ propagating obliquely through the snow pack. Also with passive microwave sensors, strong polarimetric signatures have been found over the Greenland ice sheet: in ~~(Li et al., 2008), the found~~ Li et al. (2008), the observed passive microwave signatures could not be explained by surface features, but were discussed with respect to microstructural variations of the anisotropy of snow, as predicted by Tsang (1991).

Polarimetric radar remote sensing methods ~~provide a contactless tool to measure the~~ can provide information of the dielectric anisotropy of snow ~~destruction-free, and~~ from large distances. Areas of many thousands of ~~km^2~~ square-kilometers can be observed with air- and space-borne sensors~~. They provide a~~, even repeatedly by satellites during every repeat-pass of an orbit. Remote sensing methods provide therefore a complementary tool to ~~computer tomography as large areas and volumes of natural snow can be observed.~~ the detailed ground measurements such as computer tomography or in-situ measurements. However, with radar remote sensing methods, area-, depth- or volume-averaged snow properties are measured.

Still, publications related to polarimetric propagation effects in deposited seasonal snow are rare, despite the fact that a differential propagation speed in falling snow was already noticed in 1976 for weather radars (Hendry et al., 1976). ~~Currently, polarimetric radars are only~~ Today, polarimetric upwards looking radars are used to characterize the orientation and anisotropy of falling snow ~~or rain (Garrett et al., 2012; Xie et al., 2012; Hogan et al., 2012; Noel and Chep in 1992, microwave experiments in Greenland revealed a directional propagation speed in firn (Lytle and Jezek, 1994), caused by a vertical anisotropy. In 1996, the opposite effect was observed, when the phase~~ particles or rain (e.g. Matrosov et al., 2005; Garrett et al., 2012; Xie et al., 2012; Hogan et al.,

In contrast to the observations for firn on ice sheets, where the vertical permittivity ε_z was found to be larger than the horizontal permittivity ε_x, a larger horizontal permittivity was found in freshly deposited snow using ground-based radar measurements: Chang et al. (1996) measured the propagation difference between vertically (VV) and horizontally (HH) polarized microwaves ~~,~~ by measuring the so called Copolar Phase Difference, CPD, ~~measured by a ground-based radar~~ and found that the CPD increased after snow fall. The increase of the CPD was explained by a horizontal anisotropy of the microstructure of deposited fresh snow~~(Chang et al., 1996). Both effects were observed in satellite time series of~~ . In polarimetric radar measurements of the satellite TerraSAR-X ~~, where a significant~~ (Stangl et al., 2006; Werninghaus and Buckreuss, 2010), both, vertical and horizontal anisotropies were observed at different times by Leinss et al. (2014b): a positive correlation between the CPD and the depth of fresh snow was found, ~~but also~~ indicating horizontal structures in fresh snow with $\varepsilon_x > \varepsilon_z$. They also observed the opposite effect~~was~~

observed, where a strong temperature gradient in the snow pack forced the CPD towards negative values (?)($\varepsilon_x < \varepsilon_z$).

The CPD is a very sensitive observable to measure dielectric anisotropies because relative signal delays much smaller than the ratio between the radar wavelength and the snow depth can be measured. This interferometric approach makes it possible to determine dielectric anisotropies with a precision down to $\Delta\epsilon \approx 10^{-4}$.

1.4 Paper structure

In this paper, we present and apply an electromagnetic model to determine the mean depth-averaged structural anisotropy of a dry snow pack via the dielectric anisotropy derived from the CPD measured by with polarimetric radar systems. The model consistently builds on the description of the microstructure of snowpaper is structured as follows:

- Sect. 2 revisits the Maxwell-Garnett mixing formulas to model the anisotropic dielectric permittivity from the structural anisotropy of snow. A link to the characterization of the microstructure in terms of spatial correlation functions . The model is applied on CPD measurements acquired with the SnowScat Instrument (Wiesmann et al., 2008; Werner et al., 2010) is established.
- Sect. 3 derives the CPD measured by polarimetric radar systems for a anisotropic dielectric medium of known thickness and negligible losses by scattering and absorption.
- Sect. 4 describes the experiment and the field data collected within four winter seasons from 2009 to 2013. The CPD time series Four years of CPD measurements are discussed with respect to in view marker events of snow fall, snow metamorphism and melting. For three
- Sect. 5 analyzes the CPD time series in order to determine the evolution of the depth-averaged anisotropy of the snow pack. For four selected dates, we compare the derived anisotropy with the anisotropy determined is compared with measurements obtained by computer-tomography. Furthermore, we compare the measured CPD time series of two winter seasons with space-borne observations from radar observations from the satellite TerraSAR-Xand TanDEM-X and discuss the question, of . Then we discuss whether the CPD can be used to determine the depth of fresh snow.
- Sect. 6 concludes the paper.

2 Electromagnetic model for measuring Dielectric permittivity as a function of the structural anisotropywith polarimetric radar systems

The ice matrix of snow can have two different anisotropies which both can influence the anisotropy of the dielectric permittivity. The structural anisotropy, discussed in this section, is given by an anisotropic spatial distribution of the ice matrix i.e. the shape of ice crystals. The fabric anisotropy, discussed in appendix A, is given by the crystal axis orientation of ice crystals but its effect on the permittivity of seasonal snow is small compared to the effect of the structural anisotropy.

In this section we an adapted version of the Maxwell-Garnett mixing formulas is presented to provide a relation between the structural anisotropy of snow, snow density and the effective dielectric permittivity ε_{eff}, and the Copolar Phase Difference (CPD) measured by a polarimetric, side-looking radar system. .

2.1 Definition of structural anisotropy

In the following we define the coordinate axes such that z is the vertical (parallel to gravity) and the x and y plane is parallel to the flat earth surface. We restrict our model to flat terrain and do not consider shear stress or temperature gradients not parallel to gravity, which can both occur on steep terrain.

2.1 Definition of structural anisotropy

We define the structural anisotropy, A, as the normalized difference between the characteristic horizontal dimension, a_x, and the characteristic vertical dimension, a_z, of the "grains" in the ice matrix:

$$A = \frac{a_x - a_z}{\frac{1}{2}(a_x + a_z)} \tag{1}$$

Different choices for the length scales a_x and a_z are possible (Löwe et al., 2011). Recent work for microwave modeling has mainly used the (exponential) correlation lengths, $a_x = p_{\text{ex},x}$ and $a_z = p_{\text{ex},z}$, as defined in Mätzler (2002)and derived from . The exponential correlation lengths are conveniently derived by an exponential fit to spatial correlation functions (Löwe et al., 2011).

If the anisotropy is defined as in Eq. (1), the magnitude of A $|A|$ for grains with given ratio between longest and shortest length is independent of whether the longest length is vertically or horizontally oriented. This is different for an alternative definition A' where the anisotropy is defined as the vertical-to-horizontal size ratio of ice grains. The difference of the two definitions with respect to the isotropic case ($A = 0$ and $A' = 1$) becomes clear when comparing e.g. ($a_x = 2, a_z = 1$) with ($a_x = 1, a_z = 2$). The definition A' is commonly used to simplify electromagnetic modeling. The anisotropy A' can be converted to Eq. (1) by

$$A' = \frac{a_z}{a_x} = \frac{2 - A}{2 + A} \quad \text{or} \quad A = \frac{1 - A'}{\frac{1}{2}[1 + A']}. \tag{2}$$

We note that the anisotropy A' differs from the definition in terms of the "degree of anisotropy" (DA) which is used in (Hildebrand et al., 1999; Schneebeli and Sokratov, 2004). For the DA, the absolute orientation in space is lost since the definition is based on the ratio of the largest and smallest eigenvalues of the mean intersection length (MIL) tensor. The anisotropy A' (defined as ϵ in Torquato and Lado, 1991 or $\mathcal{A}(l_c)$ in Calonne et al., 2014) can be further related to the anisotropy-parameter Q used in Calonne et al. (2014) by the definition in Löwe et al. (2013, Eq. 4).

~~In the following we define the coordinate axes such that z is parallel to the normal vector of the earth surface and the x and y plane is parallel to the flat earth surface. We restrict our model to flat terrain and do not consider shear stress or temperature gradients not parallel to gravity, which can both occur on steep terrain.~~

2.2 Relative permittivity as a function of anisotropic inclusions: Maxwell-Garnett formulas

The CPD measured by polarimetric radar systems depends on the difference of the dielectric permittivity ε_{eff} measured in the x and z direction. The aim of this subsection is to establish a link between the effective permittivity $\varepsilon_{\text{eff},i}$ for $i \in \{x, y, z\}$ and the structural anisotropy A.

The following model is based on an empirical extension of the classical Maxwell–Garnett mixing formulas for aligned mixtures of ice inclusions in a host medium of air (e.g. Polder and van Santen, 1946; Sihvola, 2000). To motivate the necessity of the empirical extension we briefly revisit the application of Maxwell–Garnett mixing formulas in the isotropic case. For isotropic snow ($A = 0$) the permittivity $\varepsilon_{\text{eff},i}$ should agree with measurements of ε for isotropic snow. However, the relative permittivity, $\varepsilon_{\text{eff, MG}}$, calculated with the Maxwell–Garnett formula underestimates the measured permittivity (Mätzler, 1996) which is slightly higher. It was found that $\varepsilon_{\text{eff, MG}}$ is equivalent with the lower Hashin–Shtrikman bound (Sihvola, 2002; Hashin and Shtrikman, 1962). The upper Hashin–Shtrikman bound is equivalent with the "inverse" Maxwell–Garnett formula, $\varepsilon_{\text{eff, MG, inv}}$, which models air inclusions in a host medium of ice (Sihvola, 2002). Therefore it is preferable to combine both bounds in a reasonable way to determine ε_{eff}. We found that the following weighted average~~agrees with (Wiesmann and Mätzler, 1999, Eqs. 45 and 46)[3] within less than $\pm 0.7\,\%$~~

~~$$\varepsilon_{\text{eff}} = (\varepsilon_{\text{eff, MG}} + \varepsilon_{\text{eff, MG, inv}} \cdot f_{\text{vol}}\varepsilon_{\text{ice}})\,/(1 + f_{\text{vol}}\varepsilon_{\text{ice}}).$$~~

$$\varepsilon_{\text{eff}} = (\varepsilon_{\text{eff, MG}} + \varepsilon_{\text{eff, MG, inv}} \cdot f_{\text{vol}}\varepsilon_{\text{ice}})\,/(1 + f_{\text{vol}}\varepsilon_{\text{ice}}), \tag{3}$$

[3] ~~Eq. (46) in Wiesmann and Mätzler (1999) has been adapted to produce correct results for pure ice ($\nu = 1$). The adapted factors are $\varepsilon_h = 1.005$ and $\varepsilon_s = 3.17^{1/3}$.~~

agrees best with values from literature (for details see Appendix B). The ice volume fraction f_{vol} relates the density of snow ρ (g/cm^3) to the volumetric mass density of air and ice by

$$\rho = f_{\text{vol}} \cdot \rho_{\text{ice}} + (1 - f_{\text{vol}}) \cdot \rho_{\text{air}} \approx f_{\text{vol}} \cdot \rho_{\text{ice}}. \tag{4}$$

In the microwave regime between 10–20 GHz, the relative permittivity of pure polycrystalline ice is given by $\varepsilon_{\text{ice}} = 3.17 \pm 0.02$, and shows a weak temperature dependence ~~(Mätzler and Wegmüller, 1987; Fujita et al., 1993; Warren and Brandt, 2~~ (Mätzler and Wegmüller, 1987; Fujita et al., 1993; Matsuoka et al., 1996 As the uncertainty for snow density measurements of some percent is larger than the temperature dependence of the permittivity, a fixed permittivity of 3.17 corresponding to approximately -10°C has been used in this paper.

According to the Maxwell–Garnett theory for isotropic mixtures, $\varepsilon_{\text{eff, MG}}$ is given by

$$\varepsilon_{\text{eff, MG}} = \varepsilon_{\text{air}} + 3 f_{\text{vol}} \varepsilon_{\text{air}} \frac{\varepsilon_{\text{ice}} - \varepsilon_{\text{air}}}{\varepsilon_{\text{ice}} + 2\varepsilon_{\text{air}} - f_{\text{vol}}(\varepsilon_{\text{ice}} - \varepsilon_{\text{air}})} \tag{5}$$

with the relative permittivity of air, $\varepsilon_{\text{air}} = 1$ (e.g. Sihvola, 2000). The "inverse" Maxwell–Garnett result, $\varepsilon_{\text{eff, MG, inv}}$, follows by swapping ε_{air} and ε_{ice} in Eq. (5) and replacing f_{vol} by $1 - f_{\text{vol}}$ (Sihvola, 2002). Note that the Maxwell–Garnett theory is a mean-field theory and additionally requires the inclusions to be much smaller than the wavelength of the microwaves in the medium ($a_x, a_y, a_z \ll \lambda/\sqrt{\varepsilon_{\text{eff}}}$), so that scattering in the snow volume can be neglected.

For non-spherical inclusions, Eq. (5) has to be adapted by introducing depolarization factors, N_i, for aligned ellipsoidal inclusions (e.g. Cohn, 1900; Polder and van Santen, 1946, or Sihvola, 2000). As settling and temperature gradient metamorphism act in the z direction, we model the elliptical inclusions as oblate or prolate spheroids which have their symmetry axis parallel to z. According to ~~(Sihvola, 2000)~~ Sihvola (2000) the permittivity of anisotropic mixtures is given for each spatial dimension $i \in x, y, z$ by

$$\varepsilon_{\text{eff, MG},i} = \varepsilon_{\text{air}} + f_{\text{vol}} \varepsilon_{\text{air}} \frac{\varepsilon_{\text{ice}} - \varepsilon_{\text{air}}}{\varepsilon_{\text{air}} + (1 - f_{\text{vol}}) N_i (\varepsilon_{\text{ice}} - \varepsilon_{\text{air}})} \tag{6a}$$

The "inverse" Maxwell–Garnett form of Eq. (6a) reads

$$\varepsilon_{\text{eff, MG, inv},i} = \varepsilon_{\text{ice}} + (1 - f_{\text{vol}}) \varepsilon_{\text{ice}} \frac{\varepsilon_{\text{air}} - \varepsilon_{\text{ice}}}{\varepsilon_{\text{ice}} + f_{\text{vol}} N_i (\varepsilon_{\text{air}} - \varepsilon_{\text{ice}})}. \tag{6b}$$

Both equations are used in Eq. (3) to calculate the effective anisotropic relative permittivities $\varepsilon_{\text{eff},x}, \varepsilon_{\text{eff},y}$ and $\varepsilon_{\text{eff},z}$ for snow. Results for the permittivity and the deviation from the isotropic case are shown in Fig. 1.

The depolarization factors N_i are assumed to be equivalent for both Eqs. (6a) and (6b) ~~and~~ as both equations describe the polarizability of elliptical particles. The depolarization

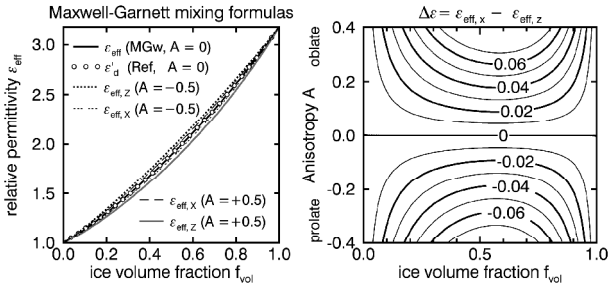

Figure 1. Left: Relative permittivity $\varepsilon_{\mathrm{eff}}$ of snow with isotropic ($A = 0$), vertically oriented ($A = -0.5$) and horizontally oriented ($A = +0.5$) inclusions calculated by the weighted Maxwell–Garnett formula (MGw), Eq. (3). The dots indicate the empirical function given by Eq. (46) in Wiesmann and Mätzler (1999). Right: the dielectric anisotropy, $\Delta\varepsilon = \varepsilon_{\mathrm{eff},x} - \varepsilon_{\mathrm{eff},z}$, as a function of ice volume fraction f_{vol} and anisotropy A according to Eq. (3).

factors N_i are given according to (Sihvola, 2000) for ellipsoidal inclusions with the dimensions a_x, a_y, a_z by the elliptic integral of second kind

$$N_i = \frac{a_x a_y a_z}{2} \int_0^\infty \frac{\mathrm{d}s}{(s+a_i^2)\sqrt{(s+a_x^2)(s+a_y^2)(s+a_z^2)}}, \quad (7)$$

where the integration variable s of unit squared-distance describes an ellipsoidal surface larger than the surface of the elliptic inclusion where $s = 0$ (Landau and Lifshitz, 1960, §4, p20-30). The dimensions $a_x = a_y$ define the (horizontal) diameter of the spheroids and a_z is their vertical length. Note that Sihvola (2000) used the ellipsoids' semi-axis. However, the depolarization factors do not depend on the absolute size of inclusions and are invariant under rescaling $a_i \to \lambda a_i$ for arbitrary λ. Consequently, it is possible to parametrize the depolarization factors directly by the anisotropy A', which can easily be verified by substituting s in Eq. (7) with the dimensionless quantity $u = s/a_x^2$. N_i is then given by

$$N_i = \frac{A'}{2} \int_0^\infty \frac{\mathrm{d}u}{(u+\delta_{A'}(i,z))\sqrt{(u+1)^2 \cdot (u+A'^2)}} \quad (8)$$

with $\delta_{A'}(i,z) = 1$ for $i \in x,y$ and $\delta_{A'}(i,z) = A'^2$ for $i = z$. Closed form expressions for the elliptic integrals can be found e.g. in ~~Sihvola (2000)~~Landau and Lifshitz (1960); Sihvola (2000). The depolarization factors satisfy $N_x + N_y + N_z = 1$ for any ellipsoid (Polder and van Santen, 1946). For spherical inclusions all three depolarization factors are $N_i = 1/3$ and Eq. (6a) is equivalent with Eq. (5).

2.3 Series expansion of permittivity from spatial correlation functions: equivalence with Maxwell-Garnett formulas

Although ice grains show a much more complex structure than simple ellipsoids, the model of ellipsoids is realistic enough for the transverse isotropic symmetry of the dielectric tensor $\overline{\overline{\varepsilon}}$. This becomes more obvious from the exact series expansion of the dielectric tensor for arbitrary anisotropic microstructures, which can be expressed in terms of spatial correlation functions (Rechtsman and Torquato, 2008). In the Appendix, we show that under the less restrictive assumption of a transverse isotropic two-point correlation function, the truncation of the exact expression using n-point correlation functions (Rechtsman and Torquato, 2008, Eq. 16) at second order ($n = 2$) *exactly* leads to the Maxwell–Garnett result (Eq. 6a) in which the depolarization factors N_i are expressed in terms of the anisotropy parameter Q as given in (Löwe et al., 2013) via $N_i = Q$ for $i = x, y$ and $N_z = 1 - 2Q$. This implies that the present dielectric model and the thermal conductivity model from (Löwe et al., 2013) are based on exactly the same microstructural parameters. In view of recent attempts to unify microstructural descriptions of snow for microwave modeling (Löwe and Picard, 2015), we also note that the Maxwell–Garnett formula (Eq. 6a) can be likewise obtained as the low-frequency limit of the quasi-crystalline approximation for aligned spheroids (Ao and Kong, 2002).

2.4 ~~Anisotropy measured by radar systems~~

3 Dielectric anisotropy measured by polarimetric radar systems

~~In the previous section, the anisotropic effective permittivity $\varepsilon_{\mathrm{eff},i}$ was derived for snow which has a spatially anisotropic microstructure. The effective permittivity can be measured when snow~~

The depth-averaged anisotropy of a snow pack of known depth and density can be estimated when it is observed with a obliquely looking polarimetric radar system ~~by analyzing the Copolar Phase Difference, CPD. The CPD is a measure for~~ and the phase difference of the backscatter coefficients of two perpendicular polarizations is analyzed. The phase difference follows from the radio-birefringence of snow and is determined by the propagation delay ~~of~~ between two orthogonally polarized microwaves ~~and is derived in this section with respect to $\varepsilon_{\mathrm{eff},i}$.~~ reflected at the bottom of the snow pack.

~~Only side-looking~~

3.1 Experimental and geometric considerations

For measuring quantitatively the dielectric anisotropy of the snow pack, the angle between the field vector of the electromagnetic field and the principal axis of the dielectric tensor $\overline{\overline{\varepsilon}}$ must be known. Two orthogonally polarized

microwaves should be be chosen such that the polarizations are delayed by different components of the dielectric tensor $\bar{\bar{\varepsilon}}$. The anisotropy of seasonal snow has the symmetry axis in the vertical, therefore one polarization must be at least partially aligned with the vertical while the other polarization must be oriented horizontally. Side-looking polarimetric radar systems like real or synthetic aperture radar systems ~~are suitable for measuring the anisotropy of snow, whereas~~ using a vertical (VV) and horizontal (HH) polarization as defined in Fig. 2 fulfill this requirement, whereas the anisotropy cannot be measured by nadir-looking radar systems ~~like~~ (e.g. ground penetrating radars~~are not. A requirement~~) as long as there is no anisotropy in the horizontal (xy-) plane.

A further requirement is that the depth where most of the microwave energy is backscattered is known. For dry snow and frequencies of a few GHz where the volume scattering contribution in shallow seasonal snow is negligible (e.g. Hallikainen et al., 1987; West et al., 1993; Tsang et al., 2007, or Leinss et al., 2015, Fig. 5), this requirement is easy to fulfill and the scattering center corresponds to the soil below the snow pack. However, for deep firn on ice sheets or glaciers it can be difficult to obtain a good estimate on the penetration depth. The following method is not suitable for wet snow, as the dielectric properties, especially absorption and the penetration depth, strongly depend on the water content.

3.2 Definition of the CPD and signal-processing basis

The Copolar Phase Difference, CPD, is a measure for phase difference resulting from different propagation speeds of two orthogonally polarized microwaves. The CPD is defined as the phase difference between the complex-valued backscatter coefficients, S_{VV} and S_{HH}. The scattering coefficient S_{VV} for the V polarization (V transmit, V receive) is defined by the coherent superposition of all scattered fields of the ensemble of scatterers contained in the corresponding range resolution cell of the radar (the pixel). The random distribution of scatterers in the resolution cell defines the unknown but deterministic scattering-phase of S_{VV}. The scattering coefficient S_{HH} is defined the same way but for perpendicular transmit (H) and receive polarization (H). If the scatterers don't have a polarization dependent scattering phase, the (random) phase values of S_{VV} and S_{HH} are spatially correlated and show a zero-phase difference, if no birefringent medium exists between the radar and the scatterers. The (complex-valued) spatial correlation function is defined by the copolar coherence

$$\gamma_{\mathrm{VV,HH}} \cdot e^{i\phi_{\mathrm{CPD}}} = \frac{\langle S_{\mathrm{VV}} \cdot S_{\mathrm{HH}}^{*} \rangle}{\sqrt{\langle |S_{\mathrm{VV}}|^2 \rangle \cdot \langle |S_{\mathrm{HH}}|^2 \rangle}}. \tag{9}$$

The magnitude of the copolar coherence is given by the correlation coefficient $\gamma_{\mathrm{VV,HH}}$ which ranges from 0 to ~~measure the anisotropy is that the two orthogonal polarized microwavesare delayed by different components of the dielectric tensor $\bar{\bar{\varepsilon}}$. The sensitivity to the anisotropy increases linearly with frequency. However, the radar system must operate at a low enough frequency (several GHz) such that microwaves can penetrate dry snow with negligible scattering or absorption losses~~ 1. The CPD is equivalent to the phase of the copolar coherence, ϕ_{CPD}. The notation $\langle \cdot \rangle$ indicates a spatial average over about 10 to several thousands of pixels containing the backscatter coefficients of each polarization and the asterisk * denotes complex conjugation.

The magnitude of the coherence is reduced when two corresponding resolution cells (of same range but different polarization) contain scatterers which do not show a correlation between orthogonal polarizations. This is the case for objects showing strong multiple scattering (e.g. ~~Hallikainen et al., 1987; West et al., 1993; Tsang et al., 2007, or Leinss et al., 2015, Fig. 5).~~ rough surfaces and strongly scattering volumes). The coherence is also reduced when the corresponding range-resolution cells, represented by S_{VV} and S_{HH}, are not perfectly overlapping and do therefore not contain exactly the same ensemble of scatterers. This occurs e.g. for large propagation delays ΔR between the two polarizations. For partially overlapping resolution cells, the coherence is reduced proportional to $1 - \Delta R/\delta r$. The coherence is totally lost when ΔR exceeds the range resolution δr of the radar system. For partially overlapping resolution cells, only scatterers which are both contained in the resolution cell of different polarizations contribute constructively to the coherence; other scatterers lead to decorrelation. The contribution of correlated scatterers to the CPD can therefore be described by two polarized waves which have a common wave front before propagating through a birefringent medium and which are scattered at exactly the same point P on the ground. This scattering geometry is the basis of Figure 2.

The dielectric anisotropy can precisely be measured with the CPD, because the CPD, defined as the phase of a signal, can be determined with a precision of a few degrees (fraction of one wavelength) relative to the total phase delay of many wavelengths which is accumulated during propagation through the snow pack (Guneriussen et al., 2001, Eq. 5), and (Leinss et al., 2015, Eq. 14). For example, for 1 m deep snow of density $\rho = 0.25\,\mathrm{g\,cm^{-3}}$ a dielectric anisotropy ~~$\epsilon_x - \epsilon_z = 10^{-4}$~~ $\Delta\varepsilon = \varepsilon_x - \varepsilon_z = 10^{-4}$ causes a CPD of 1° relative to the total phase delay of 5700° measured at a radar frequency of 10 GHz and a radar incidence angle of 40°. The dielectric anisotropy of transparent media (e.g. a dry snow pack) can therefore be measured much more accurately with the CPD compared to the time-delay between two perpendicularly polarized microwave pulses.

3.3 CPD of birefringent, non-scattering media

In order to derive the CPD, the wave propagation through snow is formulated analogue to transversely isotropic media as done in anisotropic optics (Saleh and Teich, 1991). Considering snow as transversely isotropic is reasonable since gravity and the direction of the water vapor flux in snow break isotropy in the vertical direction, therefore the optical axis is given by the z axis.

According to anisotropic optics, we define the refractive index in the z direction as the extraordinary refractive index n_e. For transversely isotropic media, the extraordinary refractive index, n_e, differs from the ordinary refractive indices, n_o, which is defined in the (x, y) plane (Fig. 2). The refractive indices are related to the relative permittivity defined in Eq. (3) together with Eqs. (6a) and (6b) by

$$n_\mathrm{o}^2 = \varepsilon_{\mathrm{eff},x} = \varepsilon_{\mathrm{eff},y} \tag{10a}$$

$$n_\mathrm{e}^2 = \varepsilon_{\mathrm{eff},z}. \tag{10b}$$

The anisotropy of snow can only be determined with polarimetric radar systems when microwaves are transmitted with a large enough incidence angle θ_0 with respect to the optical axis. The polarizations of a side-looking radar system are defined orthogonal to the propagation vector $\boldsymbol{k}$ of the incident beam such that the horizontal polarization (H) is oriented parallel to the observed surface (cf. Fig. 2). Hence, the propagation velocity of the H-polarization is ~~delayed~~ determined by the ordinary refractive index n_0. The vertical polarization (V) is defined perpendicular to H and the propagation vector $\boldsymbol{k}$. The V-polarization is not parallel to the optical axis z as for side-looking radar systems the incidence angle θ_0 can never reach $90°$. Therefore, the electric field of the V-polarization always has one component along the optical axis z and one component perpendicular to it, along x. For the V polarization, the refractive index n_V depends on the propagation angle θ_V in the medium and can be described by the refractive index ellipsoid (Saleh and Teich, 1991)

$$\frac{1}{n_\mathrm{V}^2(\theta_\mathrm{V})} = \frac{\cos^2\theta_\mathrm{V}}{n_\mathrm{o}^2} + \frac{\sin^2\theta_\mathrm{V}}{n_\mathrm{e}^2}. \tag{11}$$

The refractive indices for the H and V polarized wave are[3]

$$n_\mathrm{H} = n_\mathrm{o} \tag{12a}$$

$$n_\mathrm{V}(\theta_\mathrm{V}) = \frac{n_\mathrm{o} n_\mathrm{e}}{\sqrt{n_\mathrm{e}^2\cos^2\theta_\mathrm{V} + n_\mathrm{o}^2\sin^2\theta_\mathrm{V}}}. \tag{12b}$$

The refraction at the air-snow interface is described by Snell's law which for the H polarization is

$$n_\mathrm{air}\sin\theta_0 = n_\mathrm{H}\sin\theta_\mathrm{H}. \tag{13a}$$

[3]Note that the equation for n_V^2 in ~~(?)~~ (Leinss et al., 2014b) is an approximation of Eq. (11) for small anisotropies. The approximation follows from Eq. (11) by writing $n_\mathrm{o}^2 = \epsilon_\mathrm{eff} - \delta$ and $n_i^2 = \epsilon_\mathrm{eff} + \delta$ and applying a first order Taylor expansion in δ, neglecting terms ~~$\mathcal{O}(\delta^2/\epsilon^2)$~~ $\mathcal{O}(\delta^2/\epsilon_\mathrm{eff}^2)$.

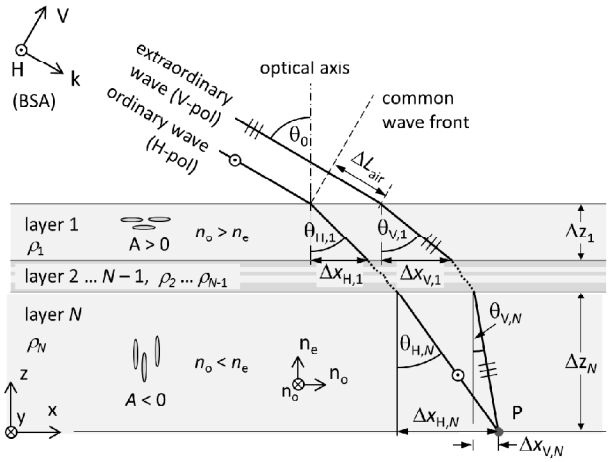

Figure 2. An electromagnetic wave (H or V polarized) is transmitted in $\boldsymbol{k}$ direction with respect to the radar coordinate system (H, k, V) and with an incidence angle θ_0 with respect to the snow surface. The electric field of the H polarized wave is perpendicular to the optical axis (z), and sees the ordinary refractive index n_o (therefore called the "ordinary wave"). The electric field of the V polarized wave has a component parallel to the optical axis and is affected by the extraordinary refractive index n_e (the "extraordinary wave"). For horizontally aligned anisotropies ($A > 0$) the extraordinary wave travels faster ($n_\mathrm{e} < n_\mathrm{o}$) whereas for vertical anisotropies the ordinary wave is faster ($n_\mathrm{o} < n_\mathrm{e}$). As refraction differs for both waves, also the optical distances differ when measured from a common wave front to the same point P on the ground. Describing the radar reflection at a common point P seems arbitrarily chosen, however only reflections from common scatterers within one radar resolution cell contribute to the CPD as described in Sect. 3.2. The structucal anisotropy of the layers is shown as expected for fresh snow (layer 1) deposited on top of old snow (layer N). The layer of fresh snow with density ρ_1 and thickness Δz_1 is drawn with horizontal structures with a anisotropy $A > 0$. The thick layer of old snow is drawn as vertical ice grains ($A < 0$) ~~recrystallized under~~ grown by temperature gradient metamorphism. The theory in this paper is true for any random layering of densities and anisotropies due to Snell's law as long as absorption or volume scattering are negligible.

For the V polarization, the refractive index n_V depends on θ_V, which in turn depends on n_V. The modified Snell's law

$$n_\mathrm{air}\sin\theta_0 = n_\mathrm{V}(\theta_\mathrm{V})\sin\theta_\mathrm{V} \tag{13b}$$

has therefore to be solved simultaneously with Eq. (12b). It follows that

$$n_\mathrm{V}(\theta_\mathrm{V}) = \sqrt{n_\mathrm{o}^2 + \left(1 - \frac{n_\mathrm{o}^2}{n_\mathrm{e}^2}\right) n_\mathrm{air}^2 \sin^2\theta_0}. \tag{14}$$

Equation (14) can be used in Eq. (13b) to calculate the angle θ_V. Note, that θ_V is only implicitly contained in Eq. (14) by θ_0 and Snell's law (13b). For a birefringent medium, θ_V does no longer describe the direction of propagation of an optical beam (which does the Poynting-Vector), but instead the direction which is perpendicular to the wave fronts (the wave vector $\boldsymbol{k}$). As we are interested in the retardation of wave fronts, we use θ_V which determines the direction of $\boldsymbol{k}$ in the birefringent medium. For multi-layer systems comprising N anisotropic layers which all have the optical axis parallel to the z axis, Eqs. (13a) and (13b) are valid for every layer because Snell's law holds at each layer-interface

$$n_j\sin\theta_j = n_{j+1}\sin\theta_{j+1} \quad \text{for } j = 0, 1 \ldots N-1 \tag{15}$$

and with $n_0 = n_\mathrm{air}$.

The difference in propagation delay between both polarizations can now be calculated. Fig. 2 shows the geometry of a multilayer system where each layer j can have a different anisotropy A_j and density ρ_j. The layers are numbered from top (1) to bottom (N). Two sinusoidal plane waves, described by $\boldsymbol{E}(t,\boldsymbol{r}) = \boldsymbol{E}_0 e^{i(\omega t - \boldsymbol{kr})}$ with the same frequency $\nu = \omega/(2\pi)$ are transmitted to the snow surface with an incidence angle θ_0. For a fixed time t, the phase difference measured along a distance r is given by $\phi = \boldsymbol{k}\cdot\boldsymbol{r}$, where the magnitude of the wave vector $|\boldsymbol{k}| = \frac{2\pi n}{\lambda_0}$ in the medium is defined by the refractive index n and the vacuum wavelength λ_0. The two paths for the ordinary (H) and extraordinary (V) waves which connect a common wave front with a point P at the snow-soil interface are shown in Fig. 2. The two-way phase difference along this path is given by

$$\phi_\mathrm{CPD} = \phi_\mathrm{VV} - \phi_\mathrm{HH} \tag{16}$$

which correspond to the measured copolar phase difference (CPD) between the VV and HH channel of a radar system. The ~~two letters corresponds to~~ letters H and V denote the polarization of the ~~transmitting (V and H) and receiving (V and H)channel~~measured signal with VV = (vertical transmit, vertical receive) and HH = (horizontal transmit, horizontal receive). For monostatic radar systems, the same coordinate system (H,k,V) is used for transmission and reception of the microwave signal, which is called "Back-Scatter Alignment" convention, BSA. The reversal of the $\boldsymbol{k}$ vector in the BSA causes a sign-change of the phase ϕ, hence the physically expected phase difference ϕ'_CPD is related to the phase difference measured in the BSA coordinate system by

~~$\phi_\mathrm{CPD} = (-1)\phi'_\mathrm{CPD}$~~

$$\phi_\mathrm{CPD} = (-1)\cdot\phi'_\mathrm{CPD} \tag{17}$$

(cf. Lüneburg and Boerner, 2004 or Lee et al., 1999, Sect. 3.1.3). With respect to Fig. 2, the polarimetric propagation delay and consequently the CPD is given by the phase accumulated during the propagation through the snow pack plus an offset in air

$$\begin{aligned}\phi'_\mathrm{CPD} &= 2\sum_{j=1}^{N}\Delta\phi_{\mathrm{V},j} - 2\sum_{j=1}^{N}\Delta\phi_{\mathrm{H},j} - 2\phi_\mathrm{air} \\ &= 2\sum_{j=1}^{N}\frac{k_{\mathrm{V},j}\Delta z_j}{\cos\theta_{\mathrm{V},j}} - 2\sum_{j=1}^{N}\frac{k_{\mathrm{H},j}\Delta z_j}{\cos\theta_{\mathrm{H},j}} - 2\phi_\mathrm{air}.\end{aligned} \tag{18}$$

The in-air phase difference $\phi_\mathrm{air} = k_0\Delta L_\mathrm{air}$ depends on the sum of horizontal displacements $\sum\Delta x_{\mathrm{V},j} - \Delta x_{\mathrm{H},j}$ and the wave vector in air, $k_0 = 2\pi n_\mathrm{air}/\lambda_0$ with $n_\mathrm{air} \approx 1$, and is given by

$$\phi_\mathrm{air} = k_0\cdot\sin\theta_0\sum_{j=1}^{N}\Delta z_j\,(\tan\theta_{\mathrm{V},j} - \tan\theta_{\mathrm{H},j}). \tag{19}$$

The ordinary and extraordinary wave vectors are given by

$$k_\mathrm{H} = \frac{2\pi n_\mathrm{H}}{\lambda_0} \quad \text{and} \quad k_\mathrm{V} = \frac{2\pi n_\mathrm{V}}{\lambda_0}. \tag{20}$$

Equation (18) can be rearranged and combined with Eqs. (19) and (20) and it follows that the CPD can be formulated in the BSA convention (cf. Eq.17) by

$$\phi_\mathrm{CPD} = (-1)\frac{4\pi}{\lambda_0}\sum_{j=1}^{N}\Delta z_j\cdot\Delta\zeta(\rho_j, A_j, \theta_0). \tag{21}$$

The contributions of individual layers of thickness Δz are given by the ~~relative~~ specific path length difference

$$\Delta\zeta(\rho, A, \theta_0) = \sqrt{n_\mathrm{V}^2 - \sin^2\theta_0} - \sqrt{n_\mathrm{H}^2 - \sin^2\theta_0}. \tag{22}$$

The ~~relative~~ specific path length difference defines the optical path length difference ~~relative to the~~ per thickness ΔZ of an anisotropic medium observed under a surface incidence angle θ_0. The refractive indices n_V and n_H are defined for each individual layer by Eqs. (12a) and (14) using the effective permittivity from Eqs. (10a) and (~~10a~~10b), which was derived in Sect. 2.2 for a given snow density ρ and structural anisotropy A.

The horizontal structures in ~~settled fresh snow causes~~ fresh snow cause a faster propagation speed for the VV polarization than for HH. Consequently, HH will have a larger phase

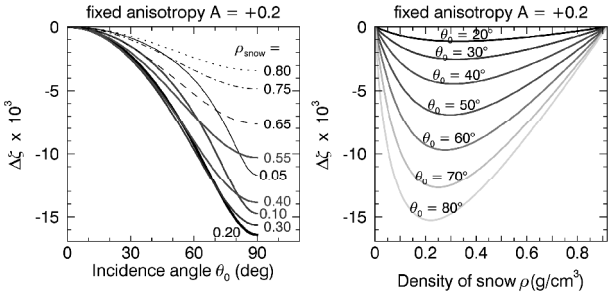

Figure 3. The ~~relative~~ specific path length difference $\Delta\zeta$, expected between vertically and horizontally polarized microwaves according to (Eq. 22), is plotted for snow with horizontally aligned oblate ice grains ($A = +0.2$) over incidence angle (left), and snow density (right).

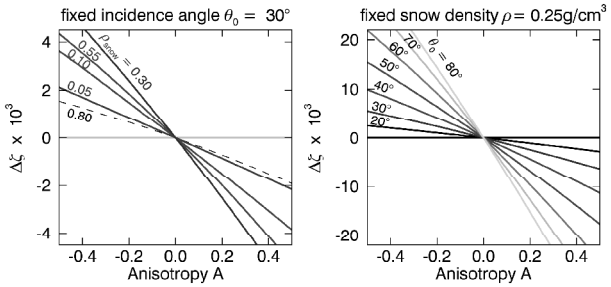

Figure 4. The ~~relative~~ specific path length difference $\Delta\zeta$, according to (Eq. 22), plotted over anisotropy for different snow densities but fixed incidence angle, $\theta_0 = 30°$, (left) and for different incidence angles but fixed snow density, $\rho = 0.25\,\mathrm{g\,cm^{-3}}$, (right).

delay than VV at the receiving antenna. This results in a positive ~~(!) copolar phase difference $\phi_{VV} - \phi_{HH}$, due to a~~ CPD, $\phi_{CPD} = \phi_{VV} - \phi_{HH}$, due to the sign-change because of the BSA.

~~The relative~~ The specific path length difference, $\Delta\zeta$, increases with incidence angle (Fig. 3, left) and with increasing densities below $0.2\,\mathrm{g\,cm^{-3}}$ (Fig. 3, right). When the snow density increases beyond $0.3\,\mathrm{g\,cm^{-3}}$, refraction reduces the alignment of the V polarization with respect to the optical axis and consequently $\Delta\zeta$ decreases (Fig. 3, right). Therefore, a broad maximum of $\Delta\zeta$ is observed for densities between 0.2 and $0.4\,\mathrm{g\,cm^{-3}}$ (Fig. 3, right), where only a weak density dependence exists.

Also, above a density of about $\rho = 0.55$, the dielectric ~~contrast $\varepsilon_x - \varepsilon_z$~~ anisotropy $\Delta\varepsilon = \varepsilon_x - \varepsilon_z$ decreases (Fig. 1, right) such that $\Delta\zeta$ vanishes at $\rho = \rho_{ice}$ where no air inclusions are present anymore. ~~A broad maximum of~~ We note here, that $\Delta\zeta$ ~~is observed for densities between 0.2 and $0.4\,\mathrm{g\,cm^{-3}}$~~ (vanishes only for dielectric isotropic (polycrystalline) ice. This is not generally the case as for ice on glaciers and ice sheets the crystal axis of ice (c-axis) can have a preferential orientation (e.g. Matsuoka et al., 1997; Fujita et al., 2014).

The weak dependence of $\Delta\zeta$ on snow density, at least for the density range of seasonal snow, allows for a quite rough estimate for snow density when the CPD is used to determine the anisotropy of snow. For seasonal snow, densities of 0.15 and $0.4\,\mathrm{g\,cm^{-3}}$ have been reported (Bormann et al., 2013). Within this range, the CPD varies by less than 20 % as shown by Fig. 3~~, right), where almost no density dependence exists~~(left).

In contrast to the ~~non-invertible density dependence of $\Delta\zeta$~~ weak density dependence, $\Delta\zeta$ depends almost linearly on anisotropy A for all densities and incidence angles (Fig. 4, left and right). Therefore, the CPD is mainly determined by snow depth Δz and the anisotropy A which makes determination of A almost independent on snow density.

~~When we use Eq.~~

3.4 Discussion of the CPD regarding literature results

For firn (with $\rho = 0.4\,\mathrm{g\,cm^{-3}}, \Delta\varepsilon = -0.05$), as observed by Fujita et al. (2014) for the upper 5 meters of the ice sheet at NEEM in the northwest of Greenland, we would expect a vertical anisotropy $A = -0.25$ ~~(?) to calculate the CPD,~~ ($A' = 1.3$). Similar firn conditions ($\rho = 0.4\,\mathrm{g\,cm^{-3}}, \Delta\varepsilon = -0.05$) have been found by Fujita et al. (2009) at Dome Fuji in Antarctica who determined a slightly lower structural anisotropy of $A' \approx 1.15$. Similar anisotropy values of $A' = 1.2$ or greater have been observed in Antarctic firn by Alley (1987). The density and dielectric measurements of both studies of Fujita indicate that a CPD of $\phi_{CPD} = -80°$ per meter would have been measured for the radar parameters of the satellite TerraSAR-X as used in the following study: in Leinss et al. (2014b) a CPD of 60–150°/m was measured for fresh snow ($\rho = 0.2$) in Finland at 32.7° and 9.65 GHz, which would correspond to a horizontal anisotropy between $A = +0.2$ and $+0.5$ ($A'^{-1} = 1.2$ and 1.7). Somewhat lower anisotropy values have been found for natural, undisturbed as well as for sieved seasonal snow where for both cases the horizontal anisotropy ($A'^{-1} = 1.12$ and 1.17) decreased and reached in one case a vertical anisotropy ($A' = 1.12$) (Schneebeli and Sokratov, 2004).

Compared to the simplified model of Leinss et al. (2014b), where refraction was not included, we get about 5–10 % lower values ~~compared to the theory in ? where refraction was not included.~~ for the CPD using Eq. (21). Refraction leads to a decreasing z component of the V polarization, consequently the ~~birefringent~~ birefringence effect is reduced as well. Using the weighted average of the two Hashin–Shtrikman bounds to calculate ε_{eff} leads to an additional decrease of up to 30 % for higher snow densities ~~,~~ compared to the model published by Leinss et al. (2014b).

~~For firn with $\rho = 0.4\,\mathrm{g\,cm^{-3}}, \Delta\varepsilon = +0.05$, as observed in Fujita et al. (2014), we would expect $\phi_{CPD} = 70°$ per meter and a vertical anisotropy $A = -0.37$ ($A' = 1.4$). In ? a CPD of 6–15/10 of fresh snow was measured at 32.7°~~

~~and 9.65 GHz, which would correspond to a horizontal anisotropy between $A = +0.2$ and $+0.5$ ($A'^{-1} = 1.2$ and 1.7). Similar anisotropy values have been observed in Alley (1987); Schneebeli and Sokratov (2004).~~

3.5 Generalization for scattering multilayer systems

Equation (21) is valid for a multi-layer system, where scattering and absorption are negligible in or between different snow layers. In the present work, we solely concentrate on non-scattering and non-absorptive media for which all scattered energy returns from the bottom of the multi-layer snow system.

For multi-layer systems ~~like snow with very large ice grains, e.g. deep multi-year firn on glaciers, but also for wet and consequently absorbing snow,~~ where scattering occurs at the snow surface, at layer boundaries or within snow layers, or where microwave-absorbing layers are present, the location of the main scattering center is difficult to define and depends strongly on the scattering and absorption properties of the snow ~~volume.~~ pack.

The scattering properties are given by the ratio of grain size to wavelength but also by the surface roughness and the dielectric contrast between neighboring layers. Scattering within the snow pack can occur e.g. in old metamorphic snow like depth hoar, in snow which contains ice layers and melt-crusts but also in deep snow on glaciers where the snow depth exceeds the penetration depth of microwaves.

In the following we briefly outline how Eq. (21) can be generalized to estimate the CPD when scattering of different layers needs to be included.

In order to generalize our model for media where volume scattering cannot be neglected, we define – possibly complex – amplitude scattering factors μ_j for each layer boundary. The scattering contribution of the first layer boundary, the air/snow interface, is given by μ_0. The phasor $e^{i\phi_1}$ ~~which results from~~ defining the CPD of the first layer contributes with ~~μ_j~~ the backscatter amplitude factor μ_1 of the first-to-second layer boundary to the total phase difference. The reflection ~~from~~ after the second layer accumulates the CPD of the first and of the second layer, so that the second phasor is given by $e^{i(\phi_1+\phi_2)}$ and so on. The total phase difference is then

$$\phi_{\mathrm{CPD}} = \mu_0 + \mu_1 \cdot e^{i\phi_1} + \mu_2 \cdot e^{i(\phi_1+\phi_2)} + \ldots$$
$$= \sum_{j=1}^{j=0}{}^{N} \mu_j \prod_{k=1}^{k=0}{}^{j} e^{i\phi_j}. \quad \text{with} \quad \phi_0 = 0. \tag{23}$$

Scattering within layers can be accounted for by subdividing a homogeneous layer into a sufficient number of finite layers.

For homogeneously scattering and/or absorbing volumes, $|\mu_j|$ would decrease exponentially, whereas μ_j can be quite heterogeneous for ice layers which occur e.g. in the percolation zone of glaciers (Parrella et al., 2015) ~~.~~ or for snow packs which contain e.g. melt crusts and ice layers. In such cases, assumptions must be made for the penetration depth or the penetration depth must be determined independently and the inversion of the CPD to determine the anisotropy can quickly be questionable.

3.6 Contribution of a rough ground surface

The method to determine the anisotropy of snow as presented in the previous sections relies on the assumption that the CPD of the underlying ground is zero or at least known (see Sect. 5.6). Radar experiments have shown that the CPD is close to zero for soil at small incidence angles but shows an increasing standard deviation for rough surfaces. It has also been found that the CPD increases to a few ten degrees with incidence angle for rough soil(Sarabandi, 1992; Oh et al., 2002). The CPD is also influenced by vegetation cover, especially for oriented vegetation (Ulaby et al., 1987). Therefore, CPD measurements of snow free ground are recommended to verify if any CPD bias exists.

4 Experimental data

For the validation of our model we analyzed radar data acquired within the Nordic Snow Radar Experiment (NoSREx) campaigns ~~(?)~~(Lemmetyinen et al., 2013). The NoSREx campaigns consisted of extensive field measurements and various active and passive microwave measurements acquired at a test site near the ~~city~~ town of Sodankylä in northern Finland. The test site, shown in Fig. 5, is an almost flat forest clearing which is surrounded by boreal forest. ~~Low~~ The test site is covered by low taiga-type vegetation ~~grows on the site on~~ which grows on mineral soil. ~~During winter, the site was covered quite homogeneously with snow. The variability of snow depth showed a standard deviation of 2–3 and was measured with seven sticks located~~ The test site is equipped with various sensors to measure meteorological data and snow properties. For the radar measurements, two sectors were defined on the test site, sector 1 ~~apart. The seven sticks are indicated by "SDvar" in Fig. 5.~~ in the center of the forest clearing, sector 2 between trees.

4.1 Microwave measurements

The radar data were acquired by the SnowScat Instrument (SSI), which was installed on a 9 m high tower~~on the test site. The SSI~~, The tower is shown in ~~the inset of~~ Fig. 5, the SSI with its two horn-antennas is shown in the inset.

SnowScat is a fully polarimetric, coherent, continuous-wave stepped-frequency, real aperture radar and operates between 9.2 and 17.8 GHz ~~(Wiesmann et al., 2008; Werner et al., 2010)~~(Wiesmann et al., 2008; We
It was originally developed and built for snow backscatter measurements within the ESA ESTEC project KuScat,

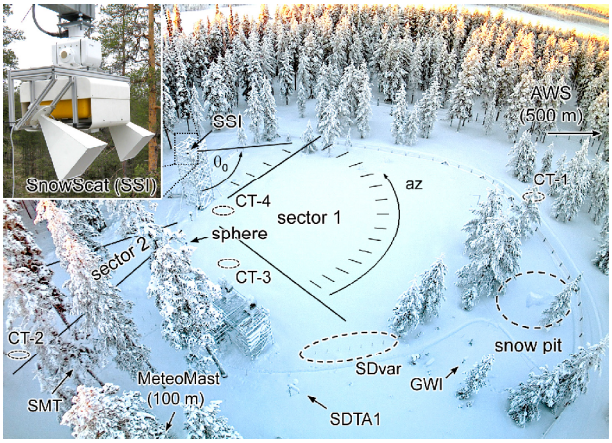

Figure 5. The radar data and meteorological measurements were acquired ~~at~~ on the above shown test site ~~near~~ nearby the town of Sodankylä, Finland. The SnowScat Instrument ~~,~~SSI ~~, is shown in the~~ (inset~~and~~) was mounted on a 9 m high tower. The reference target (sphere) used for calibration can be located behind a tree. The SSI scanned sector 1 and 2 with different azimuth (az) and incidence angles θ_0. ~~Meteorological~~ The meteorological sensors ~~are named as follows: SDTA1: Snow depth and air temperature;~~ SMT~~: Soil moisture and soil temperature; AWS: Automatic weather station. CT-1~~, ~~CT-2~~ MeteoMast,SDAT1, GWI, and ~~CT-3~~ AWS are ~~the locations of snow~~ specified in Table 1. Snow profiles ~~which~~ were ~~analyzed~~ taken at CT-1 to CT-4 for analysis by computer tomography. Snow density was measured in the snow pit, with the Gamma water Instrument (GWI), and was also derived from the snow water equivalent (SWE) determined by the SSI as described in ~~(Leinss et al., 2015)~~Leinss et al. (2015). The variability of snow depth was measured with seven sticks ~~(~~inside the ellipse "SDvar~~)~~".

contract No. 42000 20716/07/NL/EL. Both antennas of the instrument can transmit and receive in horizontal (H) and vertical (V) polarization.

~~The test site contained two sectors for which measurements were repeated~~ The (-3dB) beam width of the horn antennas ranges from 5 to 12 degree, depending on polarization and frequency.

Radar acquisitions were acquired of both sectors of the test site every four hours. The sectors were scanned in azimuth-subsectors of 6° by rotating the antennas around the vertical axis (az). The scan was done for each of the four nominal incidence angles ($\theta_0 = 30°, 40°, 50°$, and $60°$) resulting in 17×4 acquisitions for sector 1 and 5×4 acquisitions for sector 2. Each subsector was measured in all four polarization combinations~~pol $\in \{VV, HH, VH, HV\}$.~~, VV, HH, VH, and HV, using the full frequency range. A detailed description showing the acquisition geometry, the antenna patterns and the polarimetric backscatter signal ~~from the two~~ of both sectors can be found in ~~(Leinss et al., 2015)~~Leinss et al. (2015); In this publication, the snow water equivalent (SWE), later used to estimate the snow density, was determined from SSI data by means of differential radar interferometry.

In the present work, it is assumed that during dry snow conditions all energy is backscattered from the ground below the snow pack. This assumption is justified because SWE could be determined with high precision in Leinss et al. (2015), where a requirement for successful SWE measurements was a snow pack transparent for microwaves. The assumption of a transparent snow pack is further supported by the analysis of the radargrams (Fig. 9 and 10 in Leinss et al., 2014a) which show a distinct range shift of 1.2 m of the antenna pattern at the onset of snow melt. This shift measured at $\theta_0 = 40°$ is proportional to the slant range difference between the wet snow surface of 80 cm height, as observed in April 2012 and 2013, and the underlying ground which had been visible during the dry snow conditions before snow melt.

Table 1. Abbreviations for different sensors and measurements

SSI	Snow Scat Instrument (ground based radar)
sphere	Calibration target for the SSI
CT-#	Snow profile number # acquired in the field and analyzed by computer tomography (μCT)
CT-1	Profile sampling date: 03-03-2011
CT-2	Profile sampling date: 21-12-2011
CT-3	Profile sampling date: 01-03-2012
CT-4	Profile sampling date: 28-02-2013
SDAT1	Snow Depth and Air Temperature sensor no. 1
SMT	Sensors for Soil Moisture and soil Temperature
MeteoMast	Meteorological mast (snow depth, snow temperature profiles)
SDvar	Snow Depth variability course
AWS	Automatic Weather Station
GWI	Gamma Water Instrument (SWE measurement by gamma ray absorption)

4.2 Meteorological ~~measurementsSeveral instruments were installed at~~ instruments, snow depth and density determination

Several automated meteorological sensors were installed on the test site ~~which automatically measured meteorological data.~~ at the locations shown in Fig. 5~~shows the location of different sensors~~. Abbreviations for the sensors are listed in Table 1; technical details can be found in Kontu et al. (2011). Snow depth and air temperature were measured by the sensor SDTA1. Soil temperature (2 sensors at 2 cm depth) and soil moisture (4 sensors, each 2 at 2 cm and 10 cm depth) were measured by ~~two sensors~~ a sensor network named SMT. Snow depth and temperature profiles within the snowpack were measured by the meteorological mast (MeteoMast) 100 m east of the SSI. An automatic weather station (AWS),

located 500 m north of the SSI measured snow depth, air temperature, and other meteorological parameters.

4.3 ~~Snow measurements~~

~~Snow density~~ The variability of snow depth on the test site was measured with seven sticks located 1 m apart, the so called "Snow depth variability course" (SDvar). The seven sticks are located in the ellipse "SDvar" in Fig. 5. Snow depth measurements done at the seven sticks show a quite homogeneous snow depth distribution with a standard deviation of 2–3 cm during dry snow conditions. This allows for comparison of snow data measured at different locations within the test site.

The depth-averaged snow density ρ_{avg} was manually measured in the snow pit once every week. ~~Snow density~~ ρ_{avg} was also calculated from snow depth measured by SDTA1 and from SWE measurements, as SWE in mm water column equivalent = snow depth$\cdot \rho_{\mathrm{avg}}/\rho_{\mathrm{ice}}$. SWE was obtained from the SSI during dry snow conditions (Leinss et al., 2015), and from measurements of ~~the~~ gamma ray absorption within the snow pack using the Gamma Water Instrument, GWI, during wet snow conditions. ~~Details for SWE determination~~ A short description of the GWI can be found in Kontu et al. (2011) and Leinss et al. (2015).

4.3 Computer tomography profiles

The microstructure of four vertical snow profiles~~was determined at three sites~~, CT-1~~on 21 December 2011, CT-2 on 1 March 2012, and CT-3 on 28 February 2013.~~ ..CT-4, sampled in the field on the dates given in Table 1, was determined using computer tomography. The location of the ~~sites~~ profiles are shown in Fig. 5. ~~Overlapping samples where~~ For each profile, vertically overlapping samples of about 10 cm height were taken to cover entire snow depth profiles. The samples were later analyzed by computer tomography at the Institute for Snow and Avalanche Research SLF in Switzerland. For analysis by means of μCT, the snow samples had to be cast for transportation from Finland to the cold lab at SLF, Switzerland.

An analysis of the μCT data, which we used here to determine the anisotropy, was already published with respect to other snow structure parameters in Proksch et al. (2015). Here we briefly summarize the methodology of the casting and processing procedure.

The snow samples were cast using Diethly-Phthalate (DEP) to preserve the snow structure. The casting procedure as well as an accuracy analysis of cast and not-cast samples are described in Heggli et al. (2009). In the cold lab, the samples were scanned with a nominal resolution (voxel size) ranging from 10 µm for new snow to 20 µm for depth hoar. The size of the evaluated volumes ranged from 67 mm^3 for CT-1~~and~~, CT-2 and CT-3 ($512\times512\times256$ voxel with 10 µm voxelsize) to 917 mm^3 for ~~CT-3~~ CT-4 ($512\times512\times600$ voxel with 18 µm voxel size). ~~The sizes of the evaluated volumes were chosen much larger than the representative elementary volume (REV) in order to obtain reliable results from the correlation functions. The REV required to derive reliably density estimates from CT measurements was found to be between 2 and 4 (Kaempfer et al., 2005).~~

The 3-D-gray-scale images, which resulted from the scans, were filtered using a Gaussian filter (sigma = 1 voxel, filter kernel support = 2 voxel). The smoothed images were then segmented into binary images. For snow/air segmentation, the intensity threshold was chosen at the minimum between the DEP peak and the air peak in the histograms of the gray-scale images.

4.4 ~~Processing the~~ SnowScat data processing and CPD ~~retrival~~calibration

The ~~frequency-domain raw data ,~~ raw data measured by the SSI ~~,~~ in the frequency-domain for each azimuth direction az and incidence angle θ were windowed to select a specific frequency band of 2 GHz bandwidth~~which~~. The selected bandwidth was then focused into ~~the~~ range profiles of single-look-complex (SLC) format (~~details in~~ for procession details see Leinss et al., 2015). The pixels of an SLC acquisition represent the complex-valued backscatter ~~amplitude profiles~~ coefficients $S_{\mathrm{pol}}(r, \theta_0, az)$ ~~along range r. The phase of the complex signal contains information about the signal propagation delay~~of each polarization pol $\in$ {VV, HH, VH, HV}. The uncalibrated CPD ~~was~~ for each az and θ_0 was then calculated from the ~~complex-valued, copolar coherence defined as~~

$$\gamma_{\mathrm{VV,HH}} \cdot e^{i\phi_{\mathrm{CPD}}}(\theta_0, az) = \frac{\langle S_{\mathrm{VV}} \cdot S^*_{\mathrm{HH}} \rangle}{\sqrt{\langle |S_{\mathrm{VV}}|^2 \rangle \cdot \langle |S_{\mathrm{HH}}|^2 \rangle}}.$$

copolar coherence (Eq. 9) evaluated for the measured backscatter coefficients S_{VV} and S_{HH}. The ensemble averages ~~of~~ $\langle\cdot\rangle$ contained about 150–300 range-pixels ~~contained in the antenna footprint are indicated by $\langle\,\rangle$, and * is the complex conjugation. The magnitude of the coherence, $\gamma_{\mathrm{VV,HH}}$, is a measure for volume scattering and ranges ideally between 0 (only volume scattering) and 1 (only surface scattering). However, the coherence is reduced by system noise and rough surfaces~~covering the full width (-3 dB) of the antenna footprint. By summing over the antenna footprint, slightly different CPD values have been averaged due to the incidence angle variation of 5 - 8 degree within the common antenna footprint of both polarizations. Still, across the footprint, the incidence angle dependence of the CPD is sufficiently linear so that no systematic errors are expected. For noise and speckle reduction, the copolar coherences of different azimuth-subsectors with the same incidence angle were averaged. The phase $\phi_{\mathrm{CPD}} = \phi_{\mathrm{VV}} - \phi_{\mathrm{HH}}$, obtained from the averaged coherence, is the CPD in the backscatter alignment convention as defined in Eq. (16).

4.5 SnowScat calibration

The measured radar signal was calibrated by an internal calibration loop of the SSI to compensate system drifts. However, some polarization dependent signal delay still originated from the connectors of the antenna feeding cables and from the antennas themselves due to the polarization-dependent beam-pattern. In order to calibrate external offsets and drifts, the CPD was calibrated with two metallic targets.

The primary calibration target was a metallic sphere with a diameter of 25 mounted on a wooden pole for the duration of the experiment. The sphere can be located in Fig. 5 next to the SSI. A secondary target, a metallic plate was located behind trees close to sector 2. A third calibration target, a dihedral reflector, was installed during the setup phase of the experiment. The correct pointing direction to locate the sphere was determined with a precision of $\pm 0.5°$ by 2-D-scans in elevation and azimuth. The 2-D-scans showed that a possible systematic error of the CPD, caused by imprecise alignment, can be estimated to be below $\pm 10°$.

The theoretical CPD measured from a sphere (or plate) is expected to be zero due to the target symmetry. The sphere was measured every four hours and was used as a reference during the whole duration of the experiment. The plate was installed from October 2011 until June 2013 and was used to validate the calibration done with the sphere. The CPD measured for a dihedral reflector should be $180°$. The dihedral reflector was measured once, on 9 December 2009, to verify the processing sequence of the SnowScat raw data.

The CPD determined for the sphere, $\mathrm{CPD}_{\mathrm{REF}}$, was used as a reference and was subtracted from the uncalibrated CPD measurementsof snow, $\mathrm{CPD}_{\mathrm{uncal.}}$, to obtain calibrated results:

$$\mathrm{CPD}_{\mathrm{cal.}}(f) = \mathrm{CPD}_{\mathrm{uncal.}}(f) - \mathrm{CPD}_{\mathrm{REF}}(f).$$

Phase unwrapping was performed for the uncalibrated CPD and the reference CPD if necessary.

To reduce the noise of the reference measurements as much as possible, the reference, $\mathrm{CPD}_{\mathrm{REF}}$, was determined as follows: Time series $\mathrm{CPD}_{\mathrm{REF}}(t)$ were obtained for 21 different frequencies in order to sample the entire frequency spectrum between 9.2 and 17.8 of the instrument. The time series were smoothed with a median filter of 4 which preserved phase jumps in the signal. After temporal filtering, a frequency-dependent 4th order polynomial was fitted over the measured frequency spectrum of each acquisition to provide some noise reduction in the frequency domain.

The reference data are shown for all four seasons in Fig. 21. The solid black line shows the (frequency-dependent) reference, $\mathrm{CPD}_{\mathrm{REF}}$, for $f = 13.5\,\mathrm{GHz}$. Individual measurements of the sphere as well as measurements of the metallic plate are shown as dark and light gray solid dots below the black line.

The CPD was calibrated using the sphere as a reference target. The upper panels show the reference, $\mathrm{CPD}_{\mathrm{REF}}(f)$, for $f = 13.5$ (solid line) together with individual CPD measurements for the sphere and the plate (light and dark gray dots). The CPD of the metallic plate agrees within the standard deviation with measurements of the sphere and with $\mathrm{CPD}_{\mathrm{REF}}$. Deviations were found for season 3 due to a misalignment of the SSI to the sphere, and for November 2012, possibly due to snow cover of the metallic plate. The lower panels show the deviation, $\Delta\mathrm{CPD} = \mathrm{CPD}_{\mathrm{meas.}}(f) - \mathrm{CPD}_{\mathrm{REF}}(f)$, for individual measurements at all measured frequencies $f = 10$–17. The deviation at a frequency of 13.5 is shown as black dots. The standard deviation (RMSE) of ΔCPD for the whole frequency spectrum is given below the legend of the lower panel.

In the third season, between 18 November 2011 and 20 January 2012, the pointing direction (elevation angle) to the sphere was misaligned by $2°$. Therefore, the reference CPD was corrected by a frequency dependent offset to keep the CPD continuous at the start and the end of the period of misalignment.

The deviation of the raw-data of the sphere from the reference, $\Delta\mathrm{CPD} = \mathrm{CPD}(f) - \mathrm{CPD}_{\mathrm{REF}}(f)$, is shown in the lower panels for each season as scattered dots for each of the 21 analyzed frequencies. The root-mean-square-error, RMSE, was below $4°$ for the full frequency spectrum and is given for each seasons next to the graph. The error of the reference, $\mathrm{CPD}_{\mathrm{REF}}(f)$, which includes systematic and statistic errors, is estimated to be below $15°$ CPD showed some systematic drifts, therefore a metallic sphere was used for calibration of the measurements. The calibration procedure is detailed in Appendix D.

4.5 Selecting valid acquisitions

Invalid acquisitions were removed before the analysis with the help of the calibration data. Acquisitions were classified as invalid if the CPD or the Radar Cross Section (RCS) of the reference targets (sphere, plate) deviated too far from the expected values or if the temporal trend of the sphere and the plate-target plate were not in agreement. In the two seasons before 18 November 2011, where the plate target was not installed yet, the sphere showed very stable results therefore the data was considered as valid. For sector 2, which was located between trees, some subsectors at the left and right hand side were disturbed by trees (Leinss et al., 2015, Fig. 3) and were therefore excluded from the analysis.

5 Analysis

In the following sections, four

4.1 Measurements: Four years of CPD time series

Four years of CPD time series ~~measurements and the derived anisotropies are presented. First, the CPD time series are discussed with respect to meteorological dataand snow characteristics. Then, the temporal evolution of the average anisotropy is derived from CPD and snow depth measurements. The CPD measurements at different incidence angles and frequencies are used together with the obtained anisotropy to validate the electromagnetic model. For three dates anisotropy measurements are compared with anisotropy data from computer tomography. The potential of CPD measurements for fresh snow detection is discussed. Finally, we compare the CPD measurements with satellite data and discuss if the underlying soil affects the CPD measurements and the anisotropy of snow.~~

4.2 ~~Time series of CPD~~

~~Four years of CPD time series~~ data, acquired by the SnowScat instrument between 2009 and 2013, are plotted in Figs. 6 – 9 together with meteorological ~~data. Shown are the meteorological parameters snow depth (~~measurements.

The upper panels of the figures show meteorological parameters (abbreviations are given in Table 1, locations are shown in Fig. 5). The snow depth measured by the three sensor SDAT1~~), air- and soil temperature (~~, AWS and MeteoMast are shown as dashed lines, the mean and standard deviation of the snow depth variability course "SDvar" is shown as errors bars. The blue solid line shows the average snow depth of SDAT1, AWS and MeteoMast. Air- and soil temperature of the sensor SDAT1 and SMT ~~) as well as soil moisture (sensor SMT) and snow density~~are plotted below the snow depth. The second panel shows soil moisture for two locations, each at 2 and 10 cm depth, measured by the sensors of SMT (brown). The snow density (solid black line) was determined by dividing SWE, as ~~determined in (Leinss et al., 2015)~~described in Sect. 4.2, by the snow depth measured by the sensor SDAT1. Manual density measurements obtained in the snow pit are ~~also shown~~ shown as black dots.

The ~~polarimetric radar measurements are plotted in the~~ lower panels of ~~Figs. 6–9.~~ the figures show the polarimetric radar measurements. The CPD ($= \phi_{VV} - \phi_{HH}$) measured by the SSI is plotted for different incidence angles ~~,~~ θ_0 (third panel), and frequencies ~~,~~ f (forth panel). The lowest panel shows the co-polar coherence $\gamma_{VV,HH}$ for three different frequencies and the highest incidence angle $\theta_0 = 60°$.

The dark gray shading ~~in Figs. 6–9~~ for April and May in the figures indicates the period of snow melt~~in April and May~~. Snow free conditions are indicated by a light gray shading in autumn and May/June. In the following paragraphs we summarize the main characteristics of the measurements observed during the four winter seasons.

A common characteristic ~~which was~~ found in all four seasons ~~was~~ is a rising CPD during snow fall. The CPD reached its maximum typically a few days after snowfall ended. ~~During~~ The opposite trend, a gradually decreasing CPD during periods of cold temperatures without much fresh snow, ~~the CPD decreased gradually,~~ can be observed as long as temperatures were well below 0 °C. During snow melt, the CPD ~~was~~ is close to zero as the penetration of microwaves into the wet snow pack is inhibited. Soil moisture correlates well with snow melt, but does not show any influence on the CPD, even when the soil was not frozen in early winter.

The copolar coherence, $\gamma_{VV,HH}$, is shown for the highest incidence angle ($\theta_0 = 60°$) where it is most sensitive to volume scattering. During dry snow conditions, $\gamma_{VV,HH}$ ranges from 0.4 to 0.7 ~~(depending on frequency)~~with lower values for higher frequencies. Only at 16.8 GHz at 60° the coherence was found to be lower during winter (≈ 0.4) compared to snow free conditions (~~$\gamma_{VV,HH} \approx 0.5 \ldots 0.6$~~ $\gamma_{VV,HH} \approx 0.55$, horizontal dashed line "no snow"), which indicates some weak scattering in the snow volume. The highest values of $\gamma_{VV,HH} = 0.7 \ldots 0.8$ were measured during snow melt, where the microwave penetration depth is very weak (a few cm) and scattering occurs at the snow surface. After all snow has melted, the coherence decreased to $\approx 0.5 \ldots 0.6$ ~~and~~ as some volume scattering occurs at the low vegetation.

4.2 Interpretation of CPD measurements with respect to snow conditions

The four analyzed winter seasons showed quite different snow conditions. In the following~~paragraphs~~, we provide an interpretation of the measured CPD time series with respect to snow properties which were observed in the field and which were documented in ~~?, p. 399(49)~~Lemmetyinen et al. (2013, p. 425/49).

The winter of 2009–2010 was characterized by mild temperatures until mid of December which caused ~~a~~ delayed freezing of the soil compared to average years. Snow accumulation happened gradually and the mild temperatures lead to larger snow densities of 0.2 g cm^{-3} in early winter compared to other years. Due to warm temperatures, depth hoar was largely absent and melt-refreeze events in early December caused the formation of a crust ~~at the bottom of the snow pack~~ in the shallow snow pack which was later covered by snow. Later in winter, two major snow fall events occurred. The first happened during early February after which the CPD increased by more than 50° but decreased quickly due to strong temperature gradients causing a fast metamorphism into vertical structures. The second major snow fall occurred during the night from 2 to 3 March 2010, where a fast rise in temperatures together with 20 mm precipitation caused ~~strong~~ some snow settling. ~~Consequently~~ Despite additional fresh snow of low density, a slight increase in snow density can be observed in Fig. 6. The settling caused an abrupt increase of the CPD of about 20° ~~happened~~ during the night, followed by a total increase of more than 50° within the 5 following days. Snow settling and collapse of weak layers are discussed

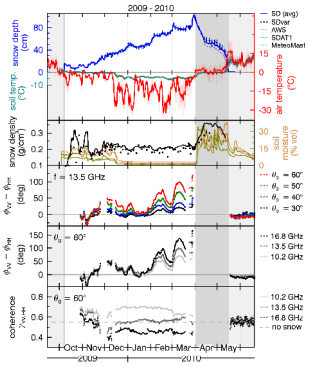

Figure 6. Winter season 2009–2010. Top ~~three~~ panels: Meteorological data measured by the sensors ~~SDAT1 and SMT; snow density as~~ described in Sect. 4.1. Bottom: CPD and copolar coherence measured by the SSI for different incidence angles and frequencies. The dark gray shading shows snow melt.

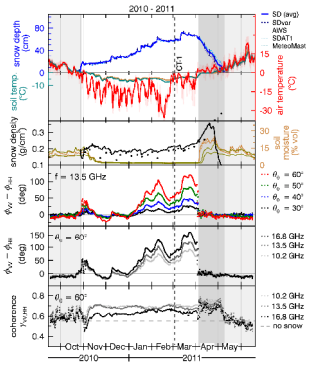

Figure 7. Winter season 2010–2011. Meteorological and radar data as shown in Fig. 6 and described in Sect. 4.1. The vertical dashed line shows the date when the profile CT-1 was acquired.

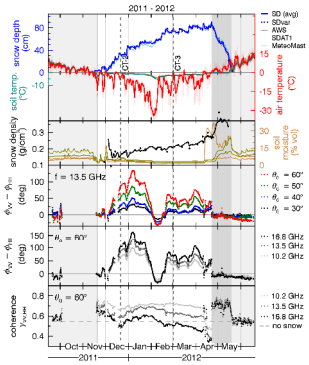

Figure 8. Winter season 2011–2012. Meteorological and radar data as shown in Fig. 6 and described in Sect. 4.1. Two vertical dashed lines shows the date when the profiles CT-2 and CT-3 were acquired.

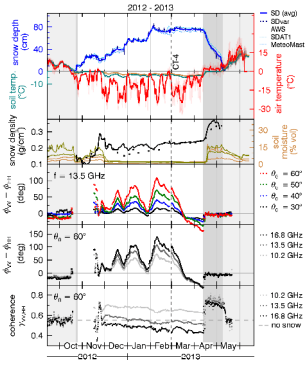

Figure 9. Winter season 2012–2013. Meteorological and radar data as shown in Fig. 6 and described in Sect. 4.1. The vertical dashed line shows the date when the profile CT-4 was acquired.

with respect to the "SnowScat anomaly on 2/3 march 2010" in Lemmetyinen et al. (2013, p.214 - 240). Our observations support their arguments, as a strong increase of the CPD is related to fresh snow, snow settling and a possible collapse of weak layers with vertical structures.

The winter of 2010–2011 was characterized by very cold temperatures and a relatively thin snow cover. The strong temperature gradients lead to a distinct layer of depth hoar. The slightly negative CPD in December indicates a weak vertical anisotropy in the snow pack. From January until March, the CPD increased with snow fall but was disrupted by a period of very cold temperatures in February during which the CPD decreased by 50°.

The winter of 2011–2012 was characterized by initially exceptionally mild temperatures and late but intense snow fall during December. The weak temperature gradient from mid December until mid January caused almost no ~~recrystallization~~ metamorphism into vertical structures. Therefore, a thick layer of horizontally oriented, settled fresh snow was preserved and a maximum CPD of $+135°$ was observed at 7 January, 9 days after 20 cm of fresh snow. Almost no depth hoar was observed due to the insulating effect of the thick snow pack. The extremely large phase differences disappeared relatively quickly during very cold air temperatures between -15 and $-35\,°C$ in the second half of January ~~and early February and~~ until mid February where the CPD even changed sign, so that a minimum CPD of $-30°$ was observed at 9 February. After various snowfall events, the negative phase differences disappeared. At 12 April, the snow surface melted and refroze afterwards. A significant drop in the copolar coherence below snow free values (Fig. 8) indicates increased volume scattering or even residual melt water in the snow pack. A change in the backscatter pattern observed in Leinss et al. (2014a, Fig. 9) supports the observation of increased volume scattering. During the time around 12 April, when the snow surface was wet snow, the CPD dropped for a few days to zero but recovered afterwards during a short period of negative temperatures before snow melt.

The winter of 2012–2013 was again characterized by very mild temperatures but early and heavy snowfall during November, followed by three additional major snowfall events, which caused a very clear peak-like signal in the CPD. The peaks appear a few days after snow fall ended which indicates that settling of fresh snow is responsible for an increase of the CPD. In February, after the last heavy snow fall, a CPD of more than $+100°$ was reached. From March until mid April, no snow fall was present and low temperatures caused a strong ~~recrystallization~~ metamorphism for a period of 6 weeks, after which a minimum CPD of $-60°$ was observed. With the onset of snow melt, the CPD jumped to zero due wet snow and the resulting ~~weak~~ small microwave penetration depth.

5 Analysis

5.1 Estimation of the average anisotropy of snow

The developed electromagnetic model ~~from Sect. ??~~ in Sect. 2 and 3 is free of fit-parameters. Therefore, the ~~measured copolar phase~~, copolar phase difference, measured and averaged over all azimuth subsectors, $\mathrm{CPD}_{\mathrm{meas.}}$, can be inverted with the additional information of snow depth and a good approximation of snow density (as discussed at the end of Sect. 3.3) to get a CPD-based estimate for the depth-average anisotropy ~~$A^{\mathrm{CPD}}_{\mathrm{avg}}$~~, $A^{\mathrm{CPD}}_{\mathrm{avg}}(t,\theta_0,f)$.

~~The average anisotropy can be estimated, because the CPD shows only a weak density dependence for the density range of seasonal snow (Bormann et al., 2013). Between densities of 0.15 and 0.4, the CPD varies by less than 20 as shown by Fig. 3a.~~

For the analysis in this section, we assumed that the snow pack ~~observed at different incidence angles~~ consisted of a single layer with ~~constant anisotropy A. Equation (21) can then be used to model the CPD for a given~~ a constant anisotropy. We further assumed that the snow properties (depth, density, anisotropy and also scattering properties of the underlying soil) do not vary spatially across the test site so that we can compare measurements done with different incidence angles and with different antenna footprints. The measurements of the snow depth variability course, SDvar, and the careful preparation of the test site's surface support these assumptions. The area observed by the SSI covers the center of the forest clearing such that variations of snow properties due to a proximity to trees should be negligible (this is only true for sector 1, not for sector 2 located between trees). A variable snow depth due to wind drifts is unlikely, as the test site is sufficiently protected by wind due to the surrounding trees of the forest clearing (Fig. 5).

The depth-average anisotropy, $A^{\mathrm{CPD}}_{\mathrm{avg}}$, is estimated from Eq. (21) using $\mathrm{CPD}_{\mathrm{meas.}}$ for the radar system parameters (microwave frequency f, incidence angle θ_0~~,~~). The required in-situ measured parameters snow depth ΔZ ~~, and snow density ρ.~~ (from SDAT1), and the depth-average snow density ρ_{avg} as shown in Figs. 6 – 9. A sketch of the processing chain to determine the anisotropy is shown in the block diagram in Fig. 10. The ice volume fraction $f_{\mathrm{vol}} = \rho_{\mathrm{avg}}/\rho_{\mathrm{ice}}$ follows from snow density. For every measurement time t, the depth-averaged, CPD-based estimate ~~$A(\theta_0, f)$ follows for each incidence angle θ_0 and frequency f~~ $A^{\mathrm{CPD}}_{\mathrm{avg}}(t,\theta_0,f)$ follows by minimization of the difference

$$\left|\mathrm{CPD}_{\mathrm{meas}}(t,\theta_0,f) - \mathrm{CPD}_{\mathrm{model}}(A_{\mathrm{avg}}(\theta_0,f,t)|, \theta_0, f)\right|. \tag{24}$$

~~The estimated anisotropy, $A^{\mathrm{CPD}}_{\mathrm{avg}}(t)$, for a given time is then computed by averaging the estimated values $A(\theta_0, f)$ over all incidence angles and frequencies. The standard deviation for each time follows directly from the difference between $A^{\mathrm{CPD}}_{\mathrm{avg}}(t)$ and the estimates $A(\theta_0, f)$ for each θ_0, and f.~~

~~The input parameters to estimate $A^{\mathrm{CPD}}_{\mathrm{avg}}(t)$ are snow depth and density as shown in~~ with respect to $A \in [-1,1]$. CPD time series at 16 different frequencies between 10 and 17 GHz and at four different incidence angles were evaluated in Eq. (24), a few of them are shown in the Figs. 6 – 9. ~~Radar measurements $\mathrm{CPD}_{\mathrm{meas}}(t,\theta_0,f)$ at 16 different frequencies between 10~~ Anisotropy values of all frequencies but only anisotropy values determined for the three larger incidence angles $\theta_0 = 40,\ 50,$ and ~~17 were used. For estimation of~~ $60°$ were later averaged to determine $A^{\mathrm{CPD}}_{\mathrm{avg}}(t)$ ~~we used only three incidence angles $\theta_0 = 40 \ldots 60°$,~~, since the CPD measurements with the smallest incidence angle ($\theta_0 = 30°$) showed the highest sensitivity to calibration errors ~~and other uncertainties.~~

~~The processing chain to determine the anisotropyis shown in the block diagram in Fig. 10. Time series of the estimated anisotropy are shown in Fig. 11.~~. The estimated anisotropy, $A^{\mathrm{CPD}}_{\mathrm{avg}}(t)$, was therefore determined from $48 (= 16 \times 3)$ estimates $A^{\mathrm{CPD}}_{\mathrm{avg}}(t,\theta_0,f)$. The standard deviation for each time t is determined by the scatter of all $64\ (= 16 \times 4)$ estimates $A^{\mathrm{CPD}}_{\mathrm{avg}}(t,\theta_0,f)$ around their average $A^{\mathrm{CPD}}_{\mathrm{avg}}(t)$. The average standard deviation of $\sigma_A \approx 0.005$ is well below the range of the obtained anisotropy between -0.05 and $+0.2$. The standard deviation varies with snow depth and is shown as a gray bar below the anisotropy.

Time series of the estimated anisotropy $A^{\mathrm{CPD}}_{\mathrm{avg}}(t)$ are shown in Fig. 11. The largest positive anisotropy $A^{\mathrm{CPD}}_{\mathrm{avg}} \approx +0.2$ was found for Dec 2011 after intense snow fall and while temperature gradient metamorphism was very weak. The largest negative anisotropies were found for Nov 2010 ($A^{\mathrm{CPD}}_{\mathrm{avg}} \approx -0.06$) where strong temperature gradients in the thin snow pack were present. Large negative anisotropies were also found in Feb 2012 ($A^{\mathrm{CPD}}_{\mathrm{avg}} \approx -0.05$) and April 2013 ($A^{\mathrm{CPD}}_{\mathrm{avg}} \approx -0.05$) after periods of very cold temperatures without precipitation. As $A^{\mathrm{CPD}}_{\mathrm{avg}}$ is the depth-averaged anisotropy of positive and negative values much larger

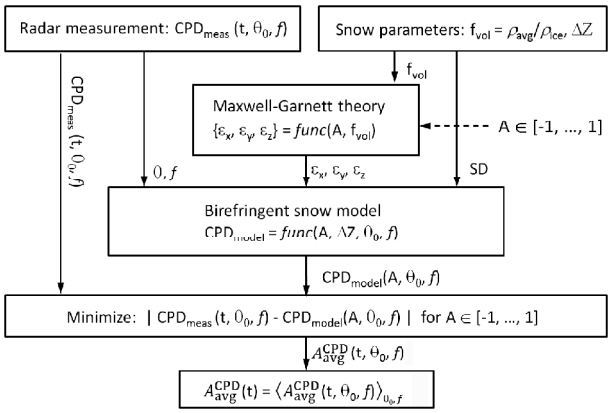

Figure 10. Processing chain used to estimate the average anisotropy of the snow pack, $A_{\mathrm{avg}}^{\mathrm{CPD}}$. The anisotropy can ~~iteratively~~ be estimated from the measured CPD, by minimizing the difference between modeled and measured data with respect to A if snow depth ΔZ and the ice volume fraction f_{vol} are known. The anisotropy ~~A~~ $A_{\mathrm{avg}}^{\mathrm{CPD}}(t, \theta_0, f)$ was calculated independently for all incidence angles, θ_0, and frequencies, f, and the results were averaged to obtain $A_{\mathrm{avg}}^{\mathrm{CPD}}(t)$.

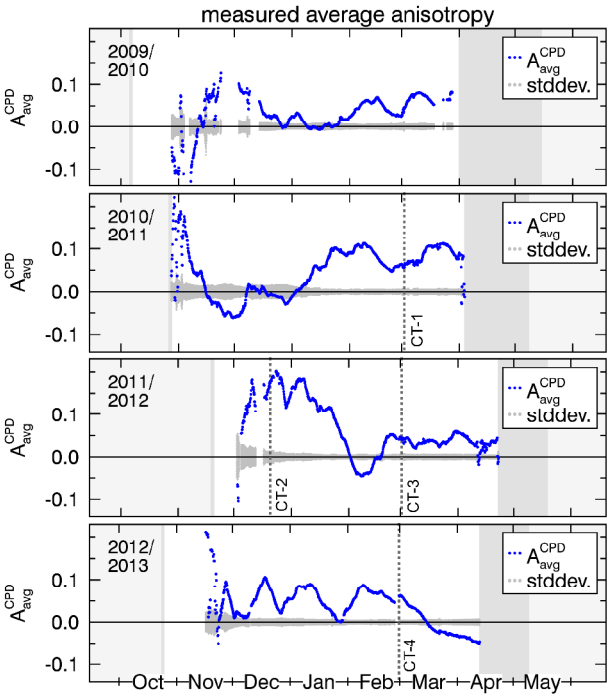

Figure 11. Average anisotropy of the snow pack, $A_{\mathrm{avg}}^{\mathrm{CPD}}$, determined during dry snow conditions for the winter seasons from 2009–2013. The anisotropy was derived from the CPD ~~which was~~ measured by the SnowScat instrument. The standard deviation of $A_{\mathrm{avg}}^{\mathrm{CPD}}$, calculated from measurements at different frequencies and incidence angles, is shown as the time-varying gray bar below the anisotropy. The dark-gray shading in April/May indicates the period of snow melt, the light-gray shadings ~~in~~ (Oct./Nov.~~and~~, May/June) indicate snow free conditions. The four dashed vertical lines show the times when the anisotropy was measured by computer tomography (CT-1, ~~CT-2~~ 2, ~~CT-3~~ 3, and 4).

anisotropies are expected to be found in individual layers (see Sect. 5.3 and Fig. 16).

While discussing the structural anisotropy of snow which has been derived from dielectric anisotropy it seems relevant to recall that single ice crystals also show a birefringence. Fujita et al. (2014) reported that the dielectric anisotropy due to oriented crystal fabrics is often much lower than dielectric anisotropy expected from a structural anisotropy. In appendix A we used the fabric measurements in snow from Riche et al. (2013) to estimate a maximum dielectric anisotropy of $\Delta\epsilon = -0.002$ which corresponds to a structural anisotropy of $A = -0.02$. This is small compared to the measurements shown in Fig. 11 and confirms therefore the statement of Fujita et al. (2014). It is worth to note, that the dielectric anisotropy due to the vertical crystal orientation of fresh snow has the opposite sign as the dielectric anisotropy due to the horizontal structural anisotropy of fresh snow.

5.2 Incidence angle and frequency dependence

The larger the incidence angle, the better are the vertically polarized microwaves aligned with the optical axis of ~~anisotropic snow~~ birefringent snow pack. The CPD must therefore increase with increasing incidence angle. This has already been observed in the CPD time series plotted for different incidence angles in the middle panel of Figs. 6–9.

The electromagnetic model presented in Sect. ~~??~~ 3 predicts a nonlinear incidence angle dependence due to refraction in the snow pack (Fig. 3, left). To verify the nonlinear incidence angle dependence, we selected five dates spread over the four winter seasons to cover the maximum available range of CPDs. For each date we used the measured snow density ~~, ρ , and the~~ and snow depth ΔZ together with the averaged CPD-based anisotropy, $A_{\mathrm{avg}}^{\mathrm{CPD}}$, to model the expected incidence angle dependence. A comparison of modeled and measured incidence angle dependence is shown in Fig. 12 (left) for the five selected dates.

The CPD is modeled to be proportional to the depth of a snow pack which is transparent for microwaves. The deeper the snow and the higher the frequency, the more wavelengths "fit" ~~into the~~ in the propagation path length through the snow volume and the higher is the expected phase difference. This frequency dependence is described by Eq. (21) which shows a linear frequency dependence ($\propto \lambda^{-1}$). Larger CPD values were indeed measured for higher frequencies as it is shown for $f = 10.2$, 13.5 and 16.8 GHz in the 2nd-last panel of Figs. 6–9. For a more quantitative insight, we plotted the CPD measured for 16 different frequencies in Fig. 12 (right). The CPD was plotted for the same five dates

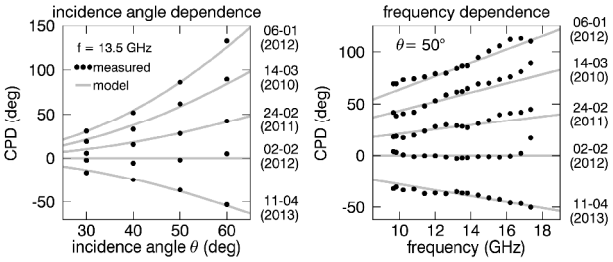

Figure 12. Left: incidence angle dependence of measured CPD vs. modeled incidence angle dependence. Right: frequency dependence of measured CPD vs. modeled linear frequency dependence.

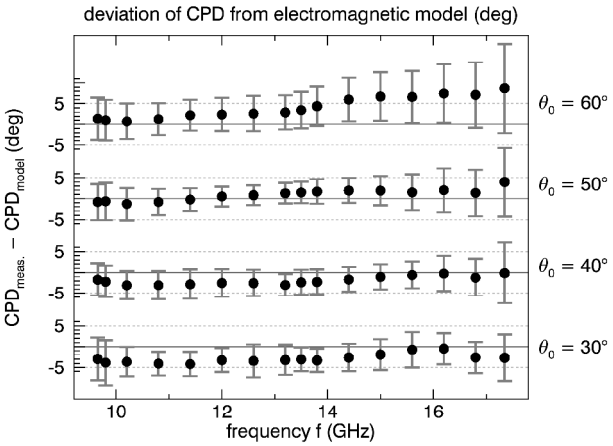

Figure 13. Deviation of measured and modeled CPD for different frequencies f and different incidence angles θ_0. Dots show the mean deviation $\mathrm{CPD}_{\mathrm{meas.}} - \mathrm{CPD}_{\mathrm{modeled}}$ of all data acquired during dry snow conditions. The error bars are the standard-deviations calculated from about 5600 measurements.

shown in Fig. 12 (left). As expected, the CPD shows approximately a linear dependence on frequency.

In order to get a better quantitative measure how well the electromagnetic model fits to ~~the~~ measured data, we did a statistical analysis and compared the modeled phase difference, $\mathrm{CPD}_{\mathrm{model}}(A^{\mathrm{CPD}}_{\mathrm{avg}}(t), \theta_0, f)$, according to Eq. (21), with the measured phase difference, $\mathrm{CPD}_{\mathrm{meas.}}(t, \theta_0, f)$. The mean deviation, as well as the standard deviation of $\mathrm{CPD}_{\mathrm{model}} - \mathrm{CPD}_{\mathrm{meas.}}$, were calculated over all acquisitions acquired during dry snow conditions separately for each incidence angle θ_0 and for each frequency f.

The mean deviation is plotted over frequency and for each incidence angle in Fig. 13. The error bars indicate the standard deviation. The mean deviation is about $\pm 4°$ (black dots in Fig. 13) and is almost always within the standard deviation (error bars). Only for $\theta = 60°$ and $f > 14\,\mathrm{GHz}$, we measure larger deviation up to $+8°$. Figure 13 shows that neither large deviations from the expected incidence angle dependence nor large deviations from the linear frequency dependence

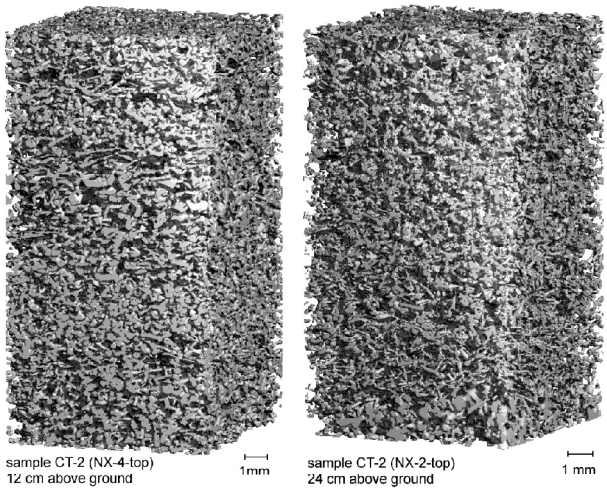

Figure 14. Two samples from the profile ~~CT-1~~ CT-2 (21 December 2011) taken ~~at a depth of~~ 12 cm (left) and 24 cm (right) above ground. Horizontal structures are clearly visible in the left image but can also be identified in ~~both images~~the right image. The CT-based average anisotropy ~~derived for~~ of the two samples are $A^{\mathrm{CT}}_{\mathrm{avg}} = +0.26$ (left) and $+0.16$ (right). The vertically resolved anisotropy, A_{CT}, determined every 2 mm depth by means of μCT, ~~are~~ is plotted in Fig. 16 (top ~~left~~right) for both samples as blue dots.

were found. The deviations of $\mathrm{CPD}_{\mathrm{meas}}$ from the $\mathrm{CPD}_{\mathrm{model}}$ are within the estimated calibration accuracy of $\pm 15°$.

As measured and modeled data agree within a few degree, we conclude that our electromagnetic model is able to explain the observed CPD by considering snow as an optically anisotropic medium. The linear dependence on frequency confirms our assumption that the CPD is a volumetric property of snow.

5.3 Validation with computer tomography

For validation we compared the CPD-based estimates ~~$A^{\mathrm{CPD}}_{\mathrm{avg}}$~~ $A^{\mathrm{CPD}}_{\mathrm{avg}}(t_i)$ to tomography based estimates ~~$A^{\mathrm{CT}}_{\mathrm{avg}}$~~ $A^{\mathrm{CT}}_{\mathrm{avg}}(t_i)$ obtained from in-situ snow measurements. The ~~dates~~four dates t_i, when the samples for computer tomography analysis were taken from the ~~three~~ four snow pits, CT-1~~, CT-2, and CT-3, are indicated~~ . . .CT-4, are indicated as dashed vertical lines in Figs. ~~8,~~ 7 - 9, and also in Fig. 11~~as dashed vertical lines. Four examples of~~ . Two examples of the 3-D images ~~of snow samples of about 2 height~~ obtained by computer tomography are shown in Figs. 14 and 15.

In order to obtain the anisotropy from the computer tomography data, the binary 3-D images were analyzed by means of spatial correlation functions according to Löwe et al. (2011). Exponential correlation lengths, $p_{\mathrm{ex},x}$, $p_{\mathrm{ex},y}$, and $p_{\mathrm{ex},z}$, were derived from the correlation functions as described by Mätzler (2002). The anisotropy determined by computer tomography, A_{CT}, is defined analogue to Eq. (1).

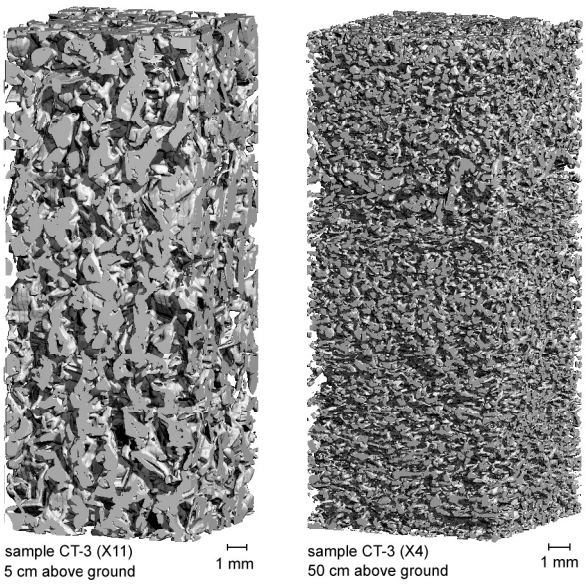

Figure 15. Two samples from the profile ~~CT-2~~ CT-3 (1 March 2012). The left profile, taken 5 cm above ground, shows old ~~recrystallized~~ metamorphic snow (depth hoar) with vertical structures ($A_{\mathrm{avg}}^{\mathrm{CT}} = -0.24$). The profile on the right, taken 50 cm above ground, shows horizontal structures ($A_{\mathrm{avg}}^{\mathrm{CT}} = +0.35$) of fresh, settled snow which fell two weeks before the sample was taken. The vertically resolved anisotropy, A_{CT}, determined every 2–5 mm depth by means of μCT, are plotted in Fig. 16 (top right) for both samples as blue dots.

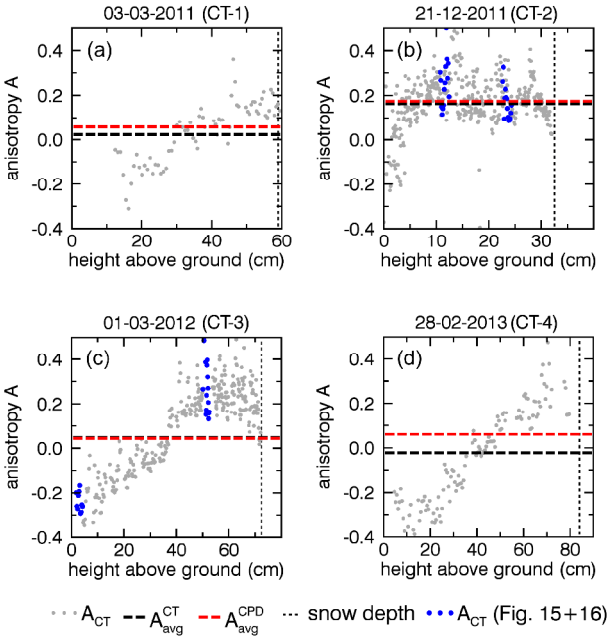

Figure 16. Vertical profiles of the anisotropy, A_{CT}, determined from computer tomography. For comparison, we plotted in each graph horizontal lines which show the depth-averaged anisotropies, $A_{\mathrm{avg}}^{\mathrm{CT}}$ together with the average anisotropy, $A_{\mathrm{avg}}^{\mathrm{CPD}}$, determined from the radar data (Fig. 11). ~~Top-left~~(a): the profile CT-1 shows 30 cm of old snow with vertical structures from Nov./Dec. 2010 which is covered by metamorphic snow which fell from mid January to early February 2011 (see Fig. 7) (b): the profile CT-2 shows homogeneously distributed positive anisotropies which result from heavy snow fall during mild temperatures in December 2011 (see Fig. 8). ~~Top-right~~(c): ~~The~~ the profile ~~CT-2~~ CT-3 shows a thick layer with vertical structures of ~~recrystallized~~ metamorphic snow in the lower ~~35~~40 cm of the snow pack. In the upper ~~35~~40 cm horizontal structures are visible which result from fresh snow fall mid of February 2012 (see Fig. 8). ~~Bottom-left~~(d): alternating snow fall and cold temperatures lead to an almost linearly increasing anisotropy in the ~~end of~~ profile CT-4 from late February 2013 (see Fig. 9).

Due to the symmetry in the x and y direction, $p_{\mathrm{ex},x}$ and $p_{\mathrm{ex},y}$ were averaged:

$$A_{\mathrm{CT}} = \frac{(p_{\mathrm{ex},x} + p_{\mathrm{ex},y}) - 2p_{\mathrm{ex},z}}{\left[\frac{1}{2}(p_{\mathrm{ex},x} + p_{\mathrm{ex},y}) + p_{\mathrm{ex},z}\right]}. \quad (25)$$

The anisotropy was determined for the entire snow profile with a vertical resolution of 1–2 mm, depending on snow grain size~~, for the entire snow profile~~. The obtained anisotropy profiles are shown in Fig. 16. For comparison, we added horizontal lines, which show the average anisotropy, $A_{\mathrm{avg}}^{\mathrm{CT}}$, determined from computer tomography and the average anisotropy, $A_{\mathrm{avg}}^{\mathrm{CPD}}$, determined from the CPD.

~~For the first two profiles,~~ The first profile shown in Fig. 16 (CT-1~~and~~) shows a slightly larger anisotropy, $A_{\mathrm{avg}}^{\mathrm{CPD}} = 0.05$, compared to the average anisotropy derived from the CT data, $A_{\mathrm{avg}}^{\mathrm{CT}} = 0.023$. For the profile CT-1 only a limited number of data points was available with missing data from the lowest 10 cm. However field observations shows depth hoar for the bottom 10 cm indicating that $A_{\mathrm{avg}}^{\mathrm{CT}}$ should even be smaller.

For the second and third profiles, CT-2 ~~,~~and CT-3, many CT data point were available and the difference in anisotropy is remarkably small and agrees within values of ~~+0.008~~ +0.008 and −0.004, or +4 and −8 % ~~. However, for the third profile, CT-3~~relative to the anisotropy measured by CT of $A_{\mathrm{avg}}^{\mathrm{CT}} = +0.16$ and $+0.05$.

For the forth profile, CT-4, a larger difference of +0.08 was observed ($A_{\mathrm{avg}}^{\mathrm{CT}} = -0.02$, $A_{\mathrm{avg}}^{\mathrm{CPD}} = +0.06$). The difference might originate from a very sparse sampling of the top snow layers (~~see~~ Fig. 16, bottom ~~left~~right), as taking samples was difficult due to soft fresh snow. No samples could be taken from the top 4 cm. ~~We~~

For CT-4, we can exclude limited penetration as a reason for the difference, despite occurring warm temperatures a few days before, because the copolar coherence (Fig. 9) and the temporal coherence (Leinss et al., 2015, Fig. 19) did not show any anomaly. However, we can not exclude the fact, that the assumption of oriented spheroids in our model is

a too strong assumption for the very dendritic shape of fresh fluffy snow.

The vertical structure of the anisotropy profiles agrees to our expectation regarding the meteorological conditions as described in the caption of Fig. 16. In the anisotropy profiles vertical structures were found in the older snow layers, as it is ~~expect for snow recrystallized by temperature gradient metamorphism~~expected for the geometry of metamorphic snow which was exposed to temperature gradients. In contrast to the old layers, the top layers show horizontally aligned structures as we expect it to be the case for fresh snow. The fact, that fresh snow is related to horizontal structures and therefore to a positive CPD, makes it possible to use the CPD for detection of fresh snow.

5.4 Correlation between fresh snow and a positive CPD

The settling of ~~snow has been shown to be responsible for~~ new snow at intermediate times can cause an increasingly positive anisotropy due to the horizontal alignment of dendrite backbones (Löwe et al., 2011). According to our theory, increasing anisotropies cause an increase of the CPD. This makes it possible to use a change in CPD to detect fresh snow as done in ~~?~~ Leinss et al. (2014b) using satellite data. ~~However,~~

As fresh snow settles within a few days after deposition, it is expected that the CPD does not increase simultaneously with the accumulation of fresh snow, but increases with a time-lag τ ~~as the snow first has to settle until an increased CPD can be observed. Further, the CPD decreases during periods of cold temperatures due to temperature gradient metamorphism. Therefore an increase of the CPD is not expected to be exactly proportional to an increase in snow depth~~after snow fall. The parameter τ characterized the time shift between snow fall and an increase of the anisotropy. A value $\tau \approx 0$ indicates that the CPD increases instantaneously with snow fall, whereas $\tau > 0$ gives an approximation for the time delay after which the growth of vertical structures driven by a temperature gradient exceeds the growth of a horizontal anisotropy due to settling. For too large temporal offsets between a change of snow depth (SD) and a change of the CPD, no correlation is expected as temperature gradient metamorphism dominates the evolution of the CPD.

In ~~this section~~ the following, we analyze the correlation between ~~fresh snow~~ changes in snow depth ΔSD and a change in CPD, ΔCPD. The correlation is defined as

$$R = \mathrm{corr}\{\mathrm{CPD}(t+\tau) - \mathrm{CPD}(t+\tau-\Delta T), \\ \mathrm{SD}(t) - \mathrm{SD}(t-\Delta T)\}, \quad (26)$$

where SD is the measured snow depth, τ the temporal offset between both time series as explained above, ΔT the sampling interval, and R is the Pearson-correlation coefficient. The ~~time~~ sampling invertal ΔT is the time difference between two measurements ~~and~~ of snow depth and CPD. ΔT

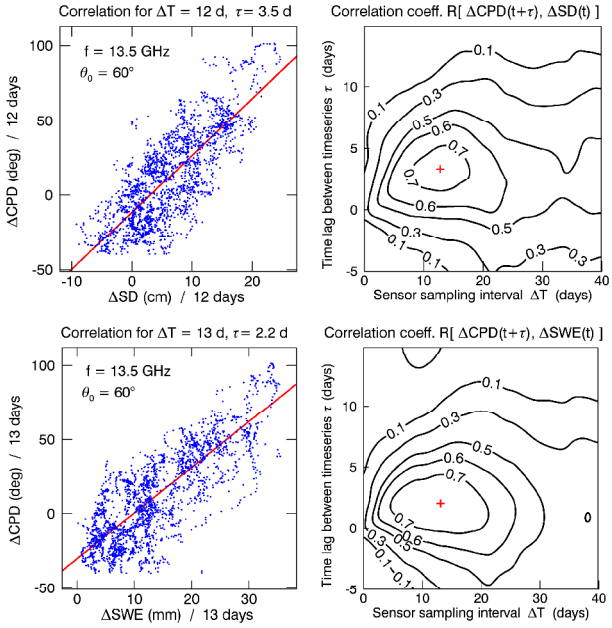

Figure 17. Left: correlation between ΔCPD and changes in snow depth ΔSD (top) and ΔSWE (bottom) within a sampling interval of $\Delta T = 12$ and 13 days. The time when the CPD difference was obtained, $t+\tau$, was shifted by $\tau = 3.5$ days (top) and $\tau = 2.2$ days (bottom) vs. the time t when the snow depth difference ΔSD was obtained because the maximum CPD was always observed when fresh snow has already settled. Right: Pearson-correlation coefficients R for different pairs of ΔT and τ shown as contour plots. The pair $(\Delta T, \tau)$ with the highest correlation coefficient is marked by a red cross.

corresponds e.g. to the repeat time of satellite acquisitions. The sampling interval ΔT needs to be large enough in order to give fresh snow some time for settling such that the CPD increases above the level of phase noise. However, the sampling time should not be too large, as minor snow fall events might be missed, and also snow metamorphosis will reduce measured values of ~~the~~ positive CPD changes ~~which~~ as they are typical for fresh snow fall.

The scatter plot in Fig. 17 (top) shows the correlation between the depth of fresh snow within 12 days and the corresponding change in CPD measured with a time-lag of 3.5 days. The scatter plot is shown for the best correlation, $R = 0.75$, which was found for different values of ΔT and τ. The correlation coefficient R is shown for all tested values of Δt and τ in the contour plot of Fig. 17 (top right). The red cross marks the pair with the highest correlation coefficient.

The range of optimal sampling intervals, ΔT, can be derived from the contour plot shown in Fig. 17. The plot shows that the optimal ΔT is between 9 and 15 days. We analyzed all frequencies and incidence angles and the best correlation coefficients, which ranged between 0.65 and 0.75,

were always found for $\Delta T = 11 \pm 3$ days and a time-lag of $\tau = 3.0 \pm 0.5$ days.

The optimal sampling interval ΔT matches the 11 day orbit repeat time of TerraSAR-X. Using time series of TerraSAR-X, a CPD change of $+10$ to $+15°$ per 10 cm of fresh snow was observed at 9.65 GHz at an incidence angle of 33° (?)(Leinss et al., 2014b). From these results we would expect that the CPD changes by 40–60° at the central frequency of the SSI of 13.5 GHz at $\theta_0 = 60°$. Here we observed a change in CPD of 38° per 10 cm of fresh snow at 13.5 GHz which fits well with respect to the uncertainty $R = 0.74$ of Fig. 17 (top left).

The availability of accurate time series of the SWE measurements published in Leinss et al. (2015) made it also possible to check if a correlation exists between ΔSWE and ΔCPD. The lower two graphs of Fig. 17 show an example for the correlation. The best correlations ($R \approx 0.65 \ldots 0.8$) were found for a sampling interval of $\Delta T = 10 \pm 3$ days with a time-lag of $\tau = 2.2 \pm 0.3$ days. The correlation with ΔSWE is slightly better compared to the correlation with ΔSD.

5.5 Comparison with satellite data

The CPD observed by the ground-based SnowScat instrument could also be measured from space with the satellite TerraSAR-X (TSX). Spatial and temporal correlations between the CPD and snow depth were published by ?Leinss et al. (2014b). Fig. 18 compares phase differences measured by TSX for the two seasons 2011–2012 and 2012–2013. The space-borne measurements show the same trends as the ground based measurements. However, the phase differences observed by TSX are about a factor 2 smaller than the CPD measured with the SSI (scatter plot in Fig. 18). The reason is very likely, that the TSX data were obtained from large open areas. In the large areas about 30% less snow depth was measured (cf. Fig. 3 in ?Leinss et al., 2014b), probably due to a stronger wind exposition compared to the more wind-protected forest clearing, where the SSI was located. Wind might also be a reason for disturbed snow settling as wind drifted snow crystals show a different microstructure than undisturbed settled snow. The lower snow depth and the stronger wind exposition might explain, why smaller phase differences were measured. Some residual vegetation and trees which were contained in the large areas observed by TSX, also decreased the measured CPD due to spatial averaging.

5.6 Effect of underlying soil

Sector 2, as shown in Fig. 5, was covered with an metallic mesh by August 2011 to isolate purely snow specific radar signatures from effects of the underlying soil. In the winter 2011/12 strong ice built up on the mesh causing high backscattering. However, we did not observe any effect on the CPD , and the data of both sectors agree very well (Fig.

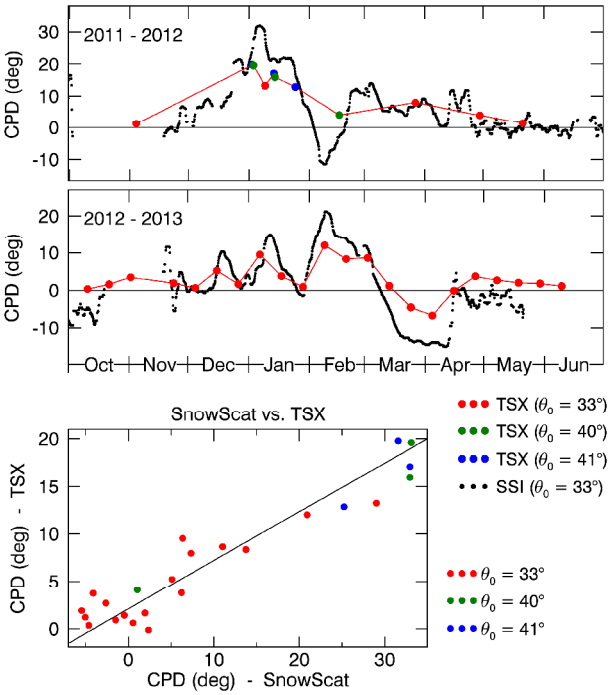

Figure 18. CPD measured by TerraSAR-X (TSX) at $\theta = 33$, 40, and 41° in comparison with measurements of the compared to SnowScat instrument (SSI) measurements ($f = 9.65$ GHz, interpolated to $\theta = 33°$). The measurements of both Both instruments show the same trend (top) but the CPD measurements of the SSI are about a factor of 2 larger than the TSX measurements (bottom). The discrepancy can be explained by different snow conditions as the TSX data were acquired over large open areas , where about 30% less snow depth was measured, compared to the test site of the SSI.

19, middle). To prevent the build up of an ice crust in the next season, the mesh was cleared from ice on 10 December 2012. 12 December 2012 (vertical dashed line). The removal of the ice crust in the season 2012/13 did again not much affect the measured CPD, and no large differences between the soil sector and the mesh-sector were found. We could speculate, that slightly larger CPD values measured between January and April 2013 might indicate the missing of a layer of vertical oriented depth hoar crystals, but the deviation could also originate from slightly different snow conditions of the two sectors. Still, the good agreement between the measurements of the soil sector and the measurements from the metallic mesh confirms again that the measured CPD is almost purely a signal resulting from the snow volume. Whereas Although the CPD signal is caused by the snow volume, temperature gradient metamorphism alters the anisotropy of snowand . As the temperature gradient is partially determined by the temperature of the underlying soil there exists an indirect effect of the soil energy balance to the evolution of the CPD.

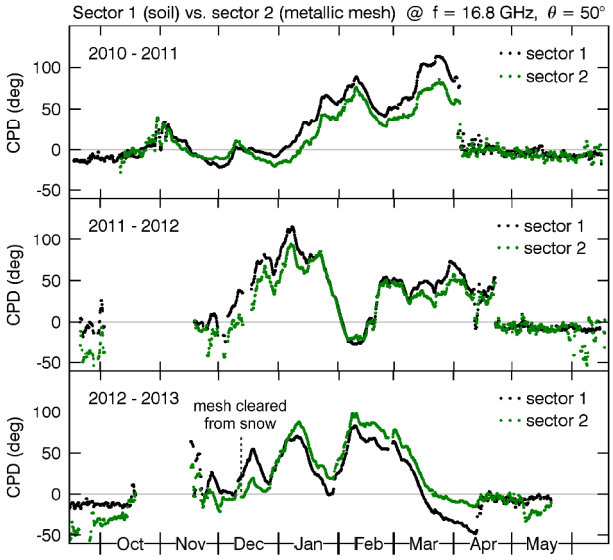

Figure 19. Comparison of the CPD measured on the two sectors of the test site. Sector 2 was located between trees behind the ~~SnowScat instrument,~~ SSI and was covered with a metallic mesh during the last two seasons of the experiment (after August 2011). Generally, the CPD on sector 2 evolves very similar to Sector 1 and ~~does not show~~ shows no large deviations.

6 Conclusions

~~In this paper, we~~ We demonstrated a contact-less ~~and destruction-free~~ technique for monitoring the temporal evolution of the depth-averaged anisotropy of a seasonal snow pack. The technique is based on measuring the birefringent dielectric properties of snow at microwave frequencies where scattering effects can be neglected. The anisotropy ~~of snow. The anisotropy~~ was determined ~~by analyzing~~ from the copolar phase differences (CPD) ~~of~~ measured by a ground based radar ~~acquisitions.~~ instrument which must be complemented by additional data for snow depth and density.

A theoretical framework was ~~provided~~developed, which describes the ~~anisotropy as vertically aligned,~~ structural anisotropy of snow as oblate or prolate spheroidal ice grains ~~,~~ with their symmetry axis in the vertical. Using Maxwell–Garnett type mixing formulas~~were then applied to determine~~ , the effective permittivity tensor was calculated to describe the ~~birefringent properties~~ microwave birefringence of snow. To ~~ensure a unified microstructure characterization with~~ make contact to the microstructure characterization in previous work, we have shown that ~~this model based on identical~~ the model of spheroidal inclusions is ~~identical~~ equivalent to a more general approach ~~to~~ for the effective permittivity tensor based on correlation functions. ~~Using the permittivity tensor, which determines the birefringence of snow,~~ From the effective permittivity tensor we calculated the birefringence and wave propagation according to anisotropic optics. The propagation delay difference of orthogonally polarized microwaves was ~~measured by the CPDwhich was then used to determine the structural anisotropy of snow~~ described in terms of the CPD. The CPD depends linearly on frequency and anisotropy but shows only a weak dependence on density for the density range of seasonal snow. The CPD was then analyzed together with the measured depth and density of the snow pack to estimate the dielectric anisotropy and to derive then the structural anisotropy averaged over the snow depth.

Four years of polarimetric radar data acquired by the SnowScat Instrument, installed at a test site near the town of Sodankylä, Finland were analyzed. ~~The temporal evolution of~~ Copolar phase differences ranging from $-30°$ to $+135°$ were measured for 50–60 cm of snow at a frequency of 13.5 GHz. The large variation of CPD values shows that the anisotropy of snow cannot be neglected when analyzing the CPD within polarimetric microwave studies of snow covered regions.

Overall, the ~~depth-averaged anisotropy of the snow pack could be observed and the anisotropy, ranging~~ depth-averaged anisotropy ranges between -0.05 and $+0.25$, ~~could be determined with a~~ with a a standard deviation of 0.005 ~~. Copolar phase differences ranging from $-30°$ to $+135°$ were measured for 50–60 deep snow at a frequency of 13.5 . The electromagnetic model was tested at~~ which was obtained from measurements of different incidence angles and frequencies. Additional uncertainties which originate from snow depth and density measurements were not taken into account, though.

The CPD obtained from the electromagnetic model with the anisotropy determined for each time, $A_{\mathrm{avg}}^{\mathrm{CPD}}(t)$, was calculated for different frequencies between 10 and 17 GHz ~~,~~ and for different incidence angles between 30 and 60° in order to analyze deviations ~~from measured data. Only small deviations of~~ between modeled and measured CPD data. The modeled CPD deviated only by 5–10° ~~were found~~ from the measured values ranging from $-30°$ to $+135°$ and the expected linear frequency dependence could be confirmed. The linear frequency dependence ~~verifies~~ confirms our assumption that the CPD is a volumetric property of snow ~~determined by its structural anisotropy~~ which is determined by the dielectric anisotropy and related to the structural anisotropy of the ice matrix and pore spaces of snow.

~~The estimated anisotropies~~ For four dates, the CPD-based anisotropy estimates were validated by micro-computed tomography (μCT) measurements for which the anisotropy was ~~determined from~~ computed directly from the two-point correlation functions~~for three dates. The depth-averaged anisotropy of two of the~~ . In two cases, μ~~CT-derived anisotropy profiles agreed~~ CT-based values for the depth averaged anisotropy agreed with their CPD based counterparts within 4 and 8 %~~with our measurements. For one~~ . In one case we found a fair agreement, while for the forth sample we found a larger deviation~~of which~~ . The

origin could only be hypothesized to result from missing snow samples~~or from too coarse assumptions~~, limitations of the Maxwell–Garnett mixing formulas or limitations of using exponential correlation lengths to evaluate the anisotropy parameter Q.

In addition, we investigated the potential of how a changing CPD can be used to detect the accumulation of fresh snow and the ~~accumulation of the water equivalent of snow~~ increase of snow water equivalent (SWE). A weak correlation was found and an optimal acquisition interval of 8–15 days was determined to detect the depth of fresh snow from CPD measurements. It was observed that the evolution of the CPD shows a delay of about 2–3 days compared to the evolution of snow depth, which indicates an average settling time of a few days.

The CPD measurements obtained from the ground based instrument SnowScat were compared with space borne ~~acquisitions by~~ data from the radar satellite TerraSAR-X analyzed over large open areas located a few hundred meters from SnowScat. Both sensors showed the same temporal trend. However, the CPD observed by TerraSAR-X was about a factor of two smaller than the measurements done by SnowScat. ~~A~~ The reason could be ~~the higher snow accumulation on the forest clearing where the SnowScat instrument was located. Stronger wind exposition and the existence of some vegetation for the~~ spatial variability of snow depth and snow properties due to wind exposition but also some disturbing vegetation cover in areas observed by ~~TSX are assumed to be a reason for the smaller measured CPD values~~TerraSAR-X.

Our study shows that remote sensing techniques allow determination of the dielectric anisotropy of the snow pack when the additional information about snow depth and a rough approximation of density is available. Currently, snow depth is mainly estimated from optical measurements such as photogrammetry (Marti et al., 2016; Bühler et al., 2015) or lidar instruments (Deems et al., 2013). However, the applicability of high frequency radar instruments are currently discussed in (Evans and Kruse, 2014). Snow density could potentially be derived from measurements of the snow water equivalent (Leinss et al., 2015) if data about the snow depth is available.

The possibility to observe the dielectric anisotropy of the snow pack by remote sensing techniques opens a ~~wide~~ new field of applications. ~~Detection of fresh snow was already discussed in the previous section. Determination of the thickness of a firnlayer on glaciers might be possible, when correct assumption for the anisotropy and the scattering properties of~~ Determination of the structural anisotropy and detection of fresh snow is discussed in this paper. In principal, the CPD measured over glaciers and ice sheets should provide some information about the structure of firn~~are made and when frequencies which penetrate deep enough into firn are used.~~. However, the interpretation is difficult, though the depth of the scattering center for firn can be determined by independent means (Weber Hoen and Zebker, 2000).

Another interesting application is using CPD measurements as ~~a proxy~~ an indicator for the thermal conductivity of the snow pack. As the dielectric anisotropy can be exactly related to the anisotropy employed for parametrization of the thermal conductivity (Löwe et al., 2013) it seems feasible to aim at a proxy for the thermal conductivity from radar measurements, given a reasonable assumption about the mean density and snow depth. Thereby, the anisotropy would reflect predominant variations in the metamorphic state of the snow pack since increasing vertical structures are indicative of depth hoar~~and of an increased vertical thermal conductivity. This is particularly interesting for~~. This might be important for the ground thermal regime in permafrost regions, ~~where~~ if large vertical structures ~~often arise from~~ are created by high temperature gradients in the ~~thin~~ shallow snow pack in early-winter. Depth hoar, with its large ~~ice~~ crystals and low ~~snow~~ density close to vegetation and soil in turn, is not only important for the survival of many rodents (Bilodeau et al., 2013) but is also very important ~~in~~ for understanding the backscattering signal from snow (King and Derksen, 2015).

The large observation time spanning four winter seasons with a sampling interval of four hours builds a unique data ~~source~~ set to study the evolution of ~~the anisotropy of snow. The data and the demonstrated measurement technique might lead to improved snow models, in order to gain a deeper~~ snow anisotropy to gain further insight into the growth mechanisms of anisotropic snow crystals. Understanding the ~~microscopic~~ structural anisotropy of snow enhances the understanding of macroscopic anisotropic properties such as thermal conductivity, mechanical stability and electromagnetic properties, especially the dielectric anisotropy. The developed method to measure snow anisotropy, its good agreement with ground-based μCT measurements, and the fair agreement with satellite-based radar measurement, provide a unique opportunity to improve snow models, and globally sense the metamorphic state of the snow pack.

Appendix: ~~Re-derivation of Maxwell–Garnett equations via correlation functions~~

Appendix A: The fabric anisotropy of snow due to crystal orientation

Single crystals of hexagonal ice are dielectrically ansiotropic, since the dielectric permittivity parallel to the c-axis, $\varepsilon_{\parallel}$, is by about $\Delta\varepsilon_{\mathrm{ice}} = \varepsilon_{\parallel} - \varepsilon_{\perp} = 0.03 \ldots 0.04$ larger compared to perpendicular permittivity $\varepsilon_{\perp}$ (Fujita et al., 1993; Matsuoka et al., 1997). Ice and snow typically occur as polycrystals which are characterized by their fabric, i.e. the distribution of c-axes. The fabric can be anisotropic as well which is described by an

orientation tensor $\mathbf{a}^{(2)}$. This second order tensor is explained in (Durand et al., 2006), nicely visualized in (Woodcock, 1977), and was used in (Riche et al., 2013) to characterize the crystals orientation in seasonal snow. The eigenvalues of $\mathbf{a}^{(2)}$ follow the relation $1 \geq \lambda_1 \geq \lambda_2 \geq \lambda_3 \geq 0$ with $\lambda_1 + \lambda_2 + \lambda_3 = 1$ (Durand et al., 2006) and give the axis of an ellipsoid.

For snow, where the symmetry axis is the vertical (z) the eigenvalues correspond to the axis of an ellipsoid aligned along the coordinate axis $i = \{x, y, z\}$. The ellipsoid can have the following three shapes: 1) for a preferential orientation of the c-axis in the horizontal plane (horizontal girdle) the eigenvalues $(0 \leq \lambda_z < 1/3 < \lambda_y \approx \lambda_z \leq 1/2)$ form an oblate spheroid. 2) for an isotropic distribution, the eigenvalues form a sphere ($\lambda_x = \lambda_y = \lambda_z = 1/3$), and 3) when the c-axis clusters around the vertical (single maximum fabric), the eigenvalues form a prolate spheroid $(0 \leq \lambda_x \approx \lambda_y \leq 1/3 \leq \lambda_z \leq 1)$.

The effective permittivity of snow, ε_{eff}, composed of air pores and a matrix of (isotropically) oriented ice crystals can be described with mixing formulas (e.g. Maxwell-Garnett as in Sect. 2.2). In the following, we parametrize the effective permittivities $\varepsilon_{i,\text{eff-oi}}$ of snow comprising oriented ice crystals by a weighted average of the two permittivities of ice, $\varepsilon_{\parallel}$ and $\varepsilon_{\perp}$. The weighting is determined by the eigenvalues of the orientation tensor. The weight for $\varepsilon_{\parallel}$ is equivalent with the eigenvalue λ_i, and the weight for $\varepsilon_{\perp}$ in the perpendicular direction follows by $(1 - \lambda_i)$. The effective permittivities for the x, y, and z-direction follow as

$$\varepsilon_{i,\text{eff-oi}} = f(\rho) \cdot \left[\lambda_i \cdot \varepsilon_{\parallel} + (1 - \lambda_i) \cdot \varepsilon_{\perp}\right]. \tag{A1}$$

The function $f(\rho) = \varepsilon_{\text{eff}}(f_{\text{vol}}, \varepsilon_{\text{air}}, \varepsilon_{\text{ice}})/\varepsilon_{\text{ice}}$ accounts for the nonlinear density dependence of the permittivity parametrized by the ice volume fraction f_{vol} and by the dielectric constant of polycrystalline of ice, ε_{ice} (cf. Eq. 3).

The dielectric anisotropy of snow due to oriented ice crystals, $\Delta\varepsilon_{\text{snow-oi}} = \varepsilon_{x,\text{eff-oi}} - \varepsilon_{z,\text{eff-oi}}$, can now be related with the dielectric anisotropy of ice $\Delta\varepsilon_{\text{ice}}$:

$$\Delta\varepsilon_{\text{snow-oi}} = \varepsilon_{x,\text{eff-oi}} - \varepsilon_{z,\text{eff-oi}} = f(\rho) \cdot (\lambda_x - \lambda_z)\Delta\varepsilon_{\text{ice}} \tag{A2}$$

For the two extreme cases of snow with completely vertically oriented ice crystals ($\lambda_{x,y} = 0, \lambda_z = 1$) follows $\Delta\varepsilon_{\text{snow-oi}} = -f(\rho)\Delta\varepsilon_{\text{ice}}$; for snow with a uniform orientation in the horizontal plane ($\lambda_{x,y} = 0.5, \lambda_z = 0$) one obtains $\Delta\varepsilon_{\text{snow-oi}} = +\frac{1}{2}f(\rho)\Delta\varepsilon_{\text{ice}}$. For the isotropic case ($\lambda_i = 1/3$) one obtains $\Delta\varepsilon_{\text{snow-oi}} = 0$. The bracked [...] in Eq. (A1) is then equivalent with the permittivity of polycrystalline ice, $\varepsilon_{\text{ice}} = 1/3 \cdot \varepsilon_{\parallel} + 2/3 \cdot \varepsilon_{\perp}$, and it follows that $\varepsilon_{\text{snow-oi}} = f(\rho)$. This one-third/two-third weighting for polycrystalline ice has also been mentioned by Fujita et al. (1993, 2000) and was experimentally observed by Matsuoka et al. (1996).

For seasonal snow, some evidence has been found that the c-axis is preferentially vertically aligned for fresh snow (single-maximum) whereas for old snow the c-axis seems to be slightly oriented in a girdle in the horizontal plane (Riche et al., 2013).The strongest (single-maximum) anisotropy observed by Riche et al. (2013), parametrized by the eigenvalues $\lambda_z = 0.53, \lambda_x = 0.22$ result with Eq. (A2) in a maximum dielectric anisotropy of $\Delta\varepsilon_{\text{snow}} \approx 0.2 \cdot (0.22 - 0.53) \cdot 0.035 = -0.002$ for the example of $f(\rho) \approx f_{\text{vol}} = 0.2$ as common in seasonal snow. According to Fig.1(right) this must be compared to a structural anisotropy of $A = -0.02$ which is small compared to the structural anisotropies observed in this paper.

Appendix B: Effective permittivity from weighted average of Maxwell–Garnett equations

The Maxwell-Garnett formulas (e.g. Eq. 3.27 in Sihvola, 2000) describe the effective permittivity of (elliptical) inclusion with a permittivity ε_i (e.g. ice) embedded in a host medium of permittivity ε_e (e.g. air) and can therefore be applied to calculate the anisotropic permittivity tensor for media with a structural anisotropy. The Maxwell-Garnett formulas can also be used in a "inverted" form, where the permittivities of inclusions and the host medium are swapped (e.g. air inclusions in ice). Both cases, the Maxwell-Garnett formula and the "inverse" Maxwell-Garnett formula, Eqs. (6a) and (6b), are equivalent with the lower and upper Hashin-Shtrikman-bounds for approximations of the exact description of dielectric mixtures (Hashin and Shtrikman, 1962; Sihvola, 2002).

For the isotropic case, the Maxwell-Garnett formulas can be compared with measurements of Mätzler (1996) and it has been found that the measurements lie well within the lower and upper Hashin-Shtrikman bound (Sihvola, 2002). However, the measurements are significantly larger than the lower Hashin-Shtrikman bound which is equivalent with the Maxwell-Garnett mixing formular for ice inclusion in air. Therefore, a combination of the Maxwell-Garnett formula and its inverse form is required for a better agreement with the measured data.

The measured data of Mätzler (1996) have been used in MEMLS-3 (Wiesmann and Mätzler, 1999, Eqs. 45/46) to fit an empirical formula to describe the permittivity of dry snow. The empirical formula is given in terms of snow density ρ and reads

$$\varepsilon_{\text{MEM-3}} = \begin{cases} 1 + 1.5995\rho + 1.861\rho^3 & \rho < 0.4\,\text{g/cm}^3 \\ \left[(1-\nu)\varepsilon_h + \nu\varepsilon_{\text{ice}}^{1/3}\right]^3 & \rho > 0.4\,\text{g/cm}^3 \end{cases} \tag{B1}$$

with the coefficients $\varepsilon_h = 1.005, \varepsilon_{\text{ice}} = 3.17$ (for $-10°$C) and $\nu = \rho/\rho_{\text{ice}}$. Note, that the original coefficients of $\varepsilon_h = 1.0, \varepsilon_{\text{ice}} = 3.215$ as given by

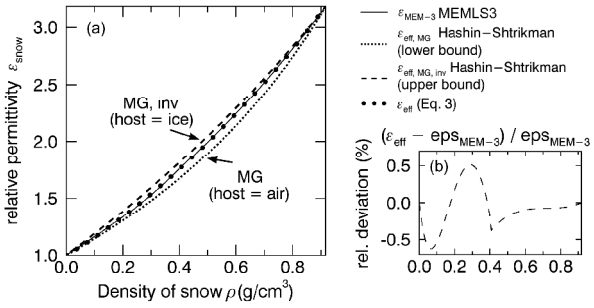

Figure B1. (a) Relative permittivity of snow $\varepsilon_{\text{MEM-3}}$ according to equation (B1) in comparison to the upper and lower Hashin-Shtrikman bound. (b) relative deviation of ε_{eff} (the weighted average of the Maxwell-Garnett formulas as given in Eq.(3)) with respect to the permittivity of dry snow as given by $\varepsilon_{\text{MEM-3}}$ in Eq. (B1).

Wiesmann and Mätzler (1999, Eqs. 45/46) have been adapted in agreement with C. Mätzler to produce correct results for pure ice ($\nu = 1$). We also note here that the exponent of 1/3 is missing for the factor ε_s (here ε_{ice}) in Wiesmann and Mätzler (1999, Eq. 46).

Fig. 20(a) shows the lower and upper Hashin-Strikman-bounds (MG and MG,inv as dashed and dotted line) and the result of Eq. (B1) (solid line). The dots on top of the solid line indicate the weighted average of both bounds as given in Eq.(3). The weighted average is motivated by the fact that for low snow densities snow can better be described by ice particles embedded in a background matrix of air, whereas for high snow densities, snow can better be described by air inclusions in ice. Fig. 20(b) shows the relative deviation (in percent) between the permittivity used in MEMLS-3 (Eq. B1) and the weighted average of the Maxwell-Garnett formula and its "inverse" form. The relative deviation $(\varepsilon_{\text{eff}} - \varepsilon_{\text{MEM-3}})/\varepsilon_{\text{MEM-3}}$ is less than $\pm 0.7\,\%$ and justifies phenomenological composition of the averaged formula.

Appendix C: Re-derivation of Maxwell–Garnett equations via correlation functions

In Rechtsman and Torquato (2008) an exact series expansion of the dielectric permittivity of arbitrary anisotropic two-phase materials was derived and related to the n-point correlation functions of the material. If the series is truncated at $n = 2$, the final result (Rechtsman and Torquato, 2008, Eq. 16) can be solved for the diagonal components, $\varepsilon_{\text{eff},i}$, $i = x, y, z$, of the effective permittivity tensor which can be written in the form

$$\varepsilon_{\text{eff},i} = \varepsilon_q + \varepsilon_q \phi_p \frac{(\varepsilon_p - \varepsilon_q)}{\varepsilon_q + (1-\phi_p)\left[\frac{1}{3} - \frac{U_i}{3\phi_p\phi_q}\right](\varepsilon_p - \varepsilon_q)}. \tag{C1}$$

The permittivities and volume fractions of the two phases which compose the microstructure are denoted by $\varepsilon_p, \varepsilon_q$ and ϕ_p, ϕ_q, respectively. The quantities U_i in Eq. (C1) are related to integrals over the two-point correlation function $C(\boldsymbol{r})$ as defined in Löwe et al. (2013, Eq. 1). In the lowest order of frequency f, contributions from scattering in the effective permittivity can be neglected (cf. Rechtsman and Torquato, 2008, Eqs. C3, C4). Then the U_i have vanishing imaginary part and are given by

$$U_x = U_y = \frac{3}{4\pi}\int_{\mathbb{R}^3} d^3r \frac{1}{r^3}\left(-1 + \frac{3}{2}\sin^2\theta\right) C(\boldsymbol{r}) \tag{C2}$$

$$U_z = \frac{3}{4\pi}\int_{\mathbb{R}^3} d^3r \frac{1}{r^3}\left(-1 + 3\cos^2\theta\right) C(\boldsymbol{r}) \tag{C3}$$

Here $r = |\boldsymbol{r}|$ is the magnitude of $\boldsymbol{r}$ and θ denotes the angle between the vertical z axis and $\boldsymbol{r}$.

If the microstructure is (statistically) transversly isotropic, it is reasonable to assume a "spheroidal symmetry" of the correlation function, viz $C(\boldsymbol{r}) = C(r/\sigma(\theta))$ with $\sigma(\theta) = 2a_x[1-(1-a_x^2/a_z^2)\cos^2\theta]^{1/2}$ as used in Löwe et al. (2013). Under this assumption, the singular integrals in C2 can be calculated as shown in Torquato and Lado (1991). The results can be inserted into the square brackets in C1 leading to

$$\left[\frac{1}{3} - \frac{U_x}{3\phi_p\phi_q}\right] = Q \tag{C4}$$

$$\left[\frac{1}{3} - \frac{U_z}{3\phi_p\phi_q}\right] = 1 - 2Q \tag{C5}$$

where the anisotropy parameter Q is defined in Löwe et al. (2013, Eq. 4) or Torquato (2002, Eqs. 17.30/17.31). Using the definition of depolarization factors from Torquato (2002, Eq. 17.25), noting their relation to Q from Torquato (2002, Eq. 17.29) on one hand, and their equivalence to the definition of N_i from Eq. (8) and from the last paragraph of Sect. 2.2 on the other hand we end up with

$$\varepsilon_{\text{eff},i} = \varepsilon_q + \varepsilon_q \phi_p \frac{(\varepsilon_p - \varepsilon_q)}{\varepsilon_q + (1-\phi_p) N_i (\varepsilon_p - \varepsilon_q)}. \tag{C6}$$

We note here that Torquato (2002, Eq. 17.25) contains a typo. Specifying p to be the ice phase and q to be the air phase in Eq. (C6), gives $\varepsilon_q = \varepsilon_{\text{air}}$, $\varepsilon_p = \varepsilon_{\text{ice}}$, $\phi_p = f_{\text{vol}}$ in the notation from Sect. 2.2, and thus Eq. (C4) coincides with the Maxwell–Garnett result Eq. (6a).

Appendix D: CPD calibration of the SnowScat data

The measured radar signal was calibrated by an internal calibration loop of the SSI to compensate system drifts. However, some polarization dependent signal delay still originated from the connectors of the antenna feeding cables and from the antennas themselves due to the polarization-dependent beam-pattern. In order to calibrate external offsets and drifts, the CPD was calibrated with two metallic targets.

The primary calibration target was a metallic sphere with a diameter of 25 cm mounted on a wooden pole for the duration of the experiment. The sphere can be located in Fig. 5 next to the SSI. A secondary target, a metallic plate was located behind trees close to sector 2. A third calibration target, a dihedral reflector, was installed during the setup phase of the experiment. The correct pointing direction to locate the sphere was determined with a precision of $\pm 0.5°$ by 2-D-scans in elevation and azimuth. The 2-D-scans showed that a possible systematic error of the CPD, caused by imprecise alignment, can be estimated to be below $\pm 10°$.

The theoretical CPD measured from a sphere (or plate) is expected to be zero due to the target symmetry. The sphere was measured every four hours and was used as a reference during the whole duration of the experiment. The plate was installed from October 2011 until June 2013 and was used to validate the calibration done with the sphere. The CPD measured for a dihedral reflector should be 180°. The dihedral reflector was measured once, on 9 December 2009, to verify the processing sequence of the SnowScat raw data.

The CPD determined for the sphere, $\mathrm{CPD}_{\mathrm{REF}}$, was used as a reference and was subtracted from the uncalibrated CPD measurements of snow, $\mathrm{CPD}_{\mathrm{uncal.}}$, to obtain calibrated results:

$$\mathrm{CPD}_{\mathrm{cal.}}(f) = \mathrm{CPD}_{\mathrm{uncal.}}(f) - \mathrm{CPD}_{\mathrm{REF}}(f). \quad \text{(D1)}$$

Phase unwrapping was performed for the uncalibrated CPD and the reference CPD if necessary.

To reduce the noise of the reference measurements as much as possible, the reference, $\mathrm{CPD}_{\mathrm{REF}}$, was determined as follows: Time series $\mathrm{CPD}_{\mathrm{REF}}(t)$ were obtained for 21 different frequencies in order to sample the entire frequency spectrum between 9.2 and 17.8 GHz of the instrument. The time series were smoothed with a median filter of 4 days which preserved phase jumps in the signal. After temporal filtering, a frequency-dependent 4th order polynomial was fitted over the measured frequency spectrum of each acquisition to provide some noise reduction in the frequency domain.

The reference data are shown for all four seasons in Fig. 21. The solid black line shows the (frequency-dependent) reference, $\mathrm{CPD}_{\mathrm{REF}}$, for $f = 13.5$ GHz. Individual measurements of the sphere as well as measurements of the metallic plate are shown as dark and light gray solid dots below the black line.

In the third season, between 18 November 2011 and 20 January 2012, the pointing direction (elevation angle) to the sphere was misaligned by 2°. Therefore, the reference CPD was corrected by a frequency dependent offset to keep the CPD continuous at the start and the end of the period of misalignment.

The deviation of the raw-data of the sphere from the reference, $\Delta\mathrm{CPD} = \mathrm{CPD}(f) - \mathrm{CPD}_{\mathrm{REF}}(f)$, is shown in the lower panels for each season as scattered dots for each of the 21 analyzed frequencies. The root-mean-square-error, RMSE, was below 4° for the full frequency spectrum and is given for each seasons next to the graph. The error of the reference, $\mathrm{CPD}_{\mathrm{REF}}(f)$, which includes systematic and statistic errors, is estimated to be below 15°.

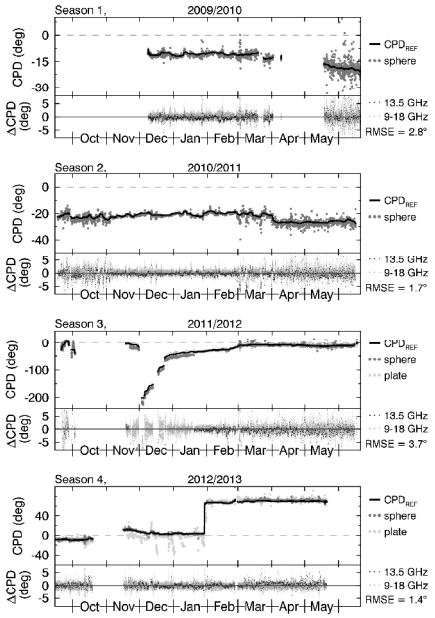

Figure D1. The CPD was calibrated using the sphere as a reference target. The upper panels show the reference, $\mathrm{CPD}_{\mathrm{REF}}(f)$, for $f = 13.5$ GHz (solid line) together with individual CPD measurements for the sphere and the plate (light and dark gray dots). The CPD of the metallic plate agrees within the standard deviation with measurements of the sphere and with $\mathrm{CPD}_{\mathrm{REF}}$. Deviations were found for season 3 due to a misalignment of the SSI to the sphere, and for November 2012, possibly due to snow cover of the metallic plate. The lower panels show the deviation, $\Delta\mathrm{CPD} = \mathrm{CPD}_{\mathrm{meas.}}(f) - \mathrm{CPD}_{\mathrm{REF}}(f)$, for individual measurements at all measured frequencies $f = 10$–17 GHz. The deviation at a frequency of 13.5 GHz is shown as black dots. The standard deviation (RMSE) of ΔCPD for the whole frequency spectrum is given below the legend of the lower panel.

Appendix E: Author contributions

S. Leinss developed the birefringence model of snow, processed and calibrated the radar data, and wrote major parts of the manuscript. H. Löwe established the link between the Maxwell-Garnett theory and the statistical description of the snow microstructure based on n-point correlation functions (Appendix A3) and did the statistical analysis of the μCT data. M. Proksch acquired the snow samples and calculated the anisotropy from the μCT data. J. Lemmetyinen provided the snow measurements and meteorological data for the test site and added extremely valuable "in-situ" knowledge. A. Wiesmann added valuable knowledge about the processing and datasets of the SnowScat instrument. I. Hajnsek carefully proofread the paper and provided the funding for this paper.

Acknowledgements. The in situ data collection was supported by the European Space Agency activity "Technical assistance for the deployment of an X- to Ku-band scatterometer during the NoSREx experiment" (ESA ESTEC Contract no. 22671/09/NL/JA/ef) ~~(?).~~ (Lemmetyinen et al., 2013). We acknowledge Margret Matzl from SLF for retrieving an additional μCT dataset from the archive. The staff at FMI-ARC is acknowledged for the collection of in situ data. We thank Anna Kontu (FMI) for providing the meteorological data and her excellent local expertise concerning ~~all~~ many experimental details at the test site. Special thank goes to Jouni Pulliainen from FMI for the initiative of setting up a test site which provides a unique amount and diversity of meteorological data and snow measurements. We thank Helmut Rott from University Innsbruck / Enveo for the encouragement to analyze the CPD of the ground based radar instrument SnowScat. We thank Christian Mätzler for adapting his model of the relative permittivity of snow in order to make it valid for high snow densities up to solid ice ~~.~~ and for providing insight in his excellent work. We also acknowledge the anonymous reviewer for the very precise feedbacks, the careful checking of references and for differencing the structural anisotropy of snow from the crystal anisotropy of ice.

References

Alley, R.: Texture of polar firn for remote sensing, Annals of Glaciology, 9, 1–4, 1987.

Ao, C. O. and Kong, J. A.: Analytical approximations in multiple scattering of electromagnetic waves by aligned dielectric spheroids, JOSA A, 19, 1145–1156, 2002.

Bilodeau, F., Gauthier, G., and Berteaux, D.: The effect of snow cover on lemming population cycles in the Canadian High Arctic, Oecologia, 172, 1007–1016, doi:10.1007/s00442-012-2549-8, http://dx.doi.org/10.1007/s00442-012-2549-8, 2013.

Bohleber, P., Wagner, N., and Eisen, O.: Permittivity of ice at radio frequencies: Part II. Artificial and natural polycrystalline ice, Cold Regions Science and Technology, 83-84, 13 – 19, doi:http://dx.doi.org/10.1016/j.coldregions.2012.05.010, http://www.sciencedirect.com/science/article/pii/S0165232X12001103, 2012.

Bormann, K. J., Westra, S., Evans, J. P., and McCabe, M. F.: Spatial and temporal variability in seasonal snow density, Journal of Hydrology, 484, 63 – 73, doi:http://dx.doi.org/10.1016/j.jhydrol.2013.01.032, http://www.sciencedirect.com/science/article/pii/S0022169413000784, 2013.

Bühler, Y., Marty, M., Egli, L., Veitinger, J., Jonas, T., Thee, P., and Ginzler, C.: Snow depth mapping in high-alpine catchments using digital photogrammetry, The Cryosphere, 9, 229–243, doi:10.5194/tc-9-229-2015, http://www.the-cryosphere.net/9/229/2015/, 2015.

Calonne, N., Geindreau, C., Flin, F., Morin, S., Lesaffre, B., Rolland du Roscoat, S., and Charrier, P.: 3-D image-based numerical computations of snow permeability: links to specific surface area, density, and microstructural anisotropy, The Cryosphere, 6, 939–951, doi:10.5194/tc-6-939-2012, http://www.the-cryosphere.net/6/939/2012/, 2012.

Calonne, N., Flin, F., Geindreau, C., Lesaffre, B., and Rolland du Roscoat, S.: Study of a temperature gradient metamorphism of snow from 3-D images: time evolution of microstructures, physical properties and their associated anisotropy, The Cryosphere, 8, 2255–2274, doi:10.5194/tc-8-2255-2014, http://www.the-cryosphere.net/8/2255/2014/, 2014.

Chang, P., Mead, J., Knapp, E., Sadowy, G., Davis, R., and McIntosh, R.: Polarimetric backscatter from fresh and metamorphic snowcover at millimeter wavelengths, IEEE Transactions on Antennas and Propagation, 44, 58 –73, doi:10.1109/8.477529, 1996.

Cohn, E.: Das elektromagnetische Feld: vorlesungen über die Maxwell'sche Theorie, S. Hirzel, 1900.

Davis, R. E. and Dozier, J.: Stereological characterization of dry Alpine snow for microwave remote sensing, Advances in Space Research, 9, 245 – 251, doi:http://dx.doi.org/10.1016/0273-1177(89)90492-4, http://www.sciencedirect.com/science/article/pii/0273117789904924, 1989.

Deems, J. S., Painter, T. H., and Finnegan, D. C.: Lidar measurement of snow depth: a review, Journal of Glaciology, 59, 467–479, 2013.

Durand, G., Gagliardini, O., Thorsteinsson, T., Svensson, A., Kipfstuhl, S., and Dahl-Jensen, D.: Ice microstructure and fabric: an up-to-date approach for measuring textures, Journal of Glaciology, 52, 619–630, doi:doi:10.3189/172756506781828377, http://www.ingentaconnect.com/content/igsoc/jog/2006/00000052/00000179/art00013, 2006.

Evan, S.: Dielectric properties of ice and snow—A review, Journal of Glaciology, 5, 773–792, 1965.

Evans, J. and Kruse, F.: Determination of snow depth using elevation differences determined by interferometric SAR (InSAR), in: Geoscience and Remote Sensing Symposium (IGARSS), 2014 IEEE International, pp. 962–965, doi:10.1109/IGARSS.2014.6946586, 2014.

Fujita, S., Mae, S., and Matsuoka, T.: Dielectric anisotropy in ice Ih at 9.7 GHz, Annals of Glaciology, 17, 276–276, http://www.igsoc.org:8080/annals/17/igs_annals_vol17_year1993_pg276-280.pdf, 1993.

Fujita, S., Matsuoka, T., Ishida, T., Matsuoka, K., and Mae: A summary of the complex dielectric permittivity of ice in the megahertz range and its application for radar sounding of polar ice sheets, in: The Physics of Ice Core Records, First edition, pp. 185–212, Hokkaido University Press, Sapporo, Japan, 2000.

Fujita, S., Maeno, H., and Matsuoka, K.: Radio-wave depolarization and scattering within ice sheets: a matrix-based model to link radar and ice-core measurements and its application, Journal of Glaciology, 52, 407–424, 2006.

Fujita, S., Okuyama, J., Hori, A., and Hondoh, T.: Metamorphism of stratified firn at Dome Fuji, Antarctica: A mechanism for local insolation modulation of gas transport conditions during bubble close off, Journal of Geophysical Research: Earth Surface, 114, 1–21, doi:10.1029/2008JF001143, http://dx.doi.org/10.1029/2008JF001143, 2009.

Fujita, S., Hirabayashi, M., Goto-Azuma, K., Dallmayr, R., Satow, K., Zheng, J., and Dahl-Jensen, D.: Densification of layered firn of the ice sheet at NEEM, Greenland, Journal of Glaciology, 60, 905–921, doi:http://dx.doi.org/10.3189/2014JoG14J006, 2014.

Garrett, T. J., Fallgatter, C., Shkurko, K., and Howlett, D.: Fall speed measurement and high-resolution multi-angle photography of hydrometeors in free fall, Atmospheric Measurement Techniques, 5, 2625–2633, doi:10.5194/amt-5-2625-2012, http://www.atmos-meas-tech.net/5/2625/2012/, 2012.

Guneriussen, T., Høgda, K. A., Johnsen, H., and Lauknes, I.: InSAR for estimation of changes in snow water equivalent of dry snow, IEEE Transactions on Geoscience and Remote Sensing, 39, 2101 – 2108, doi:http://dx.doi.org/10.1109/36.957273, 2001.

Hallikainen, M., Ulaby, F., and van Deventer, T.: Extinction Behavior of Dry Snow in the 18-to 90-GHz Range, IEEE Transactions on Geoscience and Remote Sensing, GE-25, 737 –745, doi:10.1109/TGRS.1987.289743, 1987.

Hargreaves, N.: The polarization of radio signals in the radio echo sounding of ice sheets, Journal of Physics D: Applied Physics, 10, 1285, 1977.

Hargreaves, N.: The radio-frequency birefringence of polar ice, Journal of Glaciology, 21, 301–313, 1978.

Hashin, Z. and Shtrikman, S.: A Variational Approach to the Theory of the Effective Magnetic Permeability of Multiphase Materials, Journal of Applied Physics, 33, 3125–3131, doi:http://dx.doi.org/10.1063/1.1728579, http://scitation.aip.org/content/aip/journal/jap/33/10/10.1063/1.1728579, 1962.

Heggli, M., Frei, E., and Schneebeli, M.: Instruments and Methods Snow replica method for three-dimensional X-ray microtomographic imaging, Journal of Glaciology, 55, 631–639, doi:10.3189/002214309789470932, 2009.

Hendry, A., Mccormick, G., and Barge, B.: Ku-band and S-band observations of the differential propagation constant in snow, Antennas and Propagation, IEEE Transactions on, 24, 521–525, doi:10.1109/TAP.1976.1141364, 1976.

Hildebrand, T., Laib, A., Müller, R., Dequeker, J., and Rüegsegger, P.: Direct three-dimensional morphometric analysis of human cancellous bone: microstructural data from spine, femur, iliac crest, and calcaneus, J Bone Miner Res., 14, 1167 – 74, 1999.

Hogan, R. J., Tian, L., Brown, P. R. A., Westbrook, C. D., Heymsfield, A. J., and Eastment, J. D.: Radar scattering from ice aggregates using the horizontally aligned oblate spheroid approximation, J. Appl. Meteor. Climatology, 51, 655–671, 2012.

Hörhold, M. W., Albert, M. R., and Freitag, J.: The impact of accumulation rate on anisotropy and air permeability of polar firn at a high-accumulation site, Journal of Glaciology, 55, 625–630, 2009.

Izumi, K. and Huzioka, T.: Studies of metamorphism and thermal conductivity of snow, 1, Low Temperature Science Series A, 33, 91–102, http://eprints.lib.hokudai.ac.jp/dspace/handle/2115/18276, 1975.

Jones, R. G.: The measurement of dielectric anisotropy using a microwave open resonator, Journal of Physics D: Applied Physics, 9, 819, http://stacks.iop.org/0022-3727/9/i=5/a=015, 1976.

Kaempfer, T. U. and Schneebeli, M.: Observation of isothermal metamorphism of new snow and interpretation as a sintering process, Journal of Geophysical Research: Atmospheres, 112, 1–10, doi:10.1029/2007JD009047, http://dx.doi.org/10.1029/2007JD009047, 2007.

Kaempfer, T. U., Schneebeli, M., and Sokratov, S. A.: A microstructural approach to model heat transfer in snow, Geophysical Research Letters, 32, n/a–n/a, doi:10.1029/2005GL023873, http://dx.doi.org/10.1029/2005GL023873, l21503, 2005.

King, J. and Derksen, C.: Retrieval of Tundra SWE Using Airborne Dual-frequency SAR (17.2 / 9.6 Ghz) and MEMLS-active, in: Proceedings IGARSS 2015, Milano, 2015.

Kojima, K.: Thin Section of Snow Cut by a Heated Wire., Contributions from the Institute of Low Temperature Science, 16, 47–59, 1960.

Kontu, A., Lemmetyinen, J., Takala, M., Rautiainen, K., Wiesmann, A., and Werner, C.: Technical assistance for the deployment of an X- to Ku-band scatterometer during the NoSREx experiment. Data acuisition report (D2). Contract No. 22671/09/NL/JA, Tech. rep., FMI, Enveo, Gamma Remote Sensing and ESA ESTEC, Noordwijk, 2011.

Landau, L. and Lifshitz, E.: Electrodynamics of Continuous Media, Pergamon Press, 1960.

Lee, J.-S., Grunes, M., and De Grandi, G.: Polarimetric SAR speckle filtering and its implication for classification, IEEE Transactions on Geoscience and Remote Sensing, 37, 2363 – 2373, doi:10.1109/36.789635, 1999.

Leinss, S., Lemmetyinen, J., Wiesmann, A., and Hajnsek, I.: Snow Structure Evolution Measured by Ground Based Polarimetric Phase Differences, in: EUSAR 2014; 10th European Conference on Synthetic Aperture Radar; Proceedings of, pp. 1–4, 2014a.

Leinss, S., Parrella, G., and Hajnsek, I.: Snow Height Determination by Polarimetric Phase Differences in X-Band SAR Data, IEEE Journal of Selected Topics in Applied Earth Observations and Remote Sensing, 7, 3794–3810, doi:10.1109/JSTARS.2014.2323199, 2014b.

Leinss, S., Wiesmann, A., Lemmetyinen, J., and Hajnsek, I.: Snow Water Equivalent of Dry Snow Measured by Differential Interferometry, IEEE Journal of Selected Topics in Applied Earth Observations and Remote Sensing, 8, 3773 – 3790, doi:http://dx.doi.org/10.1109/JSTARS.2015.2432031, 2015.

Lemmetyinen, J., Kontu, A., Leppänen, L., Pulliainen, J., Wiesmann, A., Werner, C., Proksch, M., and Schneebeli, M.: Technical assistance for the deployment of an X- to Ku-band scatterometer during the NoSREx experiment. NoSREx-I, -II and -III (2009 - 2012) Final report. Contract No. 22671/09/NL/JA/ef, Tech. rep., ESA ESTEC, Noordwijk, https://earth.esa.int/web/guest/campaigns, 2013.

Li, L., Gaiser, P., Albert, M., Long, D., and Twarog, E.: WindSat Passive Microwave Polarimetric Signatures of the Greenland Ice Sheet, Geoscience and Remote Sensing, IEEE Transactions on, 46, 2622–2631, doi:10.1109/TGRS.2008.917727, 2008.

Lüneburg, E. and Boerner, W.-M.: Statistical Aspects of Radar Polarimetry, in: Fields, Networks, Computational Methods, and

Systems in Modern Electrodynamics, edited by Russer, P. and Mongiardo, M., vol. 97 of *Springer Proceedings in Physics*, pp. 43–54, Springer Berlin Heidelberg, doi:10.1007/978-3-662-07221-9_5, http://dx.doi.org/10.1007/978-3-662-07221-9_5, 2004.

Lomonaco, R., Albert, M., and Baker, I.: Microstructural evolution of fine-grained layers through the firn column at Summit, Greenland, Journal of Glaciology, 57, 755–762, doi:doi:10.3189/002214311797409730, http://www.ingentaconnect.com/content/igsoc/jog/2011/00000057/00000204/art00015, 2011.

Löwe, H. and Picard, G.: Microwave scattering coefficient of snow in MEMLS and DMRT-ML revisited: the relevance of sticky hard spheres and tomography-based estimates of stickiness, The Cryosphere, 9, 2101–2117, doi:10.5194/tc-9-2101-2015, http://www.the-cryosphere.net/9/2101/2015/, 2015.

Löwe, H., Spiegel, J., and Schneebeli, M.: Interfacial and structural relaxations of snow under isothermal conditions, Journal of Glaciology, 57, 499–510, 2011.

Löwe, H., Riche, F., and Schneebeli, M.: A general treatment of snow microstructure exemplified by an improved relation for thermal conductivity, The Cryosphere, 7, 1473–1480, doi:10.5194/tc-7-1473-2013, http://www.the-cryosphere.net/7/1473/2013/, 2013.

Lytle, V. and Jezek, K.: Dielectric permittivity and scattering measurements of Greenland firn at 26.5-40 GHz, Geoscience and Remote Sensing, IEEE Transactions on, 32, 290–295, doi:10.1109/36.295044, 1994.

Marti, R., Gascoin, S., Berthier, E., de Pinel, M., Houet, T., and Laffly, D.: Mapping snow depth in open alpine terrain from stereo satellite imagery, The Cryosphere Discussions, 2016, 1–36, doi:10.5194/tc-2016-11, http://www.the-cryosphere-discuss.net/tc-2016-11/, 2016.

Matrosov, S. Y., Reinking, R. F., and Djalalova, I. V.: Inferring Fall Attitudes of Pristine Dendritic Crystals from Polarimetric Radar Data, Journal of the Atmospheric Sciences, 1, 241–250, doi:10.1175/JAS-3356.1, http://dx.doi.org/10.1175/JAS-3356.1, 2005.

Matsuoka, K., Wilen, L., Hurley, S., and Raymond, C.: Effects of Birefringence Within Ice Sheets on Obliquely Propagating Radio Waves, IEEE Transactions on Geoscience and Remote Sensing, 47, 1429–1443, doi:10.1109/TGRS.2008.2005201, 2009.

Matsuoka, T., Fujita, S., and Mae, S.: Effect of temperature on dielectric properties of ice in the range 5-39 GHz, Journal of Applied Physics, 80, 5884–5890, doi:http://dx.doi.org/10.1063/1.363582, http://scitation.aip.org/content/aip/journal/jap/80/10/10.1063/1.363582, 1996.

Matsuoka, T., Fujita, S., Morishima, S., and Mae, S.: Precise measurement of dielectric anisotropy in ice Ih at 39 GHz, Journal of Applied Physics, 81, 2344–2348, doi:10.1063/1.364238, 1997.

Mätzler, C.: Applications of the interaction of microwaves with the natural snow cover, Remote Sensing Reviews, 2, 259–387, doi:10.1080/02757258709532086, 1987.

Mätzler, C.: Microwave permittivity of dry snow, IEEE Transactions on Geoscience and Remote Sensing, 34, 573 –581, doi:10.1109/36.485133, 1996.

Mätzler, C.: Autocorrelation functions of granular media with free arrangement of spheres, spherical shells or ellipsoids, Journal of Applied Physics, 81, 1509–1517, doi:http://dx.doi.org/10.1063/1.363916, http://scitation.aip.org/content/aip/journal/jap/81/3/10.1063/1.363916, 1997.

Mätzler, C.: Relation between grain-size and correlation length of snow, Journal of Glaciology, 48, 461–466, doi:doi:10.3189/172756502781831287, http://www.ingentaconnect.com/content/igsoc/jog/2002/00000048/00000162/art00011, 2002.

Mätzler, C. and Wegmüller, U.: Dielectric properties of freshwater ice at microwave frequencies, Journal of Physics D: Applied Physics, 20, 1623, http://stacks.iop.org/0022-3727/20/i=12/a=013, 1987.

Noel, V. and Chepfer, H.: A global view of horizontally oriented crystals in ice clouds from Cloud-Aerosol Lidar and Infrared Pathfinder Satellite Observation (CALIPSO), Journal of Geophysical Research: Atmospheres, 115, 1–13, doi:10.1029/2009JD012365, http://dx.doi.org/10.1029/2009JD012365, 2010.

Oh, Y., Sarabandi, K., and Ulaby, F. T.: Semi-empirical model of the ensemble-averaged differential Mueller matrix for microwave backscattering from bare soil surfaces, IEEE Transactions on Geoscience and Remote Sensing, 40, 1348–1355, doi:10.1109/TGRS.2002.800232, 2002.

Parrella, G., Hajnsek, I., and Papathanassiou, K.: Polarimetric Decomposition of L-band PolSAR Backscattering Over the Austfonna Ice Cap, IEEE Transactions on Geoscience and Remote Sensing, n.a., n.a., 2015.

Pfeffer, W. T. and Mrugala, R.: Temperature gradient and initial snow density as controlling factors in the formation and structure of hard depth hoar, Journal of Glaciology, 48, 485–494, doi:doi:10.3189/172756502781831098, http://www.ingentaconnect.com/content/igsoc/jog/2002/00000048/00000163/art00001, 2002.

Pinzer, B. R. and Schneebeli, M.: Snow metamorphism under alternating temperature gradients: Morphology and recrystallization in surface snow, Geophysical Research Letters, 36, 1–4, doi:10.1029/2009GL039618, http://dx.doi.org/10.1029/2009GL039618, 2009.

Polder, D. and van Santen, J.: The effective permeability of mixtures of solids, Physica, 12, 257 – 271, doi:http://dx.doi.org/10.1016/S0031-8914(46)80066-1, http://www.sciencedirect.com/science/article/pii/S0031891446800661, 1946.

Proksch, M., Löwe, H., and Schneebeli, M.: Density, specific surface area and correlation length of snow measured by high-resolution penetrometry, Journal of Geophysical Research: Earth Surface, 120, 346–362, doi:10.1002/2014JF003266, 2015.

Rechtsman, M. C. and Torquato, S.: Effective dielectric tensor for electromagnetic wave propagation in random media, Journal of Applied Physics, 103, 084901, doi:http://dx.doi.org/10.1063/1.2906135, http://scitation.aip.org/content/aip/journal/jap/103/8/10.1063/1.2906135, 2008.

Riche, F., Montagnat, M., and Schneebeli, M.: Evolution of crystal orientation in snow during temperature gradient metamorphism, Journal of Glaciology, 59, 47–55, doi:doi:10.3189/2013JoG12J116, http://www.ingentaconnect.com/content/igsoc/jog/2013/00000059/00000213/art00005, 2013.

Saito, S. and Kurokawa, K.: A precision resonance method for measuring dielectric properties of low-loss solid materials in the microwave region, Proceedings of the IRE, 44, 35–42, 1956.

Saleh, B. E. A. and Teich, M. C.: Fundamentals of Photonics, John Wiley & Sons, Inc., 1991.

Sarabandi, K.: Derivation of phase statistics from the Mueller matrix, Radio Science, 27, 553–560, doi:10.1029/92RS00195, http://dx.doi.org/10.1029/92RS00195, 1992.

Schleef, S. and Löwe, H.: X-ray microtomography analysis of isothermal densification of new snow under external mechanical stress, Journal of Glaciology, 59, 233–243, http://www.scopus.com/inward/record.url?eid=2-s2.0-84881176673&partnerID=40&md5=2dd45ad6989d7ed1ff93abcecd78c02b, 2013.

Schneebeli, M. and Sokratov, S.: Tomography of temperature gradient metamorphism of snow and associated changes in heat conductivity, Hydrological Processes, 18, 3655–3665, doi:10.1002/hyp.5800, http://dx.doi.org/10.1002/hyp.5800, 2004.

Sihvola, A.: Mixing rules with complex dielectric coefficients, Subsurface Sensing Technologies and Applications, 1, 393–415, doi:10.1023/A:1026511515005, http://dx.doi.org/10.1023/A%3A1026511515005, 2000.

Sihvola, A.: How strict are theoretical bounds for dielectric properties of mixtures?, IEEE Transactions on Geoscience and Remote Sensing, 40, 880 –886, doi:10.1109/TGRS.2002.1006369, 2002.

Stangl, M., Werninghaus, R., Schweizer, B., Fischer, C., Brandfass, M., Mittermayer, J., and Breit, H.: TerraSAR-X technologies and first results, Radar, Sonar and Navigation, IEE Proceedings -, 153, 86 –95, doi:10.1049/ip-rsn:20045119, 2006.

Sugiyama, S., Enomoto, H., Fujita, S., Fukui, K., Nakazawa, F., and Holmlund, P.: Dielectric permittivity of snow measured along the route traversed in the Japanese-Swedish Antarctic Expedition 2007/08, Annals of Glaciology, 51, 9–15, doi:doi:10.3189/172756410791392745, http://www.ingentaconnect.com/content/igsoc/agl/2010/00000051/00000055/art00002, 2010.

Torquato, S.: Random heterogeneous materials, Springer, New York, 2002.

Torquato, S. and Lado, F.: Trapping constant, thermal conductivity, and the microstructure of suspensions of oriented spheroids, The Journal of Chemical Physics, 94, 4453–4462, doi:http://dx.doi.org/10.1063/1.460635, http://scitation.aip.org/content/aip/journal/jcp/94/6/10.1063/1.460635, 1991.

Tsang, L.: Polarimetic Passive Microwave Remote Sensing of Random Discrete Scatterers and Rough Surfaces, Journal of electromagnetic waves and applications, 5, 41–57, 1991.

Tsang, L., Pan, J., Liang, D., Li, Z., Cline, D., and Tan, Y.: Modeling Active Microwave Remote Sensing of Snow Using Dense Media Radiative Transfer (DMRT) Theory With Multiple-Scattering Effects, Geoscience and Remote Sensing, IEEE Transactions on, 45, 990–1004, doi:10.1109/TGRS.2006.888854, 2007.

Tyynelä, J. and Chandrasekar, V.: Characterizing falling snow using multifrequency dual-polarization measurements, Journal of Geophysical Research: Atmospheres, 119, 8268–8283, doi:10.1002/2013JD021369, http://dx.doi.org/10.1002/2013JD021369, 2014.

Ulaby, F., Held, D., Donson, M., McDonald, K., and Senior, T.: Relating polarization phase difference of SAR signals to scene properties, IEEE Transactions on Geoscience and Remote Sensing, GE-25, 83 –92, doi:10.1109/TGRS.1987.289784, 1987.

Vallese, F. and Kong, J. A.: Correlation function studies for snow and ice, Journal of Applied Physics, 52, 4921 –4925, doi:10.1063/1.329453, 1981.

Warren, S. G. and Brandt, R. E.: Optical constants of ice from the ultraviolet to the microwave: A revised compilation, Journal of Geophysical Research: Atmospheres, 113, 1–10, doi:10.1029/2007JD009744, http://dx.doi.org/10.1029/2007JD009744, 2008.

Weber Hoen, E. and Zebker, H.: Penetration depths inferred from interferometric volume decorrelation observed over the Greenland ice sheet, IEEE Transactions on Geoscience and Remote Sensing, 38, 2571 – 2583, doi:10.1109/36.885204, 2000.

Werner, C., Wiesmann, A., Strozzi, T., Schneebeli, M., and Mätzler, C.: The SnowScat ground-based polarimetric scatterometer: Calibration and initial measurements from Davos Switzerland, in: Geoscience and Remote Sensing Symposium (IGARSS), 2010 IEEE International, pp. 2363–2366, doi:10.1109/IGARSS.2010.5649015, 2010.

Werninghaus, R. and Buckreuss, S.: The TerraSAR-X Mission and System Design, IEEE Transactions on Geoscience and Remote Sensing, 48, 606 –614, doi:10.1109/TGRS.2009.2031062, 2010.

West, R., Tsang, L., and Winebrenner, D. P.: Dense medium radiative transfer theory for two scattering layers with a Rayleigh distribution of particle sizes, Geoscience and Remote Sensing, IEEE Transactions on, 31, 426–437, 1993.

Wiesmann, A. and Mätzler, C.: Microwave Emission Model of Layered Snowpacks, Remote Sensing of Environment, 70, 307 – 316, doi:http://dx.doi.org/10.1016/S0034-4257(99)00046-2, http://www.sciencedirect.com/science/article/pii/S0034425799000462, 1999.

Wiesmann, A. and Werner, C.: SnowScat, X- to Ku-Band Scatterometer Development: D13 SnowScat User Manual, Tech. Rep. ESTEC/AO1-5311/06/NL/EL, ESA ESTEC, 2010.

Wiesmann, A., Werner, C., Mätzler, C., Schneebeli, M., Strozzi, T., and Wegmüller, U.: Mobile X- to Ku-band Scatterometer in Support of the CoRe-H20 Mission, in: Geoscience and Remote Sensing Symposium, 2008. IGARSS 2008. IEEE International, vol. 5, pp. V – 244–V – 247, doi:10.1109/IGARSS.2008.4780073, 2008.

Woodcock, N.: Specification of fabric shapes using an eigenvalue method, Geological Society of America Bulletin, 88, 1231–1236, doi:10.1130/0016-7606(1977)88, http://gsabulletin.gsapubs.org/content/88/9/1231, 1977.

Xie, X., Löhnert, U., Kneifel, S., and Crewell, S.: Snow particle orientation observed by ground-based microwave radiometry, Journal of Geophysical Research: Atmospheres, 117, 1–12, doi:10.1029/2011JD016369, http://dx.doi.org/10.1029/2011JD016369, 2012.